# Guide Through the Nanocarbon Jungle

Buckyballs, nanotubes, graphene, and beyond

# Guide Through the Nanocarbon Jungle

Buckyballs, nanotubes, graphene, and beyond

**David Tománek**

*Michigan State University*

Morgan & Claypool Publishers

ISBN 978-1-627-05273-3 (ebook)
ISBN 978-1-627-05272-6 (print)

DOI 10.1088/978-1-627-05273-3

Version: 20140201

IOP Concise Physics
ISSN 2053-2571 (online)
ISSN 2054-7307 (print)

A Morgan & Claypool publication as part of IOP Concise Physics

Morgan & Claypool Publishers, 40 Oak Drive, San Rafael, CA, 94903 USA

*To my parents,*
*for their patience*

# Acknowledgments

I gratefully acknowledge the assistance of Thomas Moore who provided the graphics for figures 1, 7, 13, 14, 15, 24, 25, 34, 38, 43, 78, 82, 87 and 98. The graphic used in figure 39(b) was provided by Andras Kis. Density functional electronic structure calculations used in figures 2, 12, 39, 44 and 63 were performed by Toshihiko Fujimori, Ceren Tayran and Zhen Zhu.

I am also grateful for useful comments and suggestions by many colleagues, especially Walt A de Heer, Shigeo Maruyama, Hisanori Shinohara and Peter Thrower. I am finally indebted to Nick Frederick for a very careful proof reading.

# Contents

# About the author

## David Tománek

David Tománek studied Physics in Switzerland and received his PhD from the Free University in Berlin. While holding a position as Assistant Professor of Physics in Berlin, he got engaged in theoretical research in Nanostructures at the AT&T Bell Laboratories and the University of California at Berkeley. He established the field of Computational Nanotechnology at Michigan State University, where he holds a position as Full Professor of Physics. His scientific expertise lies in the development and application of numerical techniques for structural, electronic and optical properties of surfaces, low-dimensional systems and nanostructures.

Since he was working on his PhD Thesis, he promoted the use of computer simulations to understand atomic-level processes at surfaces and in atomic clusters. Witnessed in several hundred publications and invited talks are his results on the electronic structure, mechanical, thermal and optical properties, as well as quantum conductance of nanostructures. His contributions to Computational Nanotechnology, in particular in the field of fullerenes and nanotubes, have been rewarded by a Fellowship of the American Physical Society, the Alexander-von-Humboldt Foundation Distinguished Senior Scientist Award and the Japan Carbon Award for Life-Time Achievement.

# Introduction

*"Buckyball, onion, nanobud, peapod – what are these buzzwords about?"* was a question posed to me many times over the last decade or two. This concise glossary is designed to provide the first answer to these and similar questions, and be a guide through the jungle of the jargon that has evolved in the busy field of carbon nanostructures. It does not provide a complete review of the nanocarbon field nor should it be mistaken for a textbook. The main intention is to provide useful information about keywords and explain basic concepts in nanocarbon science to all interested parties. Many entries are accompanied by references to primary literature, which I consider useful to illustrate the context; to that degree this selection is somewhat arbitrary and surely incomplete. Non-experts may appreciate the information about properties of nanocarbons and the significance of particular synthesis and characterization techniques. Experts may find good use for simple expressions and expectation values of sizes, strain energies and electronic properties of various carbon nanostructures. In order to demystify the field, I tried my best to simplify the terminology to a large degree, trying to make it accessible to interested individuals with little more than high-school education. I hope this intention finds the approval also of those colleagues who are used to the compact scientific shorthand notation and who may find some explanations overly simplified. As the ultimate motivation to put together this glossary, I have found that the field of carbon nanostructures is too rich in beauty and possibilities to keep it only to those who specialize in particular sub-fields as researchers.

East Lansing, December 2013

### How to Find What You Are Looking For

The monograph contains the main encyclopedic part and separate appendices:

- **key entries** in the main part are typeset in boldface;
- ***italicized expressions*** in the main part refer to key entries;
- **time lines of fullerenes, nanotubes and graphene** list major discoveries that paved the way to fame for these systems;
- **tables of useful quantities** offer a quick reference for those active in nanocarbon research.

Supplementary information for each key entry in this book is provided at the URL http://www.pa.msu.edu/people/tomanek/GNJ/SI/index.html

**IOP** Concise Physics

# Guide Through the Nanocarbon Jungle

Buckyballs, nanotubes, graphene, and beyond

**David Tománek**

# A

**Achiral** is the common designation for *armchair nanotubes* and *zigzag nanotubes*. The *chiral index* $(n, m)$ in achiral *nanotubes* is characterized by either $n = m$ for armchair nanotubes or by $n = 0$ or $m = 0$ for zigzag nanotubes. Other nanotubes are called *chiral nanotubes*.

**Adamantane** with the chemical composition $C_{10}H_{16}$, shown in figure 1, is a molecule with $T_d$ symmetry, and is also the smallest *diamondoid*. The $C_{10}$ *cage*, often called the adamantane cage, is the building block of the *diamond* structure.

**Ambipolar** conductors carry electric current by both electrons and holes. In this behavior they differ from metals and doped semiconductors, where charge transport is dominated by either electrons or holes. Carbon *nanotubes* and *graphene* are ambipolar conductors.

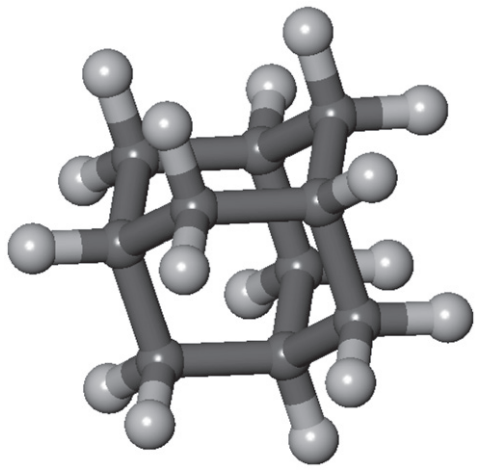

**Figure 1.** Structural model of the *adamantane* molecule with the chemical composition $C_{10}H_{16}$.

**Amorphous carbon** is a non-periodic arrangement of carbon atoms. Carbonaceous deposits commonly observed on *graphitic* carbon including *nanotubes* are often incorrectly called 'amorphous carbon' and should be more correctly referred to as *schmutz*.

**Arc evaporation** (AE), also called arc discharge, is a technique to synthesize *fullerenes* as well as *single-wall nanotubes* and *multi-wall nanotubes*. An electric arc is formed in a cooling inert gas atmosphere between electrodes connected to a 10–20 V direct current power supply. Fullerenes are found in the soot deposited on the chamber walls. *Nanotubes* form on the cathode during the evaporation of the electrode material, mostly carbon or *boron nitride* (BN), in the direction of the electric field lines. The presence of a *catalyst* in the electrodes is required to form single-wall nanotubes.

***References***

Krätschmer W, Lamb L D, Fostiropoulos K and Huffman D R 1990 Solid $C_{60}$: a new form of carbon *Nature* **347** 354

Iijima S 1991 Helical microtubules of graphitic carbon *Nature* **354** 56

The **area per atom** $A_C$ in $sp^2$ carbon nanostructures such as *graphene*, *fullerenes* and *nanotubes* is $A_C \approx 0.0262\ \text{nm}^2$.

doi:10.1088/978-1-627-05273-3ch1

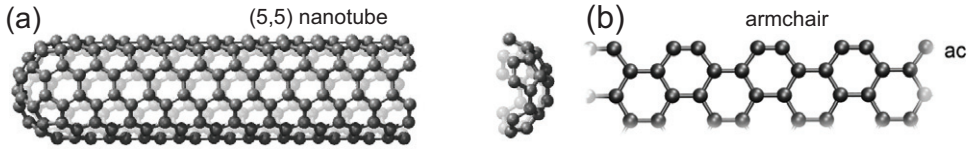


**Figure 2.** Structure of a (5, 5) *armchair nanotube* (a), terminated by an *armchair edge* (b) at one end and capped by a *dome* at the other end.

The **armchair edge** morphology of a *graphene* layer is shown in figure 2(b).

An **armchair nanoribbon** is a *graphene nanoribbon* (GNR) with an *armchair edge*. See also *graphene nanoribbon morphology*.

**Armchair nanotube** is the common name for a *nanotube* with *chiral index* $(n, n)$, referring to the *armchair edge* morphology at the open nanotube end (see figure 2).

# B

**Ball milling** (BM) is a low-cost synthesis technique of *nanotubes* and related nanostructures from layered substances, such as *graphite* and *boron nitride*. In the mechano-chemical ball-milling process that typically occurs at room temperature, the impact of a macroscopic ball on a powdered substance leads locally to a sharp temperature increase that enables rearrangement of chemical bonds.

**Ballistic** transport refers to the regime where charge carriers or lattice vibrations travel freely, without scattering. Ballistic charge transport is observed in conductors such as *nanotubes* or *graphene* and occurs without energy dissipation. The absence of scattering events in a ballistic conductor preserves the phase of the wave-packet associated with the carrier. In ballistic 1-dimensional *nanowires* such as nanotubes, *conductance* $G$ is quantized in units of the *conductance quantum* $G_0$ and is independent of the length. Scattering events transform nanotubes longer than the *electron mean free path* from ballistic to *diffusive* conductors.

**Bamboo** structure → *bucky bamboo*

**Band gap** → *fundamental band gap*

**Band structure** → *electronic band structure* or *phonon band structure*

**Battery** applications of carbon nanostructures include improvement in the number of useful charge–discharge cycles and the power delivery in Li-ion batteries (LIBs) upon addition of $\lesssim$10% *nanotubes* to the anode material consisting of *graphite*.

***Reference***

Endo M, Kim Y A, Hayashi T, Nishimura K, Matsushita T, Miyashita K and Dresselhaus M S 2001 Vapor-grown carbon fibers (VGCFs): Basic properties and their battery applications *Carbon* **39** 1287

**Bernal graphite** → *hexagonal graphite*

**Bilayer graphene** (BLG) is the simplest example of *multi-layer-graphene*, with the two layers in the preferred hexagonal (i.e. AB; see figure 44) stacking of *graphite*. The *electronic band structure* of BLG differs significantly from that of monolayer *graphene*, shown in figure 3, and that of graphite.

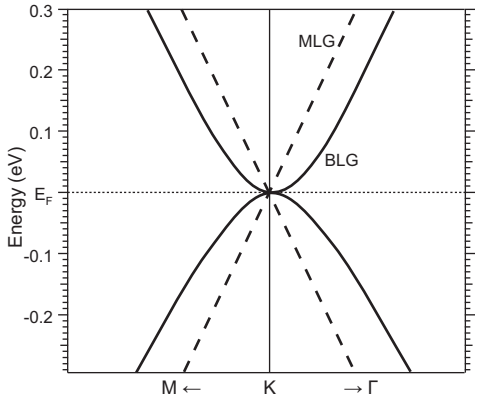


**Figure 3.** *Electronic band structure of bilayer graphene* (BLG; solid lines) in comparison to *monolayer graphene* (MLG; dashed lines) near the *Fermi point K*.

**Binding energy,** also called 'cohesive energy' $E_{coh}$, is defined as the energy investment to disassemble a structure into constituent atoms. The average atomic binding energy, $E_{coh}/n$, gradually increases with increasing number of atoms $n$ until it reaches its maximum value in the most stable bulk structure. As seen in figure 4, the equilibrium structure of small $C_n$ clusters evolves with increasing number of atoms from *chains* to rings and, for $n \geq 20$, to *fullerenes*. As shown in figure 19, transition from fullerenes to multi-wall *onion* structures is favored in structures with

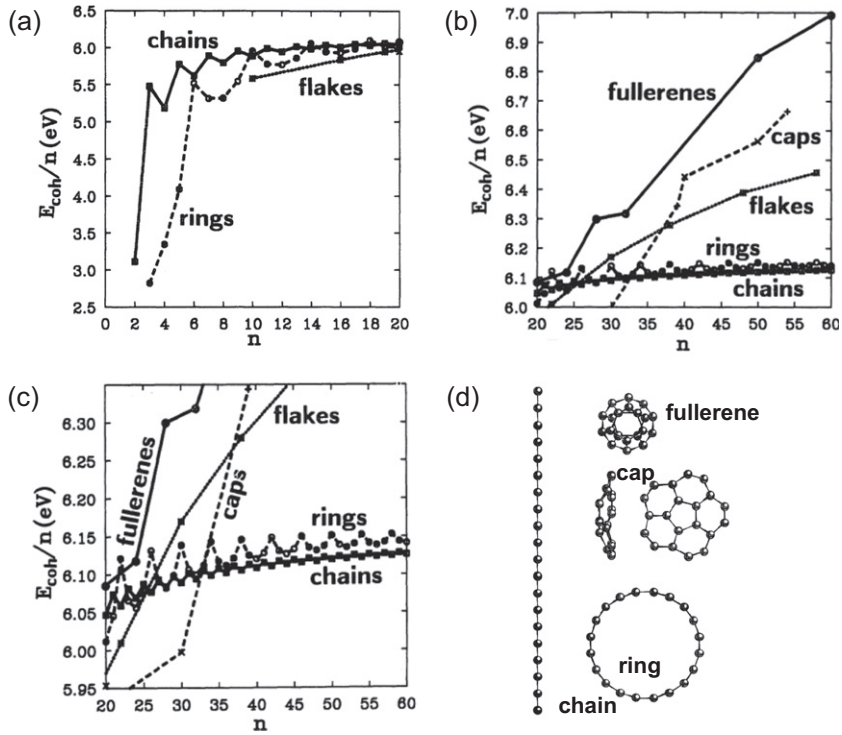


**Figure 4.** *Binding energy* per atom $E_{coh}/n$ in different structural arrangements of $C_n$. (a) Linear *chains* and rings are more stable than planar flakes for $n < 20$. (b) Absence of edges makes *fullerenes* more stable than other 2D and 1D structures for $n \geq 20$. The transition from 1D to quasi-2D fullerene structures is shown on an expanded energy scale in (c). (d) Structural *isomers* of the $C_{20}$ cluster. (Panels (a)–(c) are adapted from Tománek D and Schluter M A 1991 *Phys. Rev. Lett.* **67** 2331, © 1991 American Physical Society. Panel (d) is adapted from Brabec C J *et al* 1992 *Phys. Rev.* B **46** 7326, © 1992 American Physical Society.)

$n \gtrsim 700$ atoms by *inter-layer interactions*. For the same reason, formation of *multi-wall nanotubes* is energetically favored in large-*diameter nanotubes*, as seen in figure 61. Among the most stable bulk structures, *graphite* has the highest binding energy of $E_{coh}/n = 7.43$ eV/atom, closely followed by *diamond* with $E_{coh}/n = 7.37$ eV/atom.

***Reference***

Tománek D and Schluter M A 1991 Growth regimes of carbon clusters *Phys. Rev. Lett.* **67** 2331

A **biosensor** based on carbon *nanotubes* detects the presence of specific biomolecules that cause changes in the *conductance*, optical or *vibration spectra*. Selective antibody–antigen recognition reduces false positive results in nanotubes that are covered by specific antibodies.

***Reference***

Chen R J, Bangsaruntip S, Drouvalakis K A, Kam N W S, Shim M, Li Y M, Kim W, Utz P J and Dai H J 2003 Noncovalent functionalization of carbon nanotubes for highly specific electronic biosensors *Proc. Nat. Acad. Sci. USA* **100** 4984

**BLG** → *bilayer graphene*

**BN** → *boron nitride*

**Boron nitride** (BN) is a chemical compound with some similarities to carbon. The most stable hexagonal boron nitride (h-BN) structure is a layered substance with nearly the same lattice parameters as *graphite*. BN *nanotubes* related to BN monolayers are insulating irrespective of the *chiral index* $(n, m)$. The less stable cubic boron nitride (c-BN) structure is analogous to *diamond*.

The **Boudouard reaction** is a high-pressure disproportionation of carbon monoxide to elemental solid carbon, $2CO(g) \rightarrow C(s) + CO_2(g)$. This reaction is used in the *HiPCO process* to form *single-wall nanotubes* in the presence of a transition metal *catalyst* such as $Fe(CO)_5$.

***References***

Dai H J, Rinzler A G, Nikolaev P, Thess A, Colbert D T and Smalley R E 1996 Single-wall nanotubes produced by metal-catalyzed disproportionation of carbon monoxide *Chem. Phys. Lett.* **260** 471

Nikolaev P, Bronikowski M J, Bradley K R, Rohmund F, Colbert D T, Smith K A and Smalley R E 1999 Gas-phase catalytic growth of single-walled carbon nanotubes from carbon monoxide *Chem. Phys. Lett.* **313** 91

The **Brillouin zone** (BZ) is the *Wigner–Seitz cell* of the reciprocal lattice associated with a periodic structure. The Brillouin zones of *graphene* and *graphite* are shown in figure 5. The Fermi surface collapses to the K and K′ points in graphene and lies close to the K–H line (P line) in

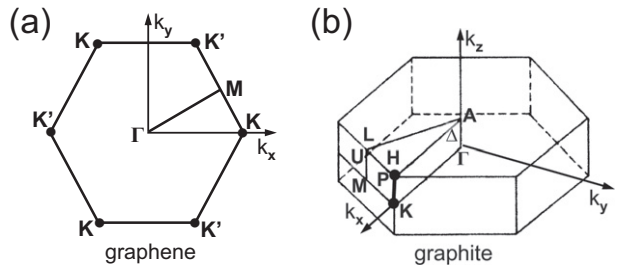


**Figure 5.** The *Brillouin zones* of *graphene* and *graphite*. Coordinates of the high-symmetry points are listed in tables 10 and 11.

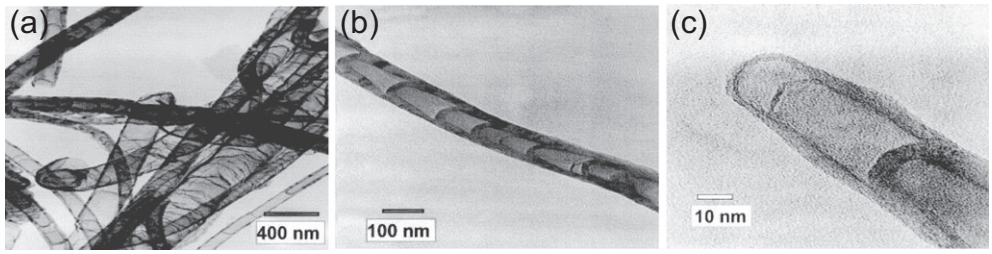


**Figure 6.** *Transmission electron microscopy* images of *bucky bamboo* grown by thermal *chemical vapor deposition* (CVD) of $C_2H_2$ at 950°C. (From Lee C J *et al* 2000 *Chem. Phys. Lett.* **323** 560, © 2000 Elsevier.)

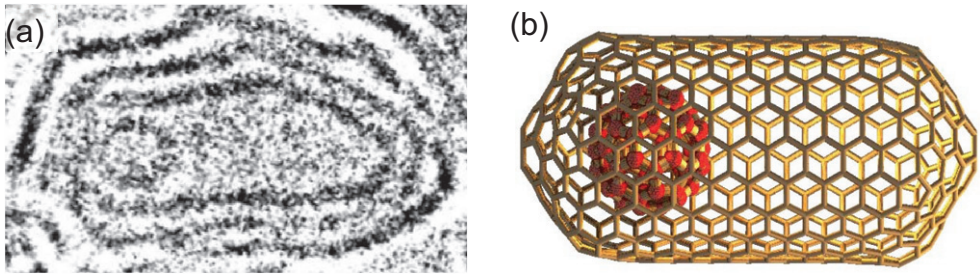


**Figure 7.** (a) High-resolution *transmission electron microscopy* image and (b) schematic structure of the *bucky shuttle*, consisting of a *fullerene* enclosed in a *capsule*. (From Kwon Y-K *et al* 1999 *Phys. Rev. Lett.* **82** 1470, © 1999 American Physical Society.)

graphite. Coordinates of the high-symmetry points of graphene are listed in table 10 and those of graphite in table 11.

**Buckminsterfullerene** → *$C_{60}$*

**Bucky bamboo** is a *multi-wall nanotube* structure with internal compartments that forms by catalytic decomposition of carbon containing gases in the *chemical vapor deposition* (CVD) process or by *arc evaporation*. *Transmission electron microscopy* images of bucky bamboo are shown in figure 6.

***Reference***

Lee C J, Park J H and Park J 2000 Synthesis of bamboo-shaped multiwalled carbon nanotubes using thermal chemical vapor deposition *Chem. Phys. Lett.* **323** 560

**Bucky onion** → *onion*

**Bucky paper** is a self-supporting layer of entangled carbon *nanotubes*. Hydrophobic carbon nanotubes float to the surface when immersed in water and aggregate to form a puffy, paper-like structure. Bucky paper may find application in mechanically strong, thermally and electrically conductive composite materials, as a nanoporous filter and as a substrate to grow biological tissue including nerve cells.

***Reference***

Rinzler A G, Liu J, Dai H, Nikolaev P, Huffman C B, Rodriguez-Macias F J, Boul P J, Lu A H, Heymann D, Colbert D T, Lee R S, Fischer J E, Rao A M, Eklund P C and Smalley R E 1998 Large scale purification of single wall carbon nanotubes: process, product and characterization *Appl. Phys.* A **67** 29

**Buckyball** → *$C_{60}$*

A **bucky shuttle** is the colloquial name for a *fullerene* or a *metallofullerene*

enclosed in a *capsule* or a *dome*-closed short *nanotube* segment. The structure is similar to a *peapod* and shown in figure 7. The enclosed fullerene can move back and forth in response to an electric field along the capsule axis.

***Reference***

Kwon Y K, Tománek D and Iijima S 1999 Bucky-shuttle memory device: synthetic approach and molecular dynamics simulations *Phys. Rev. Lett.* **82** 1470

**Buckytube** is an antiquated term for a carbon *nanotube*. The name implies that a carbon nanotube is structurally related to the *$C_{60}$* buckyball molecule.

**Bundle** of *nanotubes* → *rope* of nanotubes

# C

**$C_{60}$** is the best known *fullerene* molecule. It has the IUPAC name (C60-Ih) [5, 6] fullerene, and the structure shown in figure 8. It is also called *'buckminsterfullerene'* or simply *'buckyball'* in reference to the architect Richard Buckminster Fuller. For their role in its discovery in 1985, Harold W Kroto, Robert F Curl, and Richard E Smalley were awarded the 1996 Nobel Prize in Chemistry. The $C_{60}$ molecule in the shape of a truncated icosahedron is the smallest fullerene satisfying the *isolated-pentagon rule* (IPR). Among the possible *fullerene synthesis* routes, *arc evaporation*, followed by *fullerene separation*, is most common for $C_{60}$. A low-temperature *wet chemical synthesis* of $C_{60}$ has also been achieved.

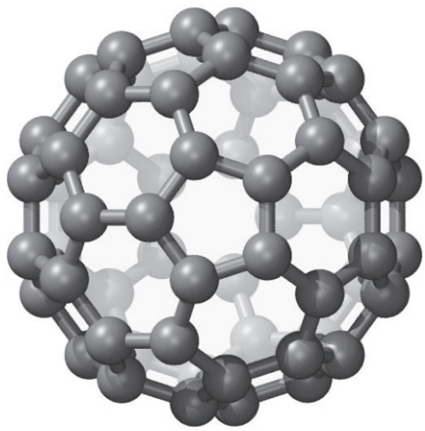

**Figure 8.** Structure of the *$C_{60}$ fullerene* molecule.

***References***

Kroto H W, Heath J R, O'Brien S C, Curl R F and Smalley R E 1985 *$C_{60}$*: buckminsterfullerene *Nature* **318** 162

A **cage**, in the context of nanocarbons, is a rigid structure with a cavity that may be sufficiently large to allow *filling* by foreign atoms. Common uses range from the small *adamantane* cage within the open structure of *diamond* to *graphitic capsules* in the shape of oblong *fullerenes*.

**Cap opening** refers to the *opening* of *dome*-closed *nanotube* ends.

**Capillary filling** of *nanotubes* by liquids, including molten metals such as lead, *fullerenes*, *diamondoids* and other small molecules, occurs in analogy to the filling of a nanopipette. Nanotubes filled with fullerenes are called *peapods*. Successful filling of nanotubes precludes *opening* their *dome*-closed ends in an oxidizing environment. Opening and filling may be achieved in a one-stage process by supplying a desired substance as part of the oxidizing environment.

***References***

Pederson M R and Broughton J Q 1992 Nanocapillarity in fullerene tubules *Phys. Rev. Lett.* **69** 2689

Ajayan P M and Iijima S 1993 Capillarity-induced filling of carbon nanotubes *Nature* **361** 333

Loiseau A and Pascard H 1996 Synthesis of long carbon nanotubes filled with Se, S, Sb and Ge by the arc method *Chem. Phys. Lett.* **256** 246

Tsang S C, Chen Y K, Harris P J F and Green M L H 1994 A simple chemical method of opening and filling carbon nanotubes *Nature* **372** 159

Zhang J, Feng Y, Ishiwata H, Miyata Y, Kitaura R, Dahl J E P, Carlson R M K, Shinohara H and Tománek D 2012 Synthesis and transformation of linear adamantane assemblies inside carbon nanotubes *ACS Nano* **6** 8674

The **capillary force** represents the force that pulls a molecule into a nanopore or nanocavity of comparable *diameter*, such as a *nanotube*. As illustrated in figure 9, $F_c = -\Delta V/\Delta x$ is the maximum negative gradient of the potential energy $V$ of a molecule near the opening of the cavity. The force is highest when the encapsulation energy $\Delta V$ is large due to a strong attractive interaction with the surrounding walls, or when the size $\Delta x$ of the molecule is small. A typical value in carbon nanotubes is $F_c \lesssim 1$ nN.

**Capillary pressure** $p_c$ is the ratio of the *capillary force* $F_c$ and the pore cross-sectional area $A$, illustrated in figure 9. In carbon *nanotubes*, very high values $p_c = F_c/A \lesssim 1$ GPa result from a small cross-sectional area. Molecules entering the constrained volume subject other enclosed molecules to pressure $p_c$, thereby facilitating fusion reactions.

***Reference***

Yoon M, Berber S and Tománek D 2005 Energetics and packing of fullerenes in nanotube peapods *Phys. Rev.* B **71** 155406

A **capsule** is a hollow structure with a *graphitic* shell consisting of an oblong *fullerene* or a short, *dome*-closed *nanotube*. Capsules often have multiple walls, such as in spherical *onions* (see figure 19).

**Carbon allotrope** is a structurally differentiated form of carbon. *Diamond*, *graphite*, *M-carbon*, *schwarzite*, *graphene*, *haeckelite*, *fullerenes*, *onions*, *nanotubes* and *nanohorns* are prominent examples of carbon allotropes. In spite of serious attempts, the nomenclature of $sp^2$ carbon allotropes, depicted in figure 10, has not yet been universally agreed upon.

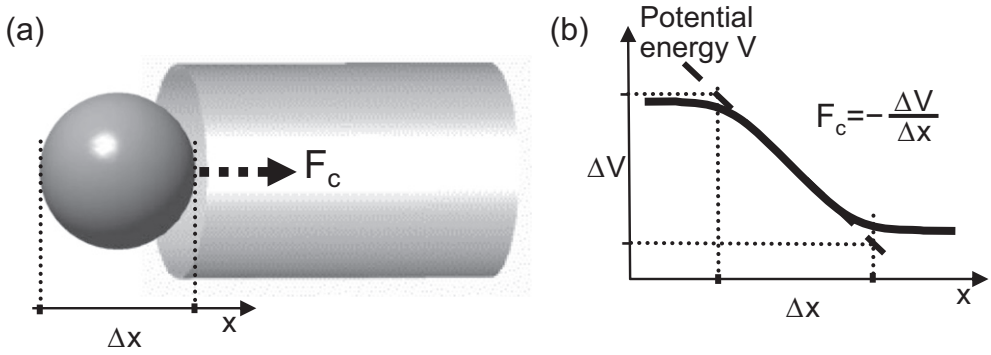


**Figure 9.** Origin of the *capillary force* $F_c$ that pulls a molecule inside a nanopore or nanocavity.

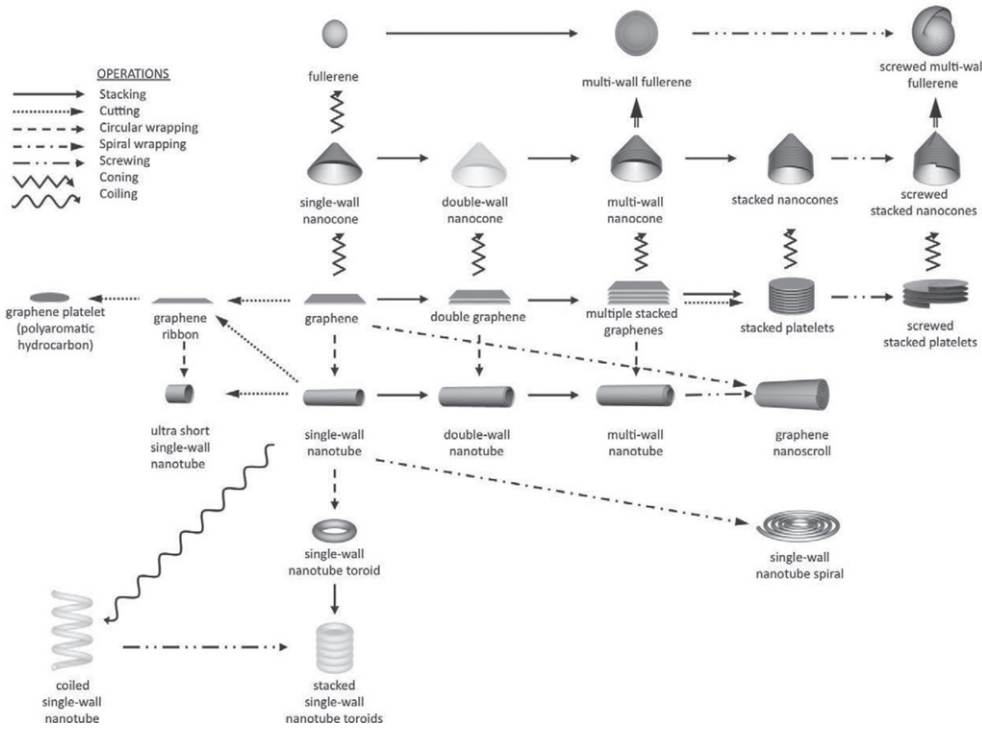


**Figure 10.** Structural forms and relationships between *sp*$^2$ hybridized *carbon allotropes*. Forms that have not yet been observed are shown faded. (From Suarez-Martinez I *et al* 2012 *Carbon* **50** 741, © 2012 Elsevier.)

***References***

Kroto H W 1992 Carbon onions introduce new flavour to fullerene studies *Nature* **359** 670

Suarez-Martinez I, Grobert N and Ewels C P 2012 Nomenclature of sp$^2$ carbon nanoforms *Carbon* **50** 741

**Carbon black** is a pure form of carbon soot.

**Carbon fiber** (CF), also called *graphite* fiber or carbon graphite, is a fiber with a typical diameter of 5–10 $\mu$m that consists of graphitized carbon. Common PAN (polyacrylonitrile)-based and pitch-based carbon fibers contain different arrangements of not rigidly connected *graphitic* layers arranged in a solid cylinder geometry. As suggested by the electron micrograph in figure 11, carbon fibers are structurally different from *multi-wall nanotubes*. Carbon fibers may be spun

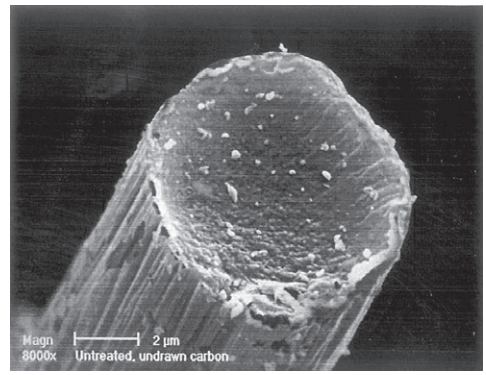


**Figure 11.** *Scanning electron microscopy* (SEM) image of an individual PAN-based *carbon fiber*. (From Chen J C and Harrison I R 2002 *Carbon* **40** 25, © 2002 Elsevier.)

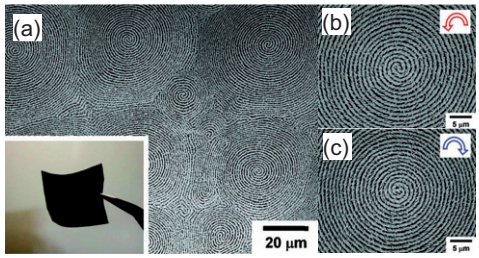


**Figure 12.** (a) *Scanning electron microscopy* (SEM) image of a helical graphite film with a multidomain morphology, obtained by *carbonization* of iodine-doped helical polyacetylene. The flexible free-standing carbon film is shown in the inset. Enlarged SEM images show (b) left-handed and (c) right-handed spiral morphologies. (From Matsushita S *et al* 2011 *J. Am. Chem. Soc.* **133** 17977, © 2011 American Chemical Society.)

into high-strength *nanotube yarns* and textiles or used as mechanical reinforcement in composite materials.

**Carbonization** is a complex process that converts an organic substance into a solid residue with increased carbon content at very high temperatures under exclusion of oxygen. The mass fraction of non-carbon elements in the residue decreases with increasing pyrolysis temperature, from typically 10 wt% at $T \approx 1200$ K to 1 wt% at $T \approx 1600$ K. Carbonization often preserves the morphology of the system, as seen in figure 12. Exposure to temperatures $T \gtrsim 2000$ K results in an increasing degree of *graphitization*.

***Reference***

Goh M, Matsushita S and Akagi K 2010 From helical polyacetylene to helical graphite: synthesis in the chiral nematic liquid crystal field and morphology-retaining carbonisation *Chem. Soc. Rev.* **39** 2466

A **carbon nanotube** is a *nanotube* with a *graphitic* wall and a typical *diameter* of a few nanometers.

A **catalyst** is a substance that plays an important role during the formation of *single-wall nanotubes*. The *catalyst material* is believed either to be atomically dispersed, in a floating catalyst, or to form nanometer-sized clusters in a supported catalyst. At the high *synthesis temperatures*, catalyst particles are believed to break down carbon feedstock to atomic carbon and precipitate it at the nanoparticle surface in the form of a growing nanotube, as illustrated in figure 58.

**Catalyst material** is almost always present during the formation of *single-wall nanotubes* (SWNTs) from carbon feedstock. Typical catalysts are nanoparticles of transition metals such as Fe, Ni, Mo, Co, Y, their mixtures or oxides.

**Catalytic growth** of *nanotubes* refers to growth in the presence of a *catalyst material* in the many techniques used for *nanotube synthesis*. Growth occurs at the interface between the open-ended nanotube and the *catalyst* particle found either at the tip during tip growth or at the bottom during root growth, shown in figure 58. Tip growth is favored when catalyst particles do not adhere strongly to a substrate.

A **chain** is a stable linear arrangement of carbon atoms that is held together by $sp^1$ bonds. Especially in odd-numbered chains, the bond lengths alternate by 0.004 nm between 0.128 nm and 0.132 nm, as seen in figure 13(a). The optimum chain structure is much closer to the *cumulenic chain* structure (C=C=C$\cdots$), connected by identical double bonds, than the *polyyne chain* structure (C−C≡C−C$\cdots$), connected by alternating single and triple

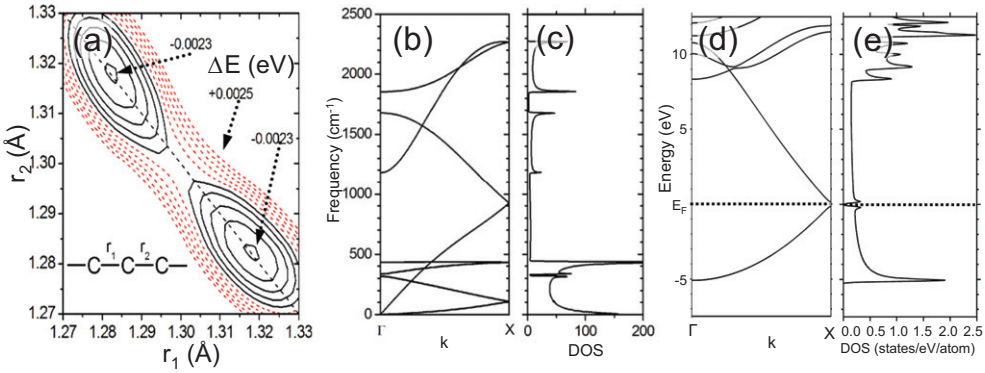


**Figure 13.** Equilibrium structure, vibrational and electronic structure of an infinite carbon *chain*. (a) Total energy contour plot $\Delta E(r_1, r_2)$ of an infinite linear carbon chain with alternating inter-atomic distances $r_1$ and $r_2$, with $\Delta E$ presented per two-atom unit cell. The schematic in the inset addresses the geometry, not the bonding character. (b) *Phonon band structure* and (c) *phonon density of states* (DOS) of a carbon chain. (d) *Electronic band structure* $E(k)$ and (e) the corresponding *electronic density of states* (DOS). (Panels (a)–(c) adapted from Zhang J *et al* 2012 *ACS Nano* **6** 8674, © 2012 American Chemical Society.)

bonds. According to table 7, a polyyne chain should display a large single/triple bond length difference of 0.03 nm; this is much larger than what is observed and is energetically unfavorable due to the rigidity of the bonds. *sp*$^2$ and *sp*$^3$ structures convert to chains at temperatures exceeding the melting point of carbon near 4000 K, benefiting from the increase in configurational and vibration entropy that outweighs the reduction of their *binding energy*. See also *chain electronic band structure* and *phonon spectrum of a chain*.

The **chain electronic band structure** $E(k)$ near the Fermi level $E_F$ is dominated by pp$\pi$ interactions and shown in figure 13(d). The *electronic density of states* (DOS), depicted in figure 13(e), is dominated by sharp peaks representing van Hove singularities that are characteristic of 1D structures. The small bond length alternation in the *chain* structure opens a small *fundamental band gap* near $E_F$ at $k = X$, which is easily visible in the DOS. The occupied states of the *electronic band structure* in figure 13(d) below $E_F$ are particularly well represented by the *Hückel molecular orbital method*. The analytic expression is $E(k) = E_F + 2\gamma_0 \cos(kd_{CC})$, where $\gamma_0 \approx -2.9$ eV is the nearest-neighbor hopping integral and $d_{CC} \approx 0.13$ nm is the interatomic distance.

The **chain phonon band structure** $\omega(k)$ is shown in figure 13(b). The *phonon density of states* (DOS), depicted in figure 13(c), is dominated by sharp peaks representing van Hove singularities that are characteristic of 1D structures.

**Chemical reactions** inside carbon *nanotubes* benefit from the presence of a rigid enclosure, which orients enclosed molecules favorably. The *capillary force* that favors entry of molecules inside a nanotube subjects the enclosed substance to a *capillary pressure* $p_c \lesssim 1$ GPa, thus accelerating a possible fusion reaction.

**Chemical vapor deposition** (CVD) is a very common process used to convert gaseous hydrocarbons to carbon *nanotubes* or to a *diamond-like carbon* (DLC) coating. The conversion occurs at high temperatures in thermal CVD, or may be assisted by a plasma in plasma-enhanced CVD (PECVD).

The **chiral angle** $\theta$ in a *nanotube* is defined as the angle in the generating *graphene* lattice between the basis vector $\mathbf{a_1}$ and the *chiral vector* $\mathbf{C_h}$ (see figure 15). It is given by

$$\theta = \sin^{-1}\left(\frac{\sqrt{3}m}{2\sqrt{n^2 + nm + m^2}}\right).$$

The **chiral index** $(n, m)$ of a *nanotube*, often called *chirality*, defines the wrapping vector or *chiral vector* $\mathbf{C_h} = n\mathbf{a_1} + m\mathbf{a_2}$ in the *graphene* plane. It is given in the basis of graphene Bravais lattice vectors $\mathbf{a_1}$ and $\mathbf{a_2}$, with $a = |\mathbf{a_1}| = |\mathbf{a_2}| = 0.246$ nm (see figure 14). Based on the morphology of the open nanotube edge, we distinguish *armchair nanotubes* with chiral index $(n, n)$ from *zigzag nanotubes* with chiral index $(n, 0)$ and other *chiral nanotubes*. Electronic *conductance* of a nanotube depends primarily on $(n, m)$ (see the labeling in figure 14).

A **chiral nanotube** is a *nanotube* with the *chiral index* $(n, m)$, where $n \neq m$ and where neither $n$ nor $m$ is equal to zero (see figure 15). Chiral nanotubes possess *handedness*, meaning that they can be either left- or right-handed.

The **chiral vector** $\mathbf{C_h} = n\mathbf{a_1} + m\mathbf{a_2}$, characterized by the *chiral index* $(n, m)$, defines a direction on the *graphene* plane. It is commonly used to describe the edges of a *graphene nanoribbon* (GNR) and the mapping of carbon atoms during the roll-up process from graphene to a *nanotube*, thereby identifying the atomic structure of the entire nanotube, as seen in figure 16. In a

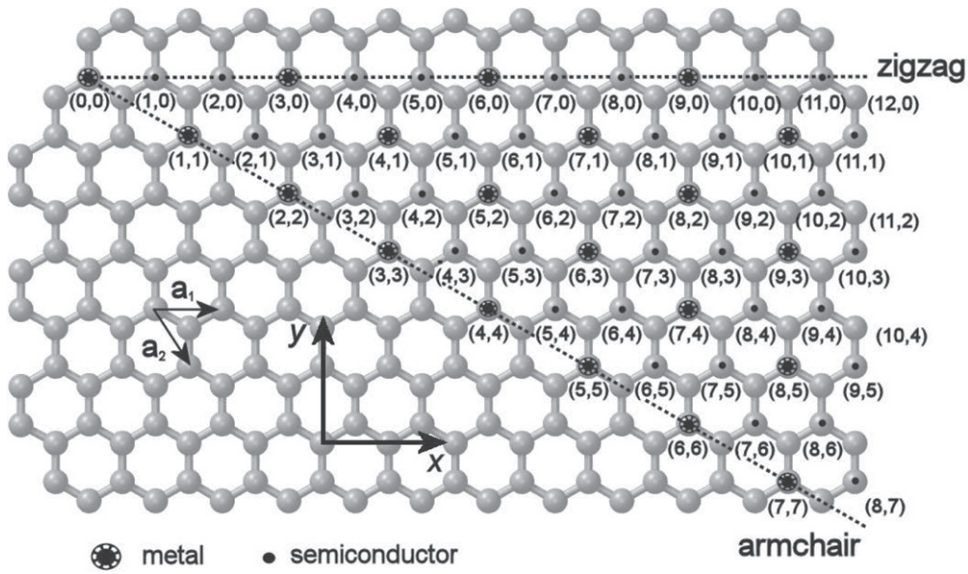


**Figure 14.** Definition of the *chiral index* $(n, m)$ of a carbon *nanotube* on the *graphene* lattice.

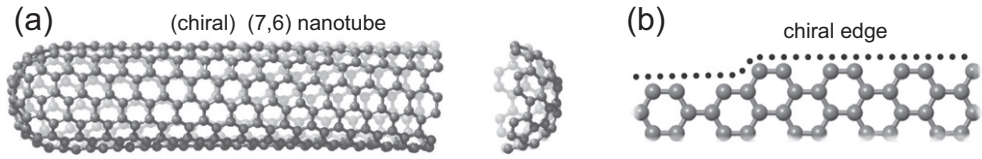


**Figure 15.** Structure of a (7, 6) *chiral nanotube* (a), terminated by a chiral edge (b) at one end and capped by a *dome* at the other end.

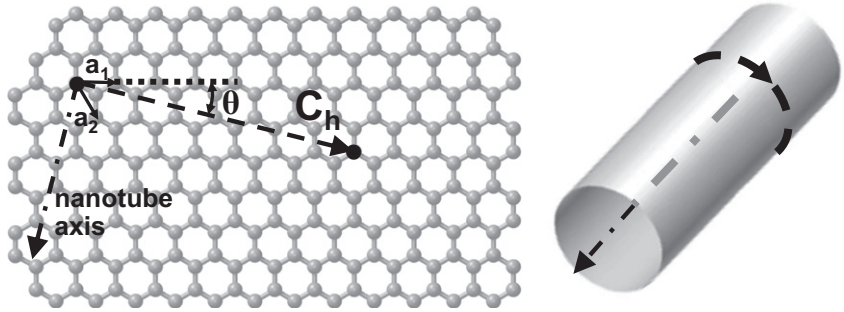


**Figure 16.** The *chiral vector* $\mathbf{C}_h$ defines the wrapping of a *graphene* monolayer to a *nanotube*.

nanotube, the chiral vector of length $|\mathbf{C_h}| \approx 0.246 \times \sqrt{m^2 + mn + n^2}$ nm is perpendicular to the axis.

**Chirality** occurs in two very different contexts in carbon physics. In most cases, it is used synonymously with the *chiral index* ($n$, $m$) and *chiral vector* to identify the structural arrangement of atoms in a *nanotube* or the morphology of a *graphene nanoribbon* edge. In *graphene* physics, chirality $\sigma \cdot \mathbf{p}/|p|$ of charge carriers is defined as the projection of the *pseudospin* $\sigma$ on the momentum direction $\mathbf{p}/|p|$. Electrons have positive chirality and holes negative chirality.

**Cohesive energy** → *binding energy*

**CoMoCAT** is a *catalyst* containing Co and Mo used in the *catalytic growth* of *single-wall nanotubes* with a narrow distribution of *diameters* $d_t \approx 0.8$ nm and *chiral indices*, mostly (6, 5) and (7, 5). The carbon feedstock in the CoMoCAT® process is CO.

***Reference***

Kitiyanan B, Alvarez W E, Harwell J H and Resasco D E 2000 Controlled production of single-wall carbon nanotubes by catalytic decomposition of CO on bimetallic Co—Mo catalysts *Chem. Phys. Lett.* **317** 497

**Composite** → *nanotube composite*

**Conductance** $G$ commonly refers to electrical conductance and is the inverse of the resistance $R = V/I$, given by the ratio of the applied voltage $V$ and the current $I$. Conductance of one-dimensional structures such as *nanotubes* may differ from that of the related layered substance. Insulating substances such as *boron nitride* yield insulating nanotubes. Metallic or semi-metallic layered substances, including *graphite*, may yield metallic, semi-metallic or semiconducting

nanotubes. The conductance of a particular *single-wall nanotube* is dominated by quantization effects that depend on its *chiral index* $(n, m)$. Carbon nanotubes, where $n-m$ is divisible by 3, are metallic or semi-metallic; all other nanotubes are semiconducting. *Armchair nanotubes* with the chiral index $(n, n)$ are truly metallic, *ambipolar* conductors. Within the *ballistic* regime, conductance of metallic or semi-metallic one-dimensional structures is quantized in units of the *conductance quantum* $G_0$. At small applied voltages, the conductance of metallic single-wall nanotubes is $G = 2G_0$, corresponding to a resistance $R = 1/G \approx 6.5\ \text{k}\Omega$.

The **conductance quantum** $G_0$ is the quantization unit of *conductance* of *nanowires* such as metallic *nanotubes* in the *ballistic* regime. Its value is $G_0 = 2e^2/h \approx (12.9\ \text{k}\Omega)^{-1}$, where $e$ is the electron charge and $h$ is the Planck constant.

**Contacts** act as quantum devices on the nanometer scale, often displaying *conductance* quantization or *Coulomb blockade* behavior. Favorable interface geometry and overlap of electronic wave functions near the Fermi level on both sides of the contact reduce the *Schottky barrier*. A low Schottky barrier and matching *work functions* on both sides of the contact improve carrier injection in ohmic contacts. Pd is considered the most favorable contact metal for *nanotubes* and *graphene*.

***Reference***

Nemec N, Tománek D and Cuniberti G 2006 Contact dependence of carrier injection in carbon nanotubes: an ab initio study *Phys. Rev. Lett.* **96** 076802

The **continuum elasticity theory** is a computational approach to determine the energy penalty due to deformation without specifying atomic positions. In *graphitic* structures this energy depends on the flexural rigidity $D = 1.41$ eV and the Poisson ratio $\alpha = 0.165$. Successful applications include the *strain energy* $\Delta E_s$ in *fullerenes* and *nanotubes* with one wall (figures 17 and 18) and *binding*


**Figure 17.** *Continuum elasticity theory* description of the energy penalty $\Delta E_s$ caused by deforming a *graphene* monolayer.

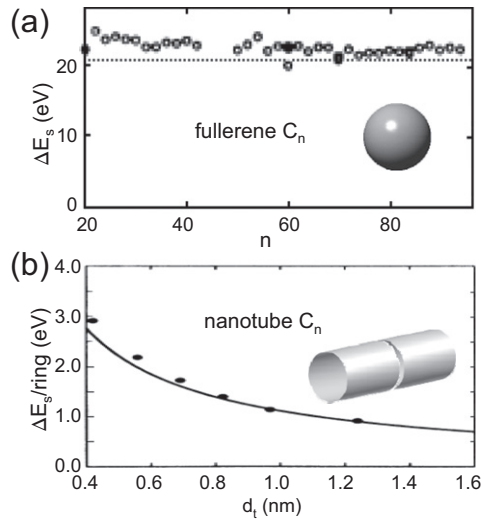


**Figure 18.** *Strain energy* in (a) $C_n$ *fullerenes* and (b) *single-wall nanotubes* with respect to a planar *graphene* monolayer. Results from *continuum elasticity theory*, shown by continuous lines, are compared to precise quantum mechanical calculations, given by the data points. Results for nanotubes with *diameter* $d_t$ are given per ring of carbon atoms along the tube perimeter, as indicated in the inset. (Based on results presented in Tománek D *et al* 1993 *Phys. Rev.* B **48** 15461, © 1993 American Physical Society.)

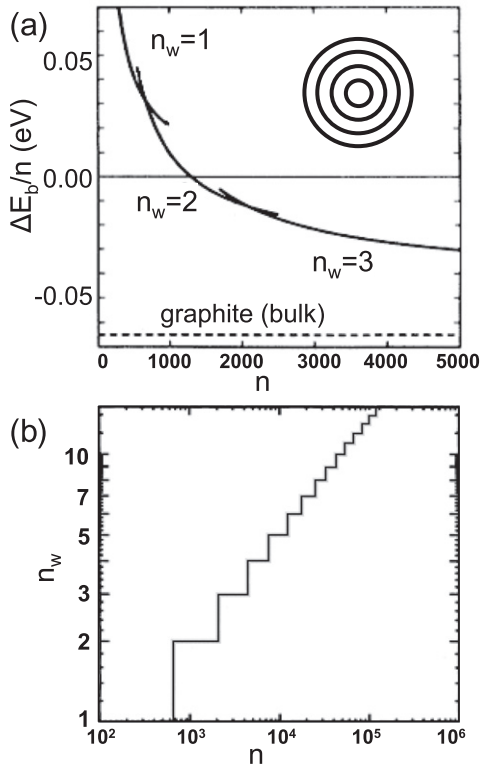


**Figure 19.** (a) Difference *binding energy* per atom $\Delta E_b/n$ in $C_n$ *onions* with $n_w$ walls with respect to a planar *graphene* monolayer. (b) Expected number of walls $n_w$ in onions with $n$ atoms. Transition from single-wall *fullerenes* to double-wall onions is expected to occur at $n \approx 700$, and to triple-wall onions at $n \approx 2000$. Presentation on the double-logarithmic scale shows the scaling $n_s \propto n^{1/3}$ for large $n$, suggesting that large onions gradually approach the bulk *graphite* structure. (Based on results presented in Tománek D *et al* 1993 *Phys. Rev.* B **48** 15461, © 1993 American Physical Society.)

*energy* in fullerenes and nanotubes with multiple walls (figures 19 and 61).

***Reference***

Tománek D, Zhong W and Krastev E 1993 Stability of multi-shell fullerenes *Phys. Rev.* B **48** 15461

**Corannulene** is an aromatic hydrocarbon molecule with the chemical formula

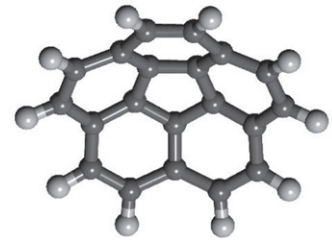

**Figure 20.** Ball-and-stick model of the $C_{20}H_{10}$ *corannulene* molecule.

$C_{20}H_{10}$, depicted in figure 20. Its basic non-planar structure (without the terminating H atoms), a pentagon surrounded by six hexagons, is seen in all *fullerenes* obeying the *isolated pentagon rule* (IPR).

The **Coulomb blockade** (CB) is a charge transport characteristic occurring in inhomogeneous *nanowires* containing *quantum dots* that are connected by tunnel junctions. Transport through a quantum dot is blocked if the Coulomb energy associated with charging a low-capacitance quantum dot with one extra electron charge $e$ exceeds the energy $eV$ provided by the applied voltage $V$ or the thermal energy $k_BT$. Transport blockage manifests itself as an infinite resistance in the current-voltage ($I$–$V$) characteristic at low applied voltages $V$ and low temperatures $T$. Coulomb blockade plays the key role in the *single-electron transistor* (SET).

The **Coulomb staircase** refers to the shape of the current–voltage ($I$–$V$) characteristic in conductors exhibiting a *Coulomb blockade*. In contrast to ohmic conductors, where $V/I = R$ is constant, the discrete energy steps associated with transferring excess electrons onto the *quantum dot* at increasing applied voltages $V$ translate to steps in $R$ and the $I$–$V$ characteristic.

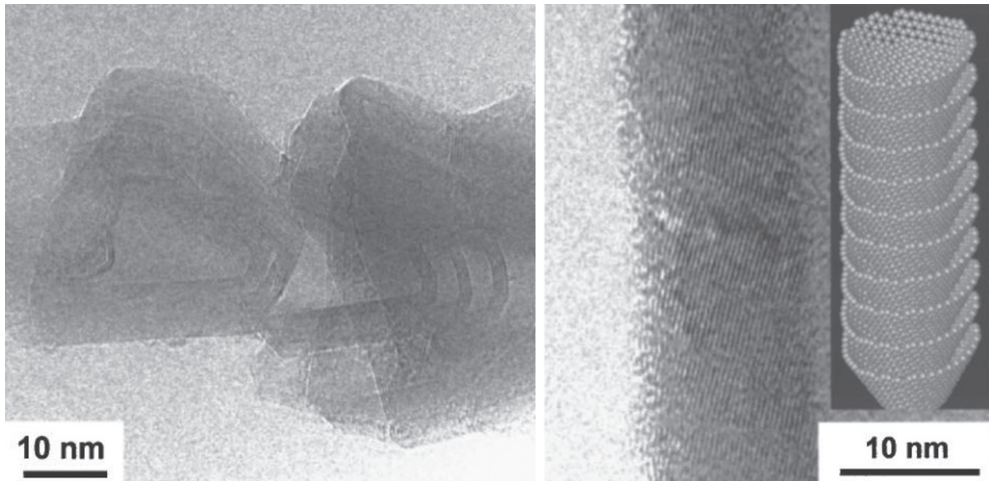


**Figure 21.** High-resolution *transmission electron microscopy* images of *cup-stacked fibers*, displaying high level of *graphitization*. The inset in the right panel illustrates the structure. (Adapted from Endo M *et al* 2002 *Appl. Phys. Lett.* **80** 1267, © 2002 American Institute of Physics.)

A **cumulenic chain** is a specific *isomer* of a *chain* of carbon atoms (C=C=C···) connected by double bonds.

**Cup-stacked fibers** are *carbon fibers* consisting of stacked truncated *graphitic* cones, as seen in figure 21. These fibers can be produced efficiently by catalytic thermal *chemical vapor deposition* (CVD).

***Reference***

Endo M, Kim Y A, Hayashi T, Fukai Y, Oshida K, Terrones M, Yanagisawa T, Higaki S and Dresselhaus M S 2002 Structural characterization of cup-stacked-type nanofibers with an entirely hollow core *Appl. Phys. Lett.* **80** 1267

**Curvature** → *Gaussian curvature* or *polyhedral curvature*

**CVD** → *chemical vapor deposition*

**Cycloaddition** is a particular chemical reaction that connects two molecules covalently by forming a cyclic adduct. The 2+2 cycloaddition, interconnecting two *graphitic* structures at the place of two facing double bonds, is depicted in figure 22. This is the first step in the *polymerization* or *fusion of fullerenes* such as $C_{60}$ and may occur as a *photochemical process* following light absorption.

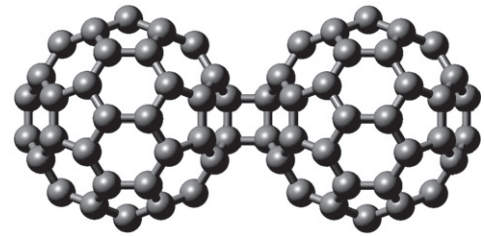

**Figure 22.** The $C_{120}$ molecule formed by covalently connecting two $C_{60}$ *fullerenes* in the 2+2 *cycloaddition* reaction.

***Reference***

Rao A M, Zhou P, Wang K-A, Hager G T, Holden J M, Wang Y, Lee W-T, Bi X-X, Eklund P C, Cornett D S, Duncan M A and Amster I J 1993 Photoinduced polymerization of solid $C_{60}$ films *Science* **259** 955

# D

The ***D*-band** is a *Raman-active* spectroscopic band commonly observed in carbon nanostructures. The *D*-band of *diamond* lies at $\omega \approx 1332\ \mathrm{cm}^{-1}$. The presence of a similar band at $\omega \approx 1350\ \mathrm{cm}^{-1}$ in *graphitic* material indicates structural disorder.

***Reference***

Ferrari A C, Meyer J C, Scardaci V, Casiraghi C, Lazzeri M, Mauri F, Piscanec S, Jiang D, Novoselov K S, Roth S and Geim A K 2006 Raman spectrum of graphene and graphene layers *Phys. Rev. Lett.* **97** 187401

**Dahlia** → *sea urchin*.

The **Debye frequency $\nu_D$** is the highest phonon frequency in a crystalline solid that is approximately described by the Debye model. $\nu_D$ is typically close to the maximum atomic vibration frequency in structures containing only carbon.

The **Debye temperature** $T_D$ is related to the *Debye frequency* $\nu_D$ by $k_B T_D = h\nu_D$; it is used in the calculation of the *specific heat* especially at low temperatures, where quantum effects dominate. The value is $T_D = 2200$ K in *diamond* and $T_D = 2750$ K (in-plane) and $T_D = 950$ K (out-of-plane) in *graphite*.

A **defect** is a deviation from the ordered structure of nanocarbons. Local defects include single or multiple vacancies, non-carbon substitutional atoms, isotopic impurities, *Stone–Thrower–Wales defects* or 5–7–7–5 defects, 5–7 defects on a *nanotube* wall such as *elbow bends*, which change the tube direction, or adjacent 5–7 defects, which change the tube *diameter*. Orientational dislocations, such as *twistons*, may strongly affect the *conductance* of carbon *nanotubes*. *Vibration spectra* and *thermal conductivity* of carbon structures depend sensitively on the *isotopic composition*, including the presence of *isotopic defects*, due to the relatively large mass difference between the predominant carbon isotopes $^{12}C$ and $^{13}C$.

***Reference***

Banhart F, Kotakoski J and Krasheninnikov A V 2011 Structural defects in graphene *ACS Nano* **5** 26

The **deformation energy** may be interpreted as a change in *strain energy*.

**Density of states (DOS)** → *electronic density of states* or *phonon density of states*

**Density, gravimetric** → *gravimetric density*

**Descartes' lost theorem**, in a form adapted to $C_n$ *fullerenes* with planar faces, states that the sum of *polyhedral curvatures* $C_i$ at all $n$ atoms amounts to $\sum_i^n C_i = 720°$. Descartes' lost theorem is equivalent to *Euler's theorem*.

***Reference***

Descartes R Elementary Treatise on Polyhedra *(unpublished, dated 1619–1621)*

**Diameter** → *diameter of a fullerene* or *diameter of a nanotube*

The **diameter of a fullerene** with a spherical shape and $n$ carbon atoms is given by $d_f \approx \sqrt{n} \times 0.0913$ nm.

The **diameter of a nanotube** with the *chiral index* $(n, m)$ and *chiral vector* $\mathbf{C_h}$ is

given by $d_t = |\mathbf{C_h}|/\pi \approx \sqrt{m^2 + mn + n^2} \times 0.0783$ nm. The most common determination of $d_t$ uses the frequency of the *radial breathing mode* (RBM). *Single-wall nanotubes* of carbon or *boron nitride* have typical diameters close to 1 nm. Free-standing nanotubes with a diameter $d_t \lesssim 0.4$ nm are structurally unstable due to the large stress. Single-wall nanotubes with a diameter $d_t \gtrsim 5.4$ nm spontaneously collapse to form a *ribbon*.

**Diamond** is a form of elemental carbon that is almost as stable as *graphite*. The diamond lattice of atoms is related to the face-centered cubic (fcc) crystal structure, with two equivalent C atoms assigned to each fcc lattice point. Each C atom is rigidly connected to its four nearest neighbors by covalent $sp^3$ bonds (see figure 23). The *gravimetric density* of diamond is $\rho = 3.52$ g cm$^{-3}$. The large *binding energy* $E_{\text{coh}} = 7.37$ eV/atom and bulk modulus $B = 442$ GPa make diamond the strongest and hardest bulk material in nature. Diamond oxidizes in air above 700 °C. Before melting in vacuum at ambient pressure, it converts to thermodynamically more stable graphite. The *thermal conductivity* of diamond is dominated by the phonon contribution and depends sensitively on the *isotopic composition* as well as temperature. 99.9% isotopically pure $^{12}$C diamond reaches the value $\kappa = 41000$ W (m·K)$^{-1}$ at 104 K, the highest measured thermal conductivity for a solid above liquid nitrogen temperature. With its *fundamental band gap* of 5.5–5.6 eV, diamond is a wide-gap insulator that is transparent in the visible range.

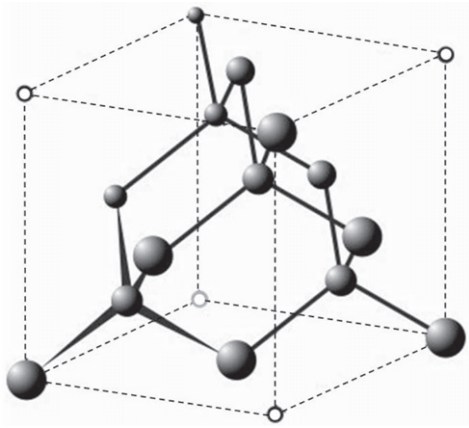

**Figure 23.** Atomic arrangement in the *diamond* lattice.

***References***


Eggert J H, Hicks D G, Celliers P M, Bradley D K, McWilliams R S, Jeanloz R, Miller J E, Boehly T R and Collins G W 2010 Melting temperature of diamond at ultrahigh pressure *Nature Phys.* **6** 40

Wei L, Kuo P K, Thomas R L, Anthony T R and Banholzer W F 1993 Thermal conductivity of isotopically modified single crystal diamond *Phys. Rev. Lett.* **70** 3764

Kresse G, Furthmüller J and Hafner J 1995 Ab initio force constant approach to phonon dispersion relations of diamond and graphite *Europhys. Lett.* **32** 729

Giustino F, Louie S G and Cohen M L 2010 Electron-phonon renormalization of the direct band gap of diamond *Phys. Rev. Lett.* **105** 265501


**Diamond-like carbon** (DLC) consists of a network of mostly $sp^3$-bonded carbon atoms. DLC is most common in coatings applied onto a substrate by *chemical vapor deposition* (CVD) in order to enhance surface hardness.

**Diamondoid** is a stable carbon *cage* molecule, consisting of one or more connected *adamantane* cages that are terminated by hydrogen or other functional groups. The simplest diamondoid is the $C_{10}H_{16}$ adamantane with one cage, followed by the $C_{14}H_{20}$ with two face-fused cages and higher polymantanes with several stable

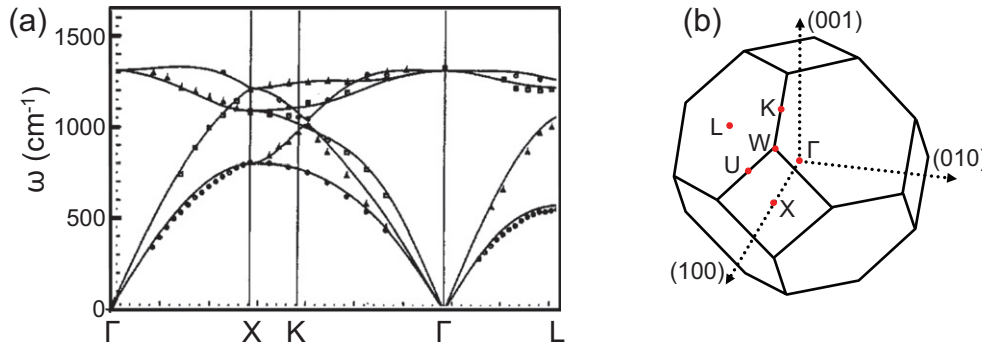


**Figure 24.** (a) *Phonon band structure* of *diamond*. The full lines represent calculations, the dots observed inelastic-neutron-scattering data from Warren J L *et al* 1967 *Phys. Rev.* **158** 805. (b) *Brillouin zone* and the most important high-symmetry points of the diamond lattice (fcc lattice with a basis, see table 9). (Results in (a) adapted from Kresse G *et al* 1995 *Europhys. Lett.* **32** 729, © 1995 Institute of Physics.)

structural *isomers*. Diamondoids occur naturally in raw oil deposits.

***Reference***

Dahl J E, Liu S G and Carlson R M K 2003 Isolation and structure of higher diamondoids, nanometer-sized diamond molecules *Science* **299** 96

**Dielectrophoresis** is a process used to separate metallic from semiconducting *nanotubes* by applying an inhomogeneous electric field to a carbon nanotube suspension held between electrodes.

***Reference***

Krupke R, Hennrich F, Löhneysen H v and Kappes M M 2003 Separation of metallic from semiconducting single-walled carbon nanotubes *Science* **301** 344

**Diffusive** transport is a conduction regime dominated by scattering of charge carriers. *Conductance* in the diffusive regime is not quantized; it is inversely proportional to the length of the carbon nanostructure, such as a *nanotube* or a *graphene nanoribbon* (GNR), and is accompanied by Joule heating. Opposite to the *ballistic* transport regime.

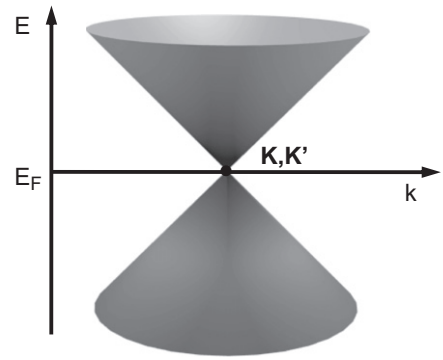


**Figure 25.** Schematic diagram of the *Dirac cone* in the *electronic band structure* $E(k)$ of a *graphene* monolayer near the *Fermi points* K and K′.

The **Dirac cone** in the *graphene electronic band structure*, shown in figure 25, received its name on account of the near-linear and isotropic band dispersion $E(k)$ near the K and K′ points in the *Brillouin zone* of *graphene*. The band dispersion in the *electronic band structure* of graphene reduces to a form analogous to the

dispersion of light or relativistic particles. It is given by $E(\Delta k_x, \Delta k_y) = E_F + \hbar v_F (\Delta k_x^2 + \Delta k_y^2)^{1/2}$, where $(\Delta k_x, \Delta k_y)$ denotes the position with respect to the *Dirac point*, $E_F$ is the Fermi energy and $v_F$ is the *Fermi velocity*. With $p = \hbar(\Delta k_x^2 + \Delta k_y^2)^{1/2}$ as momentum relative to the Fermi momentum, the form $E - E_F = v_F p$ describes formally massless particles.

**Dirac points** are the six corners of the hexagonal *Brillouin zone* of *graphene*, labelled by the letters K and K′ in figure 5(a). These points are also the *Fermi points*, representing the Fermi surface of graphene. Each of the Dirac points forms an apex of the *Dirac cone*.

**Dispersion** in common use of the term describes the separation of *single-wall nanotubes* from a nanotube *rope*, which is commonly achieved by ultrasonication in the presence of a *surfactant*. In a different context, dispersion relations describe the energy dependence $E(\mathbf{k})$ of allowed electronic states on the wavevector $\mathbf{k}$ in the *electronic band structure* and the frequency dependence $\omega(\mathbf{k})$ on $\mathbf{k}$ in the *phonon band structure* of a periodic structure.

***Reference***

O'Connell M J, Bachilo S M, Huffman C B, Moore V C, Strano M S, Haroz E H, Rialon K L, Boul P J, Noon W H, Kittrell C, Ma J, Hauge R H, Weisman R B and Smalley R E 2002 Band gap fluorescence from individual single-walled carbon nanotubes *Science* **297** 593

A **dome** is the common name for the capping structure at the end of a *nanotube*. The dome structure, illustrated in figure 26, consists of a *fullerene* hemisphere.

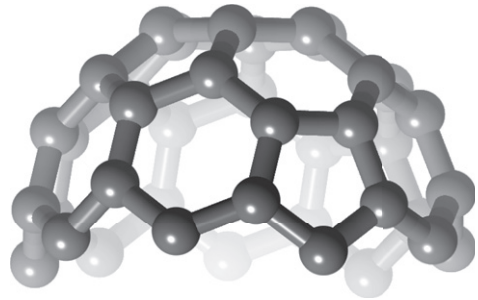

**Figure 26.** Structural model of a *dome* terminating a (9, 0) *zigzag nanotube*.

According to *Euler's theorem*, a dome must contain exactly six pentagons and an undefined number of hexagons. The number of distinguishable dome structures increases with a high power of $\approx 8.7$ of the *diameter*.

**Doping** is a process that introduces free charge carriers into semiconducting carbon nanostructures. Exposure to oxygen in the air causes p-doping of *nanotubes*. n-doping is achieved by alkali metal intercalation or by annealing nanotubes in vacuum. Exposure of *graphite* to large quantities of a foreign substance, such as metal atoms, may lead to the formation of *graphite intercalation compounds* (GICs).

A **double-wall nanotube** (DWNT) is a *multi-wall nanotube* with only two walls. Common mass production techniques including *chemical vapor deposition* (CVD) and pulsed arc-discharge with selected metal *catalysts* lead to a DWNT yield of up to 80–90%. Synthesis of even higher *purity* pristine DWNTs may be achieved by *fusion of fullerenes* inside a *peapod*, as seen in figures 36 and 37. In most cases, improved *graphitization* and a smaller number of *defects* in the inner wall make DWNTs more suitable

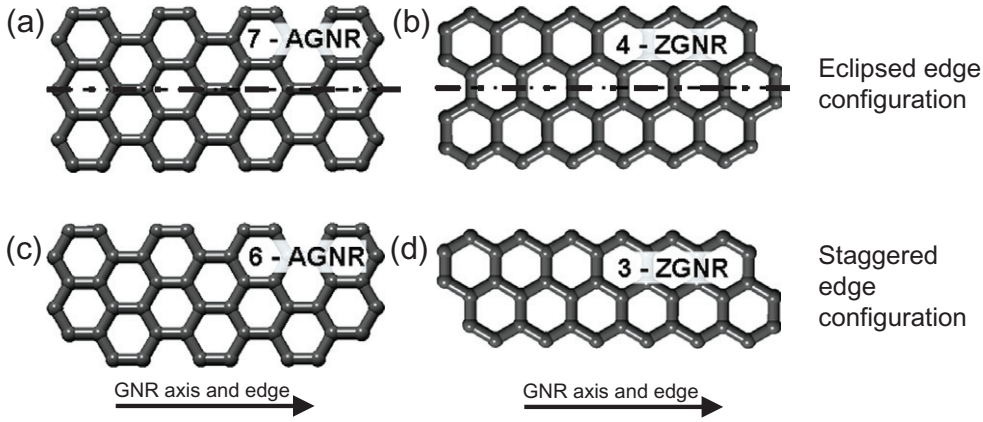


**Figure 27.** Schematic representation of common *graphene nanoribbons* (GNRs). (a, c) *Armchair nanoribbons* and (b, d) *zigzag nanoribbons* with (a, b) an *eclipsed edge configuration* and (c, d) a *staggered edge configuration*. The nomenclature used to describe the *graphene nanoribbon morphology* is illustrated in figure 42.

candidates for encapsulation than *single-wall nanotubes* (SWNTs).

***References***

Hutchison J L, Kiselev N A, Krinichnaya E P, Krestinin A V, Loutfy R O, Morawsky A P, Muradyan V E, Obraztsova E D, Sloan J, Terekhov S V and Zakharov D N 2001 Double-walled carbon nanotubes fabricated by a hydrogen arc discharge method *Carbon* **39** 761

Hiraoka T, Kawakubo T, Kimura J, Taniguchi R, Okamoto A, Okazaki T, Sugai T, Ozeki Y, Yoshikawa M and Shinohara H 2003 Selective synthesis of double-wall carbon nanotubes by CCVD of acetylene using zeolite supports *Chem. Phys. Lett.* **382** 679

Sugai T, Yoshida H, Shimada T, Okazaki T and Shinohara H 2003 New synthesis of high-quality double-walled carbon nanotubes by high-temperature pulsed arc discharge *Nano Lett.* **3** 769

Pfeiffer R, Holzweber M, Peterlik H, Kuzmany H, Liu Z, Suenaga K and Kataura H 2007 Dynamics of carbon nanotube growth from fullerenes *Nano Lett.* **7** 2428

**DWNT** → *double-wall nanotube*

# E

An **eclipsed edge configuration** in a *graphene nanoribbon* (GNR) is a structure where the edges are mirror images with respect to the GNR axis. The difference between the eclipsed and the *staggered edge configuration* is shown in figure 27.

The **edge energy** is the energy needed to cleave an infinite layer divided by the length of both edges. The precise value depends on the edge morphology. In *graphene*, the average value is $\varepsilon_e \approx 10.1\,\text{eV nm}^{-1}$ for a bare *armchair edge* and $\varepsilon_e \approx 11.8\,\text{eV nm}^{-1}$ for the less stable bare *zigzag edge*. Edge saturation by adsorbed hydrogen or other atoms stabilizes the edge, thus reducing the edge energy.

***References***

Okada S 2008 Energetics of nanoscale graphene ribbons: edge geometries and electronic structures *Phys. Rev.* B **77** 041408(R)

Liu Y, Dobrinsky A and Yakobson B I 2010 Graphene edge from armchair to zigzag: the origins of nanotube chirality? *Phys. Rev. Lett.* **105** 235502

An **edge state** is an electronic or phonon state localized mostly at the edge. Edge states in a 2D monolayer structure such as *graphene* are the counterpart of surface states in a 3D structure. At the *zigzag edge* of graphene, an electronic edge state is formed by the non-bonding C2$p_\pi$ orbitals that hybridize to a flat band. This edge state causes a sharp peak in the *electronic density of states* at the Fermi energy, leading to a magnetic instability. The electronic structure and transport of graphene flakes and *graphene nanoribbons* (GNRs) depends sensitively on the precise edge structure due to the dominant role of edges states near the Fermi level.

***Reference***

Fujita M, Wakabayashi K, Nakada K and Kusakabe K 1996 Peculiar localized state at zigzag graphite edge *J. Phys. Soc. Japan* **65** 1920

An **elbow bend** is caused by substituting one or more hexagon pairs by pentagon–heptagon pairs on opposite sides of a *nanotube*, as shown in figure 28. This *defect* changes the *chiral index* ($n$, $m$) and thus modifies the electronic structure of the nanotube.

**Electroluminescence** (EL) is light emission caused by the recombination of electrons and holes carried to the same location by an electric current. *Graphitic* carbon nanostructures may exhibit electroluminescence owing to the *ambipolar* transport character of *graphene* and carbon *nanotubes*, specific examples being *light-emitting diodes* and *light-emitting transistors* consisting of individual *single-wall nanotubes*. Electroluminescence differs from incandescence, which is associated with the black body radiation caused by Joule heating of carbon *nanowires* to high temperatures by passing an electric current.

**Electron affinity** (EA) of a molecule or a finite system is the energy gain associated with bringing an extra electron from infinitely far away and placing it in the lowest unoccupied molecular orbital (LUMO). The electron affinity of the $C_{60}$ molecule is EA = 2.65 eV. This relatively large value makes $C_{60}$ an antioxidant.

The **electron mean free path** is the average distance an electron travels without collisions. In *graphene* and conducting carbon *nanotubes*, the electron mean free path at room temperature exceeds several hundred nanometers.

***Reference***

Purewal M S, Hong B H, Ravi A, Chandra B, Hone J and Kim P 2007 Scaling of resistance and electron mean free path of single-walled carbon nanotubes *Phys. Rev. Lett.* **98** 186808

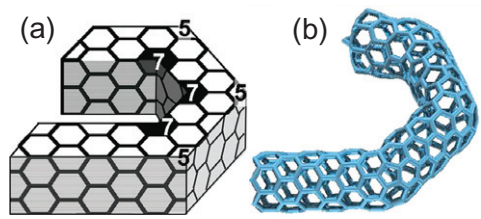


**Figure 28.** (a) Schematic representation and (b) optimized atomic structure of a set of *elbow bends* on a *nanotube*, constituting a *hook*.

**Electron mobility** $\mu$ is the quantity relating the average speed, called drift velocity $v_d$, of an electron in response to the applied electric field $E$ by $v_d = \mu E$. Electron mobility is limited by scattering from *defects* and lattice vibrations, and is typically reduced in structures deposited on a substrate. High mobility in *graphitic* materials including *graphene* and *nanotubes* results from the absence of backscattering due to the conservation of *pseudospin*. Extremely high room temperature values of $\mu \approx 79\,000$ cm$^2$ V$^{-1}$ s$^{-1}$ have been observed in semiconducting carbon nanotubes and values in excess of 15 000 cm$^2$ V$^{-1}$ s$^{-1}$ have been observed in free-standing graphene. These values exceed those for all known semiconductors.

***References***

McEuen P L, Bockrath M, Cobden D H, Yoon Y-G and Louie S G 1999 Disorder, pseudospins, and backscattering in carbon nanotubes *Phys. Rev. Lett.* **83** 5098

Dürkop T, Getty S A, Cobas E and Fuhrer M S 2003 Extraordinary mobility in semiconducting carbon nanotubes *Nano Lett.* **4** 35

Ando T, Nakanishi T and Saito R 1998 Berry's phase and absence of back scattering in carbon nanotubes *J. Phys. Soc. Japan* **67** 2857

Katsnelson M I, Novoselov K S and Geim A K 2006 Chiral tunnelling and the Klein paradox in graphene *Nature Phys.* **2** 620

The **electronic band structure** $E(\mathbf{k})$ describes the dispersion of electronic quantum states as a function of the electron momentum $\mathbf{k}$ and is closely related to the *electronic density of states* (DOS). Most important for electric *conductance* are the electronic states near the Fermi level $E_F$. See also *chain electronic band structure*, *graphene electronic band structure*, *graphene nanoribbon electronic band structure*, *graphite electronic band structure*, *nanotube electronic band structure*, and *Dirac cone*.

The **electronic density of states** (DOS) $N(E)$ enumerates the number of electronic quantum states at energy $E$ that are allowed to be occupied. $N(E)$ in clusters or *quantum dots*, such as *fullerenes* or *diamondoids*, consists of discrete levels. In one-dimensional wires, such as *nanotubes*, $N(E)$ is continuous and dominated by peaks called van Hove singularities (see figure 29). $N(E)$ is also continuous in two-dimensional systems, such as *graphene* (see figure 30), and three-dimensional systems, such as *diamond*. Crucial for *conductance* is

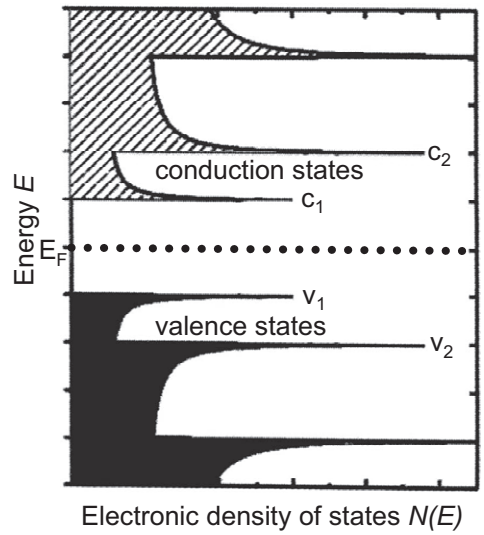


**Figure 29.** *Electronic density of states* (DOS) of a semiconducting carbon *nanotube*. The DOS is dominated by van Hove singularities at $v_1$, $v_2$, . . . in the occupied (valence) part of the spectrum and at $c_1$, $c_2$, . . . in the unoccupied (conduction) part of the spectrum. $N(E) = 0$ within the *fundamental band gap* in the energy range between the $v_1$ and $c_1$ states. In conducting carbon nanotubes, $N(E)$ has a non-zero but constant small value in the energy range between $E(v_1)$ and $E(c_1)$.

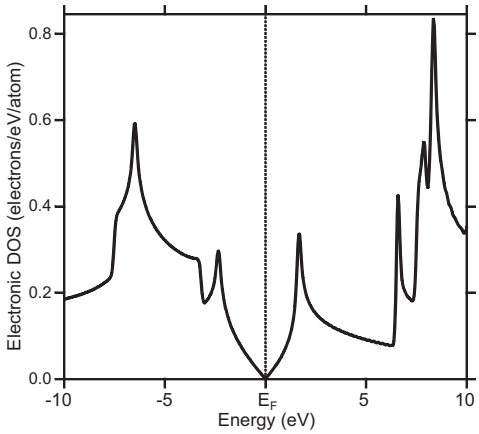


**Figure 30.** *Electronic density of states* (DOS) $N(E)$ of a *graphene* monolayer. This semi-metal has zero *fundamental band gap* and also vanishing DOS at the Fermi level $E_F$.

the behavior of $N(E)$ near the Fermi level $E_F$, the highest occupied level: $N(E_F) = 0$ in insulators, whereas $N(E_F)$ is non-zero in conductors.

**Endofullerene** → *endohedral fullerene*

**Endohedral fullerene** A@$C_n$, also called 'endofullerene', is a *fullerene* that contains an atom or an atomic aggregate A inside the hollow $C_n$ *cage*. The endohedral configuration, denoted by the '@' sign, is opposite to the *exohedral* configuration.

***Reference***

Chai Y, Guo T, Jin C, Haufler R E, Chibante L P F, Fure J, Wang L, Alford J M and Smalley R E 1991 Fullerenes with metals inside *J. Phys. Chem.* **95** 7564

**Euler's theorem** relates the number of corners or vertices ($V$), polygonal faces ($F$) and edges ($E$) by the expression $V + F - E = 2$ in any convex polyhedron (object of topological genus 0, with no holes and related to a sphere). It is equivalent to *Descartes' lost theorem* describing relations between face angles. One of its important consequences for $n$-atom *fullerenes* containing only pentagonal and hexagonal faces is that the number of pentagons $p = 12$ and the number of hexagons is $n/2 - 10$. Another consequence is that $C_{20}$ with 12 pentagonal faces is the smallest fullerene. For an object with topological genus 1, related to a donut, Euler's theorem reads $F + V - E = 0$. Perfect *nanotubes*, which may be viewed as a segment of the donut, contain hexagons only. Pentagons and heptagons appear in pairs at *defect* sites, causing local bending or *diameter* change.

The **eutectic** point in a composition–temperature ($x$–$T$) *phase diagram* refers to the chemical composition $x_e$ and the lowest temperature $T_e$ at which a eutectic mixture of compounds melts. A eutectic mixture is a system that melts at a lower temperature than the constituent compounds. $x_e$ is known as the eutectic composition and $T_e$ as the eutectic temperature. The eutectic point plays an important role in the *catalytic growth* of *vapor-grown carbon fibers* (VGCFs) and *nanotubes*. $T_e$(Ni–C) = 1326°C and $T_e$(Fe–C) = 1154°C in eutectic mixtures of *graphite* with nickel and iron, two important *catalysts* in the formation of filamentous carbon.

***Reference***

Tibbetts G G and Balogh M P 1999 Increase in yield of carbon fibres grown above the iron/carbon eutectic *Carbon* **37** 241

**Excited state dynamics** describes atomic motion in a structure where the electrons are not in the ground-state configuration. The nature of chemical bonds in the excited state differs from that in the

electronic ground state, which may fundamentally change chemical reactions. Electronic excitation can be induced by absorption of energetic electrons or light (leading to *photochemical processes*), or by energetic collisions with ions, used in focused ion beam (FIB) lithography. Electronic excitations may last in excess of a picosecond in nanostructures. They may decay non-radiatively by coupling to electrons first and later to vibration modes.

***References***

Krasheninnikov A V, Miyamoto Y and Tománek D 2007 Role of electronic excitations in ion collisions with carbon nanostructures *Phys. Rev. Lett.* **99** 016104

Miyamoto Y, Rubio A and Tománek D 2006 Real-time ab initio simulations of excited carrier dynamics in carbon nanotubes *Phys. Rev. Lett.* **97** 126104

An **exciton** is an electronic state formed by the Coulomb binding between an excited electron and a hole. In most bulk semiconductors, excitons with typical binding energies of a few meV do not change the *optical properties*. In semiconducting *nanotubes*, significantly reduced screening of the Coulomb interaction increases the electron–hole pair binding energy to a large fraction of an electron-volt, which becomes comparable to the *fundamental band gap*. Bright (dark) excitons can (cannot) be observed optically. The presence of excitonic states in the band gap strongly modifies the optical spectrum of nanotubes and related low-dimensional objects. In particular, the ratio of the second and first observed optical transition energies $R_{\mathrm{exp}} = E_{22}/E_{11}$ in the *photoluminescence* spectrum deviates strongly from $R_{\mathrm{Hu}} = 2$ based on the otherwise successful simple *Hückel molecular orbital method*. *Two-photon absorption* spectroscopy allows detailed observations of excitons. Reliable theoretical description of excitonic states in extended nanostructures may be obtained by solving the Bethe–Salpeter equation, which correctly addresses electronic many-body interactions.

***References***

Wang F, Dukovic G, Brus L E and Heinz T F 2005 The optical resonances in carbon nanotubes arise from excitons *Science* **308** 838

Kane C L and Mele E J 2003 Ratio problem in single carbon nanotube fluorescence spectroscopy *Phys. Rev. Lett.* **90** 207401

Spataru C D, Ismail-Beigi S, Benedict L X and Louie S G 2004 Excitonic effects and optical spectra of single-walled carbon nanotubes *Phys. Rev. Lett.* **92** 077402

**Exfoliation**, also known as peeling, is the disassembly of a layered structure into constituent layers. Exfoliation energy describes the associated energy investment. The exfoliation energy of *graphite* amounts to 0.06 eV/atom. See also *graphite binding*.

**Exohedral.** A configuration in the context of *fullerenes* or *nanotubes* that refers to atoms attached from outside to the hollow fullerene *cage* or the nanotube.

# F

**Fermi points** lie on the Fermi surface of a system. In semimetallic *graphene*, the Fermi surface consists of the six corners of the hexagonal *Brillouin zone*, labelled by the letters K and K′ in figure 5(a). These points are also the *Dirac points* in graphene.

The **Fermi velocity** $v_F$ is the average speed of conduction electrons at the Fermi level $E_F$. $v_F \approx 10^6$ m s$^{-1}$ in *graphene*.

The **field emission** of carbon *nanotubes* growing vertically on a substrate is described well by the *Fowler–Nordheim* relationship.

The **filling** of *graphitic* nanoparticles including *fullerenes* in the *arc evaporation* process is achieved by adding a specific substance to the electrode material. Graphitic particles formed in this way or by high-temperature electron irradiation of carbon material mostly resemble *capsules* or *onions*. The graphitic shell typically subjects the enclosed substance to high pressure that suppresses structural *defects* and may change the crystal structure, as seen in figure 32 and figure 75. *Endohedral fullerenes* are a special case of filled graphitic nanoparticles. *Single-wall nanotubes* may be filled by fullerenes or *metallofullerenes* that subsequently convert to pristine or metal-filled *double-wall nanotubes*. Filling of existing *nanotubes* precludes *opening* their closed ends and may be understood as *capillary filling*.

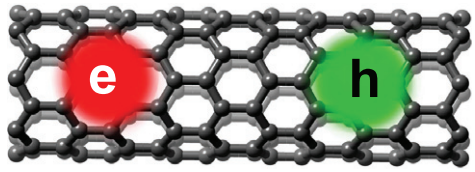


**Figure 31.** Schematic visualization of a bound electron–hole (e–h) pair, called an *exciton*, in a *nanotube*.

***References***

Saito Y 1995 Nanoparticles and filled nanocapsules *Carbon* **33** 979

Seraphin S, Zhou D and Jiao J 1996 Filling the carbon nanocages *J. Appl. Phys.* **80** 2097

Kitaura R, Imazu N, Kobayashi K and Shinohara H 2010 Fabrication of metal nanowires in carbon nanotubes via versatile nano-template reaction *Nano Lett.* **8** 693

**Foam** is a porous 3D structure consisting predominantly of $sp^2$ bonded carbon atoms. Mostly hypothetical foam structures are predicted to combine unusual electronic structure with favorable *mechanical properties*. Rigid networks of polymerized *fullerenes* and *schwarzites* may be considered special cases of a foam structure.

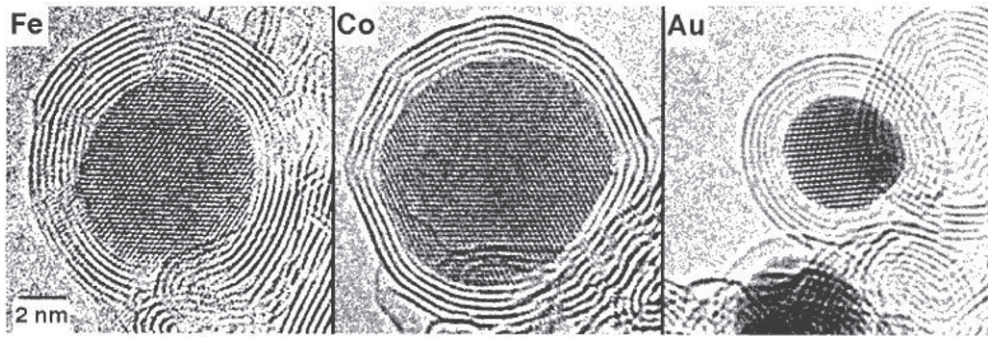


**Figure 32.** *Transmission electron microscopy* images of iron, cobalt and gold nanocrystals encapsulated inside a carbon *onion* under electron irradiation at high specimen temperature. (Adapted from Banhart F 1999 *Rep. Prog. Phys.* **62** 1181, © 1999 Institute of Physics.)

***Reference***

Zhu Z and Tománek D 2012 Formation and stability of cellular carbon foam structures: an ab initio study *Phys. Rev. Lett.* **109** 135501

**Folded graphene nanoribbon** is a structure consisting of a contiguous *graphene nanoribbon* (GNR) with one or more layers that appear to have been folded to form looped edges, as seen in figure 33. The edge structure is closely related to that of a *ribbon* formed of a collapsed *nanotube* with a wide *diameter*.

***Reference***

Lopez-Bezanilla A, Campos-Delgado J, Sumpter B G, Baptista D L, Hayashi T, Kim Y A, Muramatsu H, Endo M, Achete C A, Terrones M and Meunier V 2012 Geometric and electronic structure of closed graphene edges *J. Phys. Chem. Lett.* **3** 2097

The **Fowler–Nordheim** relationship describes the electron emission from a surface normal to which a strong local electric field $E$ has been applied. The tunneling electron current density is given by

$$J = aE^2 \exp\left(-\frac{b\Phi^{3/2}}{\beta E}\right),$$

where $\Phi$ is the *work function*, $a$ and $b$ are constants, and $\beta$ is the field amplification factor. For a sparse array of vertically aligned *nanotubes* of *radius* $r$ and height $h$, the large value of $\beta = h/r$ contributes significantly to high observed current densities $J \lesssim 10^9$ A cm$^{-2}$, which correspond to currents of $\lesssim 1\ \mu$A per nanotube.

The **fractional quantum Hall effect** → *quantum Hall effect*

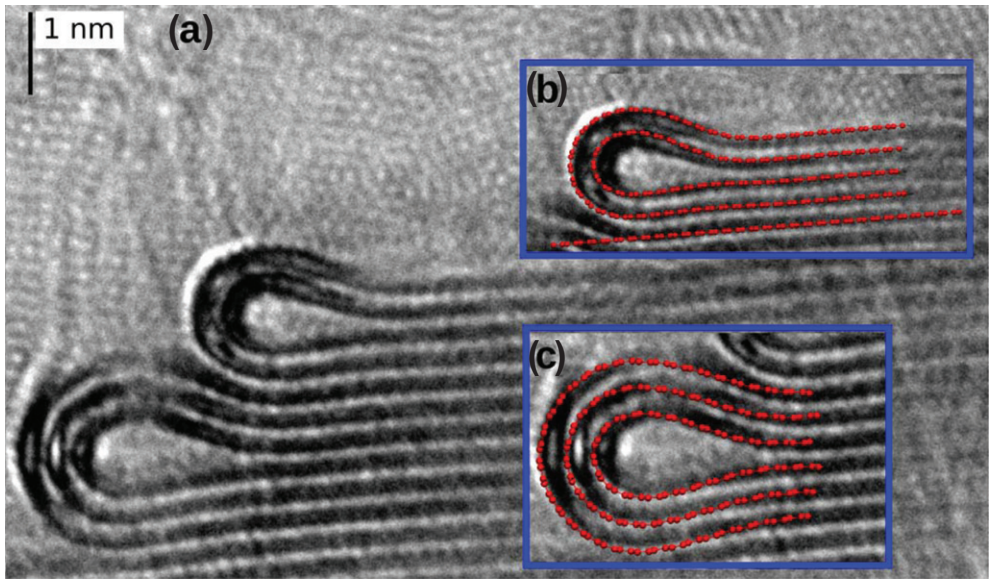


**Figure 33.** (a) High-resolution *transmission electron microscopy* image of *folded graphene nanoribbons* with two or three layers. Superposition of the image (a) and calculated equilibrium structure in the folded region is shown in (b) and (c). (Adapted from Lopez-Bezanilla A *et al* 2012 *J. Phys. Chem. Lett.* **3** 2097, © 2012 American Chemical Society.)

A **fullerene** is a molecule with a hollow *cage* structure consisting of *graphitic* carbon. The name reflects structural relationship to geodesic *domes* constructed by the architect Richard Buckminster Fuller. The most noted fullerene is the $C_{60}$ molecule, called also *buckminsterfullerene* or simply *buckyball*. The smallest fullerene is the $C_{20}$. Among the possible *fullerene synthesis* routes, *arc evaporation* is most common. Selected fullerenes with less than 100 carbon atoms are shown in figure 34. Larger fullerenes, such as the one shown in figure 35, have not been observed as single-wall structures, but may form

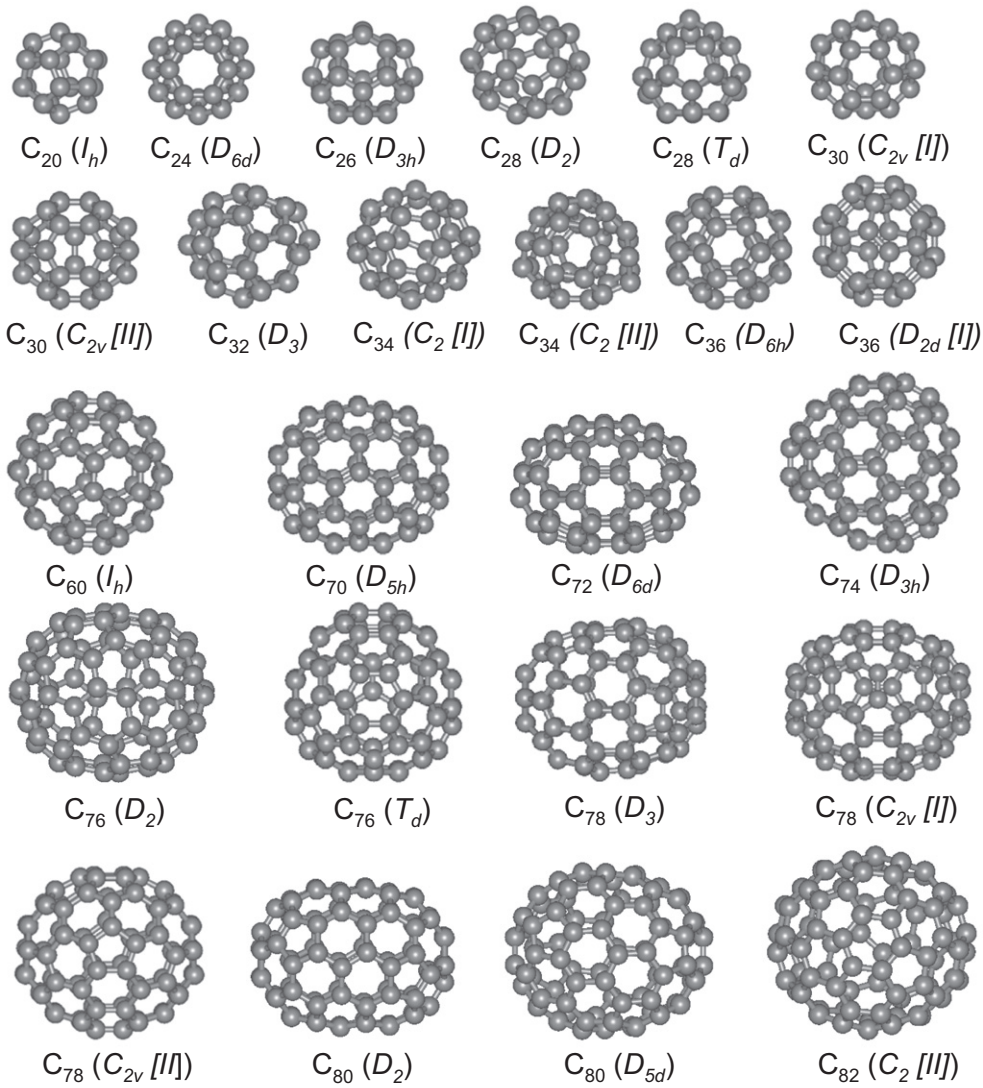


**Figure 34.** Structural models of selected $C_n$ *fullerenes* with $n < 100$ atoms. Most stable *isomers* with $n \geq 60$ atoms comply with the *isolated pentagon rule* (IPR).

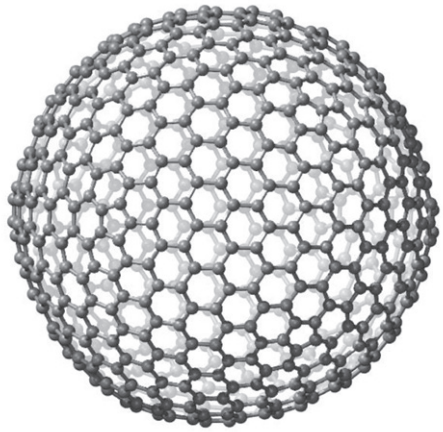

**Figure 35.** Structure of a very large $C_{720}$ *fullerene*, which may form a wall in an *onion*, shown schematically in figure 67.

walls in multi-wall fullerenes, called *onions*. The time line of fullerene discoveries is listed in table 1.

***Reference***

Fowler P W and Manolopoulos D E 2006 An atlas of fullerenes *Dover*

A **fullerene isomer** is a well-defined structure of a *fullerene*. The number of *isomers*, corresponding to the number of ways to distribute 12 pentagons and $n/2-10$ hexagons on a $C_n$ surface, increases rapidly with the size $n$.

**Fullerene separation** from soot containing a mixture of *fullerene* and *metallofullerene* molecules with different sizes can be achieved efficiently by high-pressure liquid chromatography (HPLC) with suitable columns, such as the 'buckyclutcher' or 'buckyprep' columns.

***References***

Shinohara H, Yamaguchi H, Hayashi N, Sato H, Ohkohchi M, Ando Y and Saito Y 1993 Isolation and spectroscopic properties of $Sc_2@C_{74}$, $Sc_2@C_{82}$, and $Sc_2@C_{84}$ *J. Phys. Chem.* **97** 4259

Shinohara H 2000 Endohedral metallofullerenes *Rep. Prog. Phys.* **63** 843

**Fullerene synthesis** can be achieved by high-temperature processes such as *pulsed laser vaporization* (PLV) or, most commonly, *arc evaporation* (AE). A low-temperature *wet chemical synthesis* of $C_{60}$ has also been achieved.

**Fullerite** → *solid $C_{60}$*

**Functionalization** is a common way to modify the properties, particularly the *fundamental band gap* and conductivity, of carbon nanostructures including *fullerenes* and *nanotubes* by covalent or non-covalent attachment of atoms, radicals and molecules. End-functionalization of open-ended nanotubes typically involves strong covalent bonds, whereas sidewall functionalization involves weaker adsorption bonds and is often reversible. Examples are attachment of H and F atoms or silyl radicals to fullerenes and nanotube sidewalls. Non-covalent sidewall functionalization occurs when nanotubes are exposed to *surfactants*, such as sodium dodecyl sulphate (SDS) to facilitate their *dispersion* in a solvent. Polymer molecules, including bio-polymers such as single-stranded DNA, bind weakly to *graphitic* systems through $p_\pi$–$p_\pi$ interactions. Their propensity to wrap around the nanotube is used to separate individual nanotubes from *ropes* and for *sorting of nanotubes*.

***References***

Dettlaff-Weglikowska U, Skákalová V, Graupner R, Jhang S H, Kim B H, Kim M-G, Ley L, Park Y W, Berber S, Tománek D and Roth S 2005 Effect of $SOCl_2$ treatment on electrical and mechanical properties of

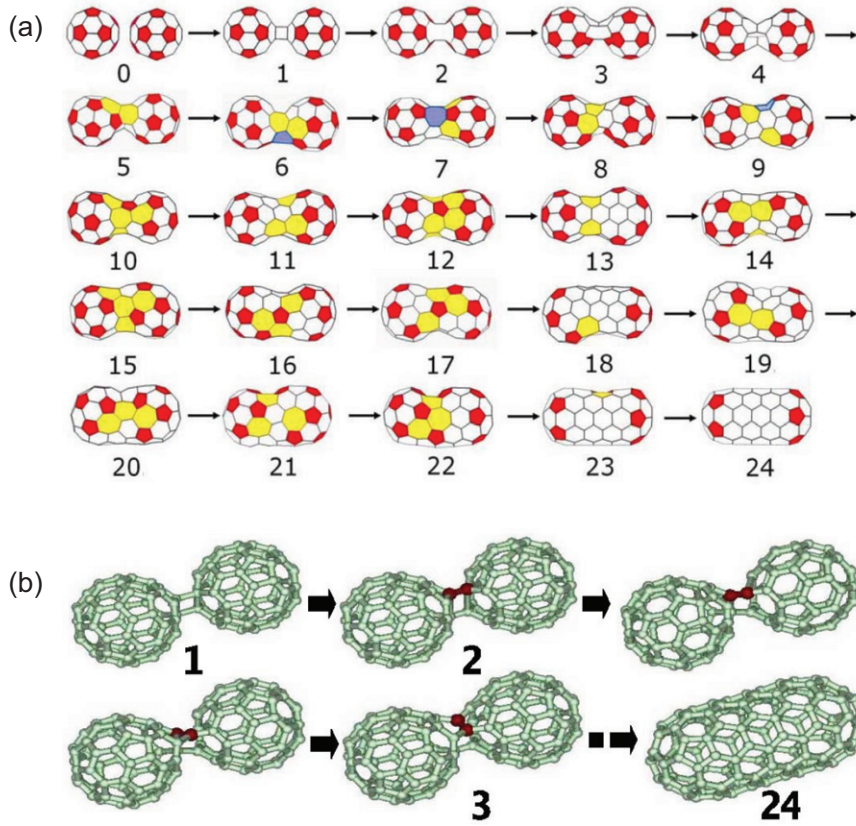


**Figure 36.** Microscopic mechanism of the *fusion of fullerenes* that may occur in *peapods*, as seen in figure 37. (a) Optimum pathway for the $2C_{60} \rightarrow C_{120}$ fusion reaction starting with a 2+2 *cycloaddition* and involving the smallest number of generalized *Stone–Wales transformations*. (b) Snapshots of selected optimized structures. (From Seungwu Han *et al* 2004 *Phys. Rev.* B **70** 113402, © 2004 American Physical Society.)

single wall carbon nanotube networks *J. Am. Chem. Soc.* **127** 5125

Chang K, Berber S and Tománek D 2008 Transforming carbon nanotubes by silylation: An *ab initio* study *Phys. Rev. Lett.* **100** 236102

The **fundamental band gap** $E_g$, often referred to as 'band gap' or 'HOMO-LUMO gap', spans the energy range between the highest occupied state (top of the valence band in semiconductors or the highest occupied molecular orbital, HOMO) and the lowest unoccupied state (bottom of the conduction band in semiconductors or the lowest unoccupied molecular orbital, LUMO). In semiconducting carbon nanostructures, $E_g$ ranges from zero in semi-metallic *graphene* to 5.5 eV in *diamond*.

The **fusion of fullerenes** may occur by a sequence of *Stone–Wales transformations*. Detailed structural changes during the fusion of two *$C_{60}$ fullerenes* to a $C_{120}$ *capsule* are depicted in figure 36. *Transmission electron microscopy* (TEM) images of fullerene fusion to a capsule inside a *peapod* are shown in figure 37.

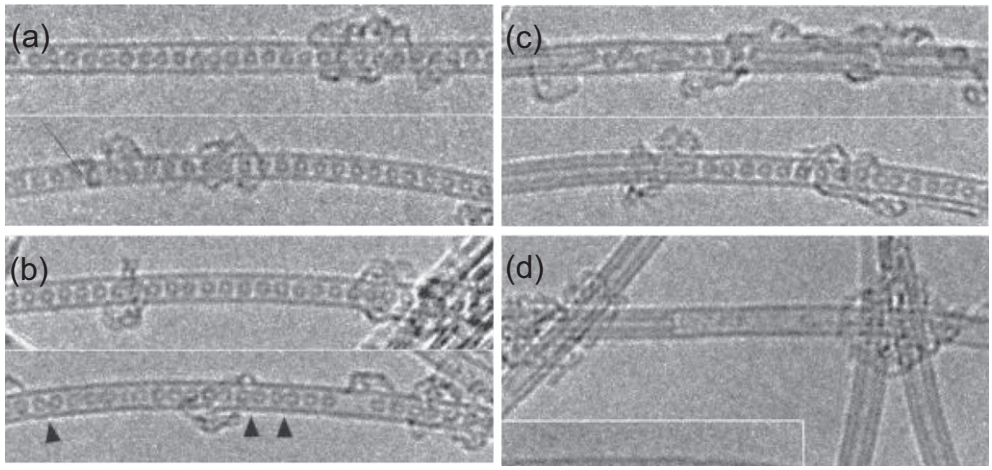


**Figure 37.** Time sequence of high-resolution *transmission electron microscopy* images of the *fusion of fullerenes* inside a *single-wall nanotube*. The images have been accumulated over many hours of observation, while the *peapods* have been heated in vacuum to temperatures between 800 and 1200°C. The onset of fusion at 800°C is indicated by black arrows in (b). Progressive fusion at 1000°C is seen clearly in (c). The completion of the conversion process from *fullerenes* to a long *capsule* at 1200°C is seen in (d). (Adapted from Bandow S *et al* 2001 *Chem. Phys. Lett.* **337** 48, © 2001 Elsevier.)

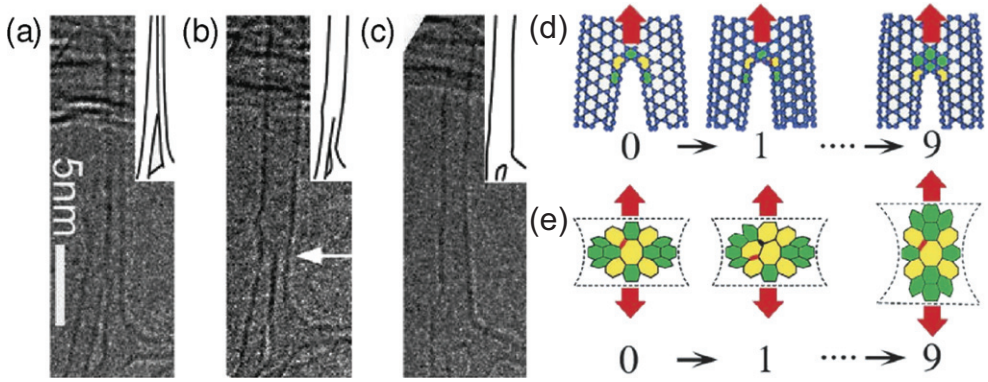


**Figure 38.** Microscopic mechanism of the *fusion of nanotubes*. (a)–(c) Time sequence of *transmission electron microscopy* observations of a transforming *Y*-junction of *single-wall nanotubes*. Selected steps within a possible sequence of generalized *Stone–Wales transformations* constituting this process are shown in (d) by ball-and-stick models and in (e) by corresponding *Schlegel diagrams*. (Adapted from Yoon M *et al* 2004 *Phys. Rev. Lett.* **92** 075504, © 2004 American Physical Society.)

***References***

Ueno H, Osawa S, Osawa E and Takeuchi K 1998 Stone-Wales rearrangement pathways from the hinge-opened [2+2] C-60 dimer to IPR C-120 fullerenes. Vibrational analysis of intermediates *Fullerene Sci. Technol.* **6** 319

Han S, Yoon M, Berber S, Park N, Osawa E, Ihm J and Tománek D 2004 Microscopic mechanism of fullerene fusion *Phys. Rev.* B **70** 113402

The **fusion of nanotubes**, shown in figure 38, may occur in a 'zipper mechanism' in

analogy to the *fusion of fullerenes* as a sequence of generalized *Stone–Wales transformations*.

***Reference***

Yoon M, Han S, Kim G, Lee S, Berber S, Osawa E, Ihm J, Terrones M, Banhart F, Charlier J-C, Grobert N, Terrones H, Ajayan P M and Tománek D 2004 The zipper mechanism of nanotube fusion: Theory and Experiment *Phys. Rev. Lett.* **92** 075504

# G

The ***G*-band** is a *Raman-active* spectroscopic band associated with high-frequency vibrations near 1600 $cm^{-1}$ in *graphitic* carbon nanostructures (see figure 77). In *single-wall nanotubes* the *G*-band splits into a $G^+$ mode at $\approx$1590 $cm^{-1}$ and a $G^-$ mode at $\approx$1570 $cm^{-1}$. The $G^-$ line shape allows one to distinguish between metallic and semiconducting nanotubes. Metallic nanotubes exhibit an additional band at $\approx$1550 $cm^{-1}$, which originates from the coupling of the electronic continuum to in-plane atomic vibrations and can be fitted with a Breit–Wigner–Fano (BWF) line shape.

***References***

Ferrari A C, Meyer J C, Scardaci V, Casiraghi C, Lazzeri M, Mauri F, Piscanec S, Jiang D, Novoselov K S, Roth S and Geim A K 2006 Raman spectrum of graphene and graphene layers *Phys. Rev. Lett.* **97** 187401

Zhao J, Jiang C, Fan Y, Burghard M, Thomas B and Mews A 2002 Diameter-dependent combination modes in individual single-walled carbon nanotubes *Nano Lett.* **2** 823

**Gaussian curvature** is a parameter used to characterize the local morphology at nanocarbon surfaces. Its value is given by $K = \kappa_1\kappa_2$, where $\kappa_1$ and $\kappa_2$ are the principal curvatures at that point. Positive Gaussian curvature occurs in convex structures such as a sphere or an ellipsoid, and is introduced by pentagons or lower polygons in a plane tiled by hexagons. Negative Gaussian curvature occurs at saddle-points or in hyperboloids and is introduced by heptagons or higher polygons in a plane tiled by hexagons. A plane or the surface of a cylinder has zero Gaussian curvature. *Fullerenes* have a positive Gaussian curvature, *graphene* and *nanotubes* have zero Gaussian curvature, and *schwarzites* have a negative Gaussian curvature.

**GIC** → *graphite intercalation compound*

**GNR** → *graphene nanoribbon*

**Graphane** is a hydrogenated *graphene* monolayer with the chemical formula $(CH)_n$, where $n$ is large. Covalent C–H bonds convert the $sp^2$ bonding character of graphene to $sp^3$ character, thereby opening a *fundamental band gap*.

***Reference***

Elias D C, Nair R R, Mohiuddin T M G, Morozov S V, Blake P, Halsall M P, Ferrari A C, Boukhvalov D W, Katsnelson M I, Geim A K and Novoselov K S 2009 Control of graphene's properties by reversible hydrogenation: evidence for graphane *Science* **323** 610

**Graphene**, also called monolayer graphene (MLG), is a monolayer of *graphite*. The planar structure is tiled by hexagons with carbon atoms at the vertices, so that each carbon atom has three co-planar nearest neighbors (see figure 39). The interatomic distance in

graphene is $d_{CC} = 0.142$ nm. The Bravais lattice underlying the honeycomb lattice of graphene is spanned by lattice vectors $\mathbf{a_1}$ and $\mathbf{a_2}$, closing an angle of 60°, with $a = |\mathbf{a_1}| = |\mathbf{a_2}| = 0.246$ nm defining the *lattice constant*. The rhombic primitive unit cell and the hexagonal *Wigner–Seitz cell* with the full symmetry of the lattice, shown by the shaded areas in figure 39, contain two atoms and have the same area of $A = 0.0524$ nm$^2$. The time line of graphene discoveries is listed in table 3.

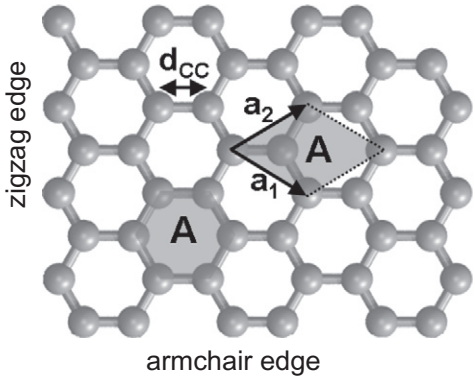


**Figure 39.** Structure of a *graphene* monolayer, spanned by the basis vectors $a_1$ and $a_2$. $A$ is the area of the unit cell.

The **graphene electronic band structure** describes the dispersion of electronic quantum states as a function of the electron momentum $(k_x, k_y)$. Electronic states near the Fermi level $E_F$ that are most important for electric *conductance* are shown schematically in figure 40 and are represented in the *Hückel molecular orbital method* by

$$E(k_x, k_y) = E_F \pm \gamma_0 \times \left[1 + 4\cos\left(\frac{k_x a}{2}\right)\cos\left(\frac{\sqrt{3}k_y a}{2}\right) + 4\cos^2\left(\frac{k_x a}{2}\right)\right]^{1/2},$$

where $\gamma_0 \approx -2.9$ eV is the nearest-neighbor hopping integral and $a = 0.246$ nm is the *lattice constant*. The six corners of the hexagonal *Brillouin zone*, labelled by the letters K and K′ (see figure 5), form the Fermi surface and are the *Dirac points* in this semi-metal with zero *fundamental band gap* and vanishing *electronic density of states* at $E_F$.

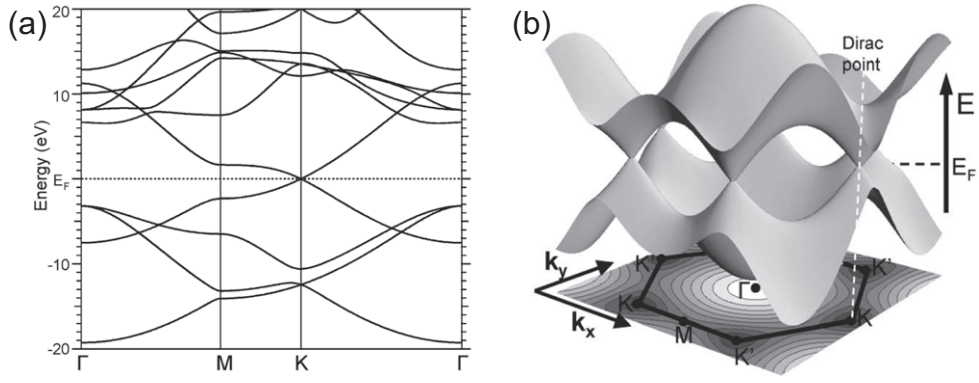


**Figure 40.** *Electronic band structure* of a *graphene* monolayer (a) along high-symmetry lines and (b) across the entire *Brillouin zone*, delimited by the solid black lines in the plane. See table 10 for the high-symmetry points of the Brillouin zone.

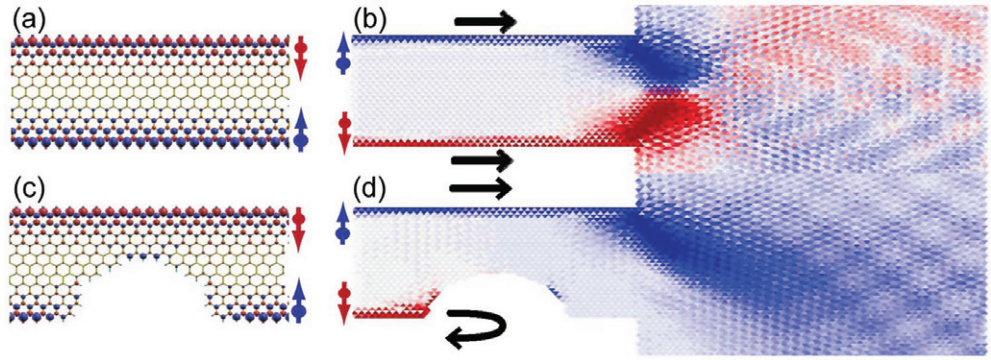


**Figure 41.** Ground state distribution of electron spins and transport in *graphene nanoribbons* (GNRs) with a *zigzag edge*. (a) Electrons associated with *edge states* carry opposite spin on opposite sides of the GNR. (b) Due to the balance of opposite spins carried along a defect-free edge, no net spin is injected in the *graphene* lead on the right. Edge *defects* do not modify spin distribution (c), but can block individual spin conduction channels (d), causing spin polarization of the current entering the graphene lead on the right. (Adapted following Wimmer M *et al* 2008 *Phys. Rev. Lett.* **100** 177207, © 2008 American Physical Society.)

A **graphene nanoribbon** (GNR) is a narrow strip of *graphene*. *Graphene nanoribbon morphology* differs from that of a *ribbon* formed from a collapsed *nanotube*, where all atoms maintain their three-fold coordination. Similar to nanotubes, quantum confinement perpendicular to the GNR axis causes significant changes in the *graphene nanoribbon electronic band structure*. Depending on the edge morphology and the width, graphene nanoribbons may be metallic, semimetallic or semiconducting. Electronic transport in metallic GNRs is dominated by the current along the edge and depends strongly on the edge morphology, in particular the presence of *defects* (see figure 41).

***References***

Barone V, Hod O and Scuseria G E 2006 Electronic structure and stability of semiconducting graphene nanoribbons *Nano Lett.* **6** 2748

Wimmer M, Adagideli I, Berber S, Tománek D and Richter K 2008 Spin transport in rough graphene nanoribbons *Phys. Rev. Lett.* **100** 177207

The **graphene nanoribbon electronic band structure** depends on the *graphene nanoribbon morphology*, illustrated in figure 42, and is dominated by *edge states*. *Zigzag nanoribbons* (ZGNRs) display a sharp peak in the *electronic density of states* at the Fermi level, which is caused by a flat band characteristic of the *zigzag edge* of *graphene* and leads to a net spin polarization of the edge. A small *fundamental band gap* opens up due to the antiferromagnetic coupling between the two spin-polarized edges. Calculations using the *Hückel molecular orbital method* suggest that *armchair nanoribbons* (AGNRs) can be either semimetallic or semiconducting. An $N$-AGNR with $N$ linear rows of atoms, as shown in figure 42(b), is semimetallic if $N = 3p + 2$, with $p$ an integer, and semiconducting otherwise. The *fundamental band gap* in semiconducting AGNRs scales approximately as $E_{\text{gap}}(N\text{-AGNR}) = 0.9\ \text{eV}\ \ \text{nm}/W$, where $W$ denotes the GNR width. GNRs with *Klein edges* are always semiconducting.

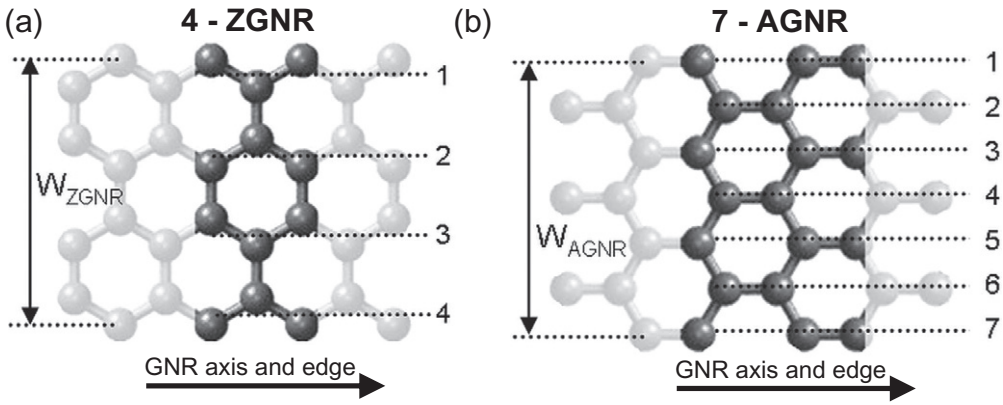


**Figure 42.** Schematic representation of the *graphene nanoribbon morphology*. (a) A *zigzag nanoribbon* with 4 zigzag rows of atoms (4-ZGNR) and (b) an *armchair nanoribbon* with 7 linear rows of atoms (7-AGNR). Both nanoribbons have the *eclipsed edge configuration*.

***References***

Nakada K, Fujita M, Dresselhaus G and Dresselhaus M S 1996 Edge state in graphene ribbons: Nanometer size effect and edge shape dependence *Phys. Rev.* B **54** 17954

Son Y-W, Cohen M L and Louie S G 2006 Energy gaps in graphene nanoribbons *Phys. Rev. Lett.* **97** 216803 2007 *ibid.* **98** 089901(E)

Han M Y, Özyilmaz B, Zhang Y and Kim P 2007 Energy band-gap engineering of graphene nanoribbons *Phys. Rev. Lett.* **98** 206805

Tao C, Jiao L, Yazyev O V, Chen Y-C, Feng J, Zhang X, Capaz R B, Tour J M, Zettl A, Louie S G, Dai H and Crommie M F 2011 Spatially resolving edge states of chiral graphene nanoribbons *Nat. Physics* **7** 616

**Graphene nanoribbon morphology** is determined by edge morphology and the width $W_{\mathrm{GNR}}$. The parallel *graphene nanoribbon* (GNR) edges are characterized by the direction of the *chiral vector* on a *graphene* plane. In analogy to carbon *nanotubes*, the morphology of GNRs is characterized by the *chiral index* $(n, m)$ defining the edge translation vector and classified as either armchair, zigzag or chiral. The width of a *zigzag nanoribbon* with $N$ zigzag rows of atoms ($n$-ZGNR), shown in figure 42(a), is $W_{\mathrm{ZGNR}} = (0.213N - 0.142)$ nm. The width of an *armchair nanoribbon* with $N$ linear rows of atoms ($n$-AGNR), shown in figure 42(b), is $W_{\mathrm{AGNR}} = (N - 1)\ 0.213$ nm. Depending on the value of $N$, the edges can have the *eclipsed edge configuration* or the *staggered edge configuration*, depicted in figure 27.

**Graphene nanoribbon synthesis** involves lithography of pre-formed *graphene* monolayers, or can be achieved by *chemical vapor deposition* (CVD). *Graphene nanoribbons* (GNRs) with uniform width can be formed by chemical unzipping of carbon *nanotubes* along their axis, as illustrated in figure 43.

***References***

Kosynkin D V, Higginbotham A L, Sinitskii A, Lomeda J R, Dimiev A, Katherine P B and Tour J M 2009 Longitudinal unzipping of carbon nanotubes to form graphene nanoribbons *Nature* **458** 872

Jiao L, Zhang L, Wang X, Diankov G and Dai H 2009 Narrow graphene nanoribbons from carbon nanotubes *Nature* **458** 877

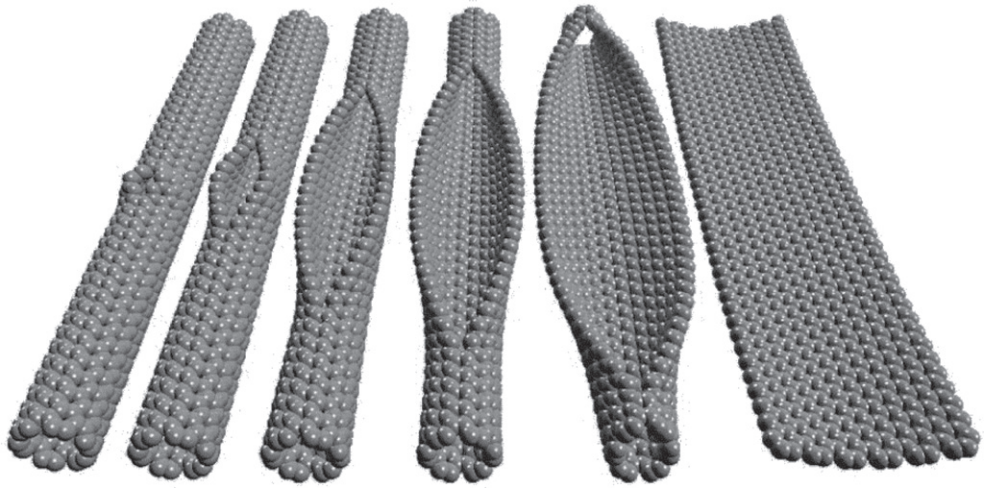

**Figure 43.** Idealized representation of the gradual unzipping of a carbon *nanotube* wall to a *graphene nanoribbon* (GNR). Oxygenated sites are not shown. (Adapted from Kosynkin D V *et al* 2009 *Nature* **458** 872, © 2009 Nature Publishing Group.)

Campos-Delgado J, Romo-Herrera J M, Jia X, Cullen D A, Muramatsu H, Kim Y A, Hayashi T, Ren Z, Smith D J, Okuno Y, Ohba T, Kanoh K, Kaneko K, Endo M, Terrones H, Dresselhaus M S and Terrones M 2008 Bulk production of a new form of $sp^2$ carbon: crystalline graphene nanoribbons *Nano Lett.* **8** 2773

Tapasztó L, Dobrik G, Lambin P and Biró L P 2008 Tailoring the atomic structure of graphene nanoribbons by scanning tunnelling microscope lithography *Nature Nanotechnol.* **3** 397

**Graphene strip** → *graphene nanoribbon* (GNR)

**Graphene synthesis** techniques include mechanical *exfoliation* of *graphite* by the 'scotch tape' technique, chemical exfoliation of graphite, high-temperature precipitation at the surface of silicon carbide or *chemical vapor deposition* (CVD) on a metal substrate.

***References***

Acheson E G 1907 Deflocculated graphite *J. Frankl. Inst.* **164** 375

Berger C, Song Z, Li T, Li X, Ogbazghi A Y, Feng R, Dai Z, Marchenkov A N, Conrad E H, First P N and de Heer W A 2004 Ultrathin epitaxial graphite: 2D electron gas properties and a route toward graphene-based nanoelectronics *J. Phys. Chem.* B **108** 19912

Novoselov K S, Jiang D, Schedin F, Booth T J, Khotkevich V V, Morozov S V and Geim A K 2005 Two-dimensional atomic crystals *Proc. Natl. Acad. Sci.* **102** 10451

Bae S, Kim H, Lee Y, Xu X, Park J-S, Zheng Y, Balakrishnan J, Lei T, Kim H R, Song Y L, Kim Y-J, Kim K S, Özyilmaz B, Ahn J-H, Hong B H and Iijima S 2010 Roll-to-roll production of 30-inch graphene films for transparent electrodes *Nature Nanotech.* **5** 574

**Graphite** is the most abundant and stable form of elemental carbon, displaying a large *binding energy* of $E_{coh}/n = 7.43$ eV/atom. The layered structure of graphite consists of *graphene*

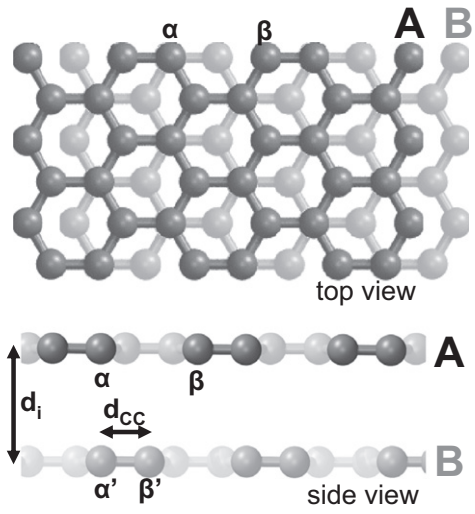


**Figure 44.** Schematic view of the *hexagonal graphite* structure with AB layer stacking.

layers separated by $d_i = 0.34$ nm and held together by weak *inter-layer interactions*. Most common forms for graphite exhibit hexagonal (AB; see figure 44) and rhombohedral (ABC) stacking of adjacent layers. In the unit cell of the dominant *hexagonal graphite* structure, containing four atoms in two layers, $\alpha$ atoms with neighbors in the adjacent layer are inequivalent to $\beta$ atoms with neighbors in every other layer (see figure 44). The unit cell of *rhombohedral graphite* contains two atoms in one layer.

**Graphite binding** is strongly anisotropic in its nature. It consists of strong in-plane $\sigma$ bonds providing the rigid network of $sp^2$ hybrid orbitals within a *graphene* layer with a large *binding energy* of $E_{coh} = 7.37$ eV/atom, and of weak inter-layer bonds. These inter-layer bonds contribute only 0.06 eV/atom, the *exfoliation* energy, to the binding energy of *graphite*. The *inter-layer interaction* consists partly of very weak covalent bonds, which are responsible for the preferential stacking of layers, and a van der Waals attraction. The covalent interaction is caused by the weak pp $\sigma$ bond between atoms in the $\alpha$ *sublattice*, which have neighbors above and below in neighboring layers, as illustrated in figure 44. Atoms in the $\beta$ sublattice, which have no such neighbors, display a very different *electronic band structure* from atoms in the $\alpha$ sublattice, as seen in figure 45(b).

***References***

Zacharia R, Ulbricht H and Hertel T 2004 Interlayer cohesive energy of graphite from thermal desorption of polyaromatic hydrocarbons *Phys. Rev.* B **69** 155406

Spanu L, Sorella S and Galli G 2009 Nature and strength of interlayer binding in graphite *Phys. Rev. Lett.* **103** 196401

**Graphite electronic band structure** describes the dispersion of electronic quantum states $E(k)$ as a function of the electron momentum **k**, as shown in figure 45. It is closely related to *graphene electronic band structure*. The weak *inter-layer interaction* removes the equivalence between the $\alpha$ and $\beta$ atoms in the 4-atom unit cell (see figure 44). The band dispersion along the K–H line normal to the layers gives rise to a nonzero *electronic density of states* at the Fermi level, as seen in figures 45(b) and 45(c).

A **graphite intercalation compound** (GIC) is a *graphite*-based structure containing a substance (typically metal atoms) intercalated in between the layers. The observed inhomogeneous distribution of intercalants is characterized as *staging* and illustrated in figure 87.

**Graphitic** structures are layered carbon structures with atoms arranged in a similar way as in *graphene*.

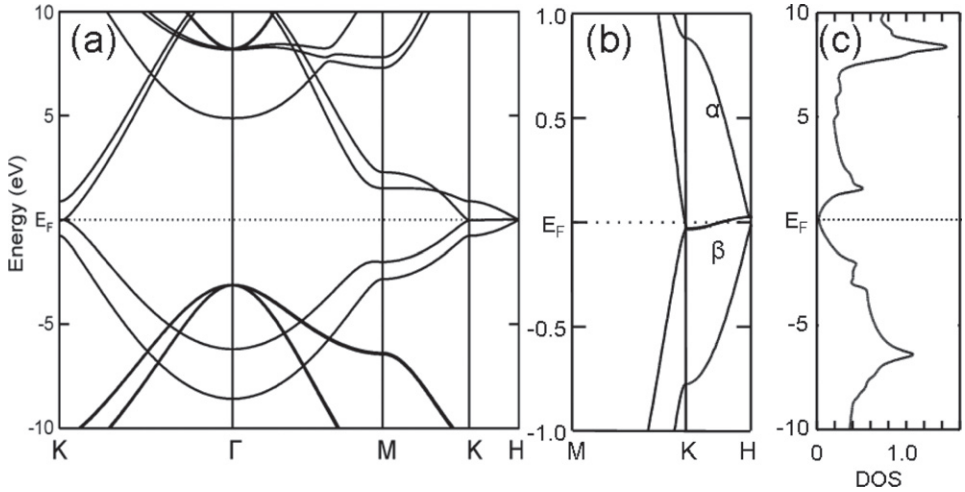


**Figure 45.** (a) *Graphite electronic band structure* along high-symmetry lines in the *Brillouin zone*, shown in figure 5. (b) Representation on an expanded energy scale, depicting differences in the band dispersion between the $\alpha$ and $\beta$ *sublattices* (see figure 44) along the K–H line near the Fermi level. (c) *Electronic density of states* of *graphite*.

**Graphitization** is the solid-state transformation of thermodynamically unstable non-graphitic carbon into *graphitic* material by heat treatment. Graphitization is completed at $T \approx 2500$ K.

**Gravimetric density** for carbon structures ranges from $\rho = 2.27$ g cm$^{-3}$ for *graphite* to $\rho = 3.54$ g cm$^{-3}$ for *diamond*. The gravimetric density of *fullerenes* and *nanotubes* depends on their packing structure, but is close to the graphite value due to the similar value of the *inter-layer distance* $d_i \approx 0.34$ nm in all *graphitic* structures.

The **growth process** of carbon nanostructures and their resulting shape depends sensitively on the carbon feedstock (carbon-containing substance), its concentration, other elements present including carrier gas and catalytically active substances, temperature, local environment including existing template structures, and specific conditions including deviation from thermal equilibrium. Optimized conditions have been developed for *fullerene synthesis*, *nanohorn synthesis*, *nanotube synthesis*, *graphene synthesis*, and *graphene nanoribbon synthesis*. Insight into the microscopic growth mechanism, including *catalytic growth*, may be provided by *molecular dynamics* (MD) simulations, illustrated in figure 58. Schematic growth process of *fullerenes* and *nanotubes* is illustrated in figure 46.

# H

**Haeckelite** is a planar $sp^2$ bonded carbon structure containing not just hexagonal carbon rings, as shown in figure 47. A large number of possible haeckelite structures results from the possibility of arranging atoms to form squares, pentagonal, heptagonal and octagonal rings in different ways. Haeckelite structures are less stable than *graphene* but may interconnect graphene flakes growing on a substrate.

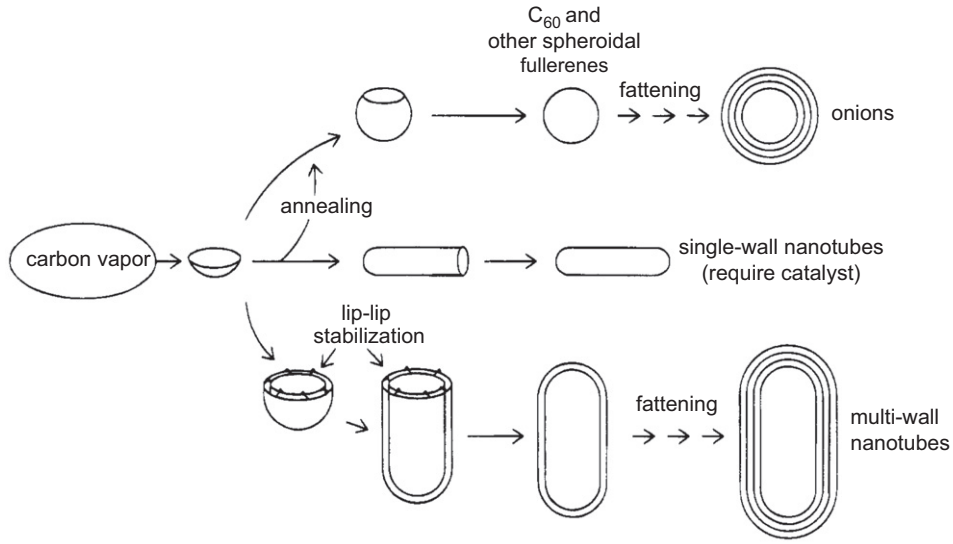


**Figure 46.** Schematic *growth process* of *fullerenes* and *nanotubes* with single or multiple walls from carbon vapor at very high temperatures. Branching occurs following nucleation of a *graphene* flake with a pentagonal *defect*. Single-wall *fullerenes* form and eventually fatten to *onions* at low carbon densities (upper branch). *Multi-wall nanotubes*, stabilized by *lip–lip interactions*, form at high carbon densities. The presence of a *catalyst* is needed to prevent premature *dome* closure of *single-wall nanotubes*. (Adapted from Guo T *et al* 1995 *J. Phys. Chem.* **99** 10694, © 1995 American Chemical Society.)

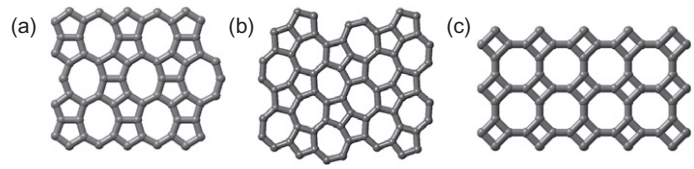


**Figure 47.** Structural models of *haeckelites* consisting of carbon forming (a) pentagons and octagons, (b) pentagons and heptagons, and (c) octagons and squares.

In analogy to 3D structures including *fullerenes*, *nanotubes* and *schwarzites*, which are based on the structural motif of planar *graphene*, similar 3D structural counterparts of haeckelites have been postulated, including fullerenes and nanotubes containing a large fraction of non-hexagonal rings.

***Reference***

Terrones H, Terrones M, Hernández E, Grobert N, Charlier J-C and Ajayan P M 2000 New metallic allotropes of planar and tubular carbon *Phys. Rev. Lett.* **84** 1716

**Handedness** is the property of a *nanotube* that depends on its *chiral index* ($n$, $m$) and, to a lesser degree, on the nanotube edge, as illustrated in figure 48. For each left-handed ($n$, $m$) nanotube there is an equally stable right-handed ($m$, $n$) counterpart. *Achiral zigzag nanotubes* and *armchair nanotubes* do not possess handedness.

***References***

Liu Z, Suenaga K, Yoshida H, Sugai T, Shinohara H and Iijima S 2005 Determination of optical isomers for left-handed

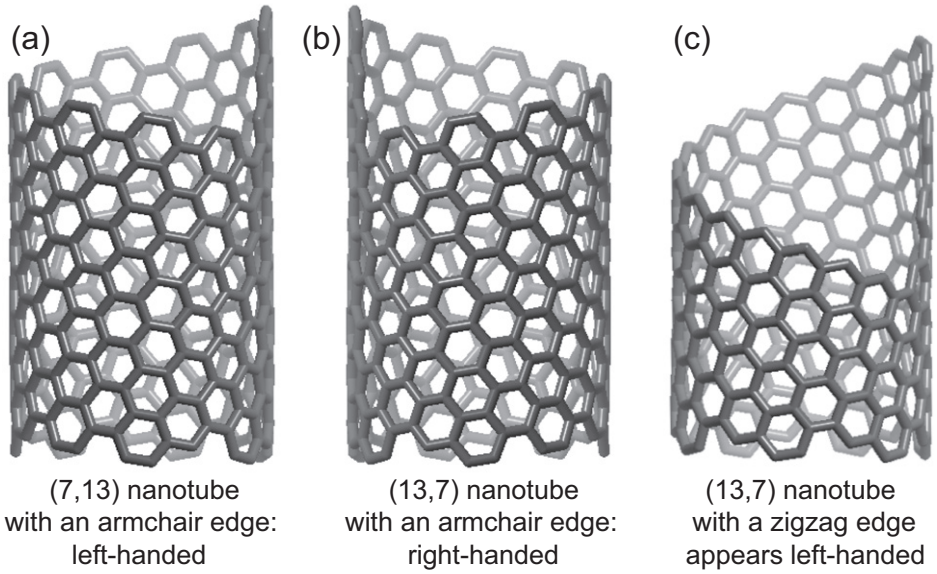


**Figure 48.** (a) A left-handed (7, 13) and (b) a right-handed (13, 7) *nanotube* with an *armchair edge* forming a helix. (c) The same (13, 7) nanotube with a *zigzag edge* forming a helix appears to be left-handed.

or right-handed chiral double-wall carbon nanotubes *Phys. Rev. Lett.* **95** 187406

Samsonidze G G, Grüuneis A, Saito R, Jorio A, Souza Filho A G, Dresselhaus G and Dresselhaus M S 2004 Interband optical transitions in left- and right-handed single-wall carbon nanotubes *Phys. Rev.* B **69** 205402

**Heat capacity** → *specific heat*

**Helical nanotubes**, also called coils or nanocoils and shown in figure 49, differ from *chiral nanotubes* by not having a straight axis. Helical *nanotubes* form under specific conditions during *catalytic growth* in the *chemical vapor deposition* (CVD) process. Carbon feedstock is typically acetylene and ethylene, and catalytic particles include cobalt and iron-coated indium tin oxide. The typical growth temperature of helical nanotubes is around 700°C, significantly lower than used for straight nanotubes. Spontaneous coiling in *helical ropes* occurs in *ropes* containing *nanotubes* with different *chiral indices*.

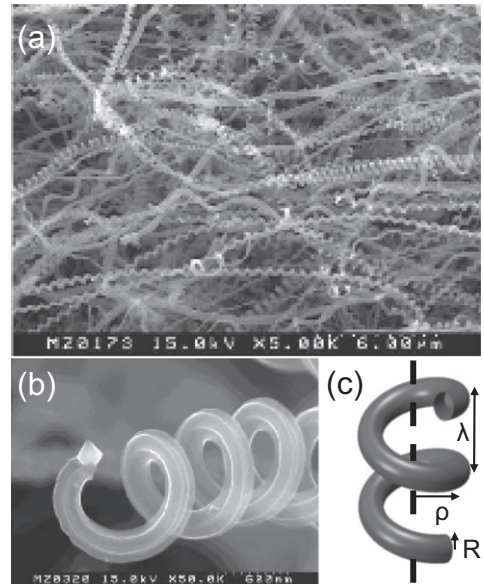


**Figure 49.** (a), (b) *Scanning electron microscopy* (SEM) images of *helical nanotubes*, adapted from Zhang M *et al* 2000 *Japan J. Appl. Phys.* **39** L1242, © 2000 The Japan Society of Applied Physics. Each nanotube helix grows with its own diameter $\rho$ and pitch length $\lambda$, defined in (c).

***References***

Bernaerts D, Zhang X B, Zhang X F, Amelinckx S, Van Tendeloo G, Van Landuyt J, Ivanovd V and Nagy J B 1995 Electron microscopy study of coiled carbon tubules *Phil. Mag.* A **71** 605

Zhang M, Nakayama Y and Pan L 2000 Synthesis of carbon tubule nanocoils in high yield using iron-coated indium tin oxide as catalyst *Japan. J. Appl. Phys.* **39** L1242

**Helical ropes** are *ropes* of mostly *single-wall nanotubes* with a helical pitch. Spontaneous coiling occurs in ropes containing *nanotubes* with different *chiral indices*. *Nanotube yarn*, shown in figure 66, is formed by twisting a nanotube rope. As shown in figure 50, twisted nanotube ropes may be used for torsional and tensile actuation and energy storage.

***References***

Teich D, Seifert G, Iijima S and Tománek D 2012 Helicity in ropes of chiral nanotubes: calculations and observation *Phys. Rev. Lett.* **108** 235501

Lima M D, Li N, Jung de Andrade M, Fang S, Oh J, Spinks G M, Kozlov M E, Haines C S, Suh D, Foroughi J, Kim S J, Chen Y, Ware T, Shin M K, Machado L D, Fonseca A F, Madden J D W, Voit W E, Galvão D S and Baughman R H 2012 Electrically, chemically, and photonically powered torsional and tensile actuation of hybrid carbon nanotube yarn muscles *Science* **338** 928

Teich D, Fthenakis Z G, Seifert G and Tománek D 2012 Nanomechanical energy storage in twisted nanotube ropes *Phys. Rev. Lett.* **109** 255501

**Herringbone fiber** → *cup-stacked fiber*

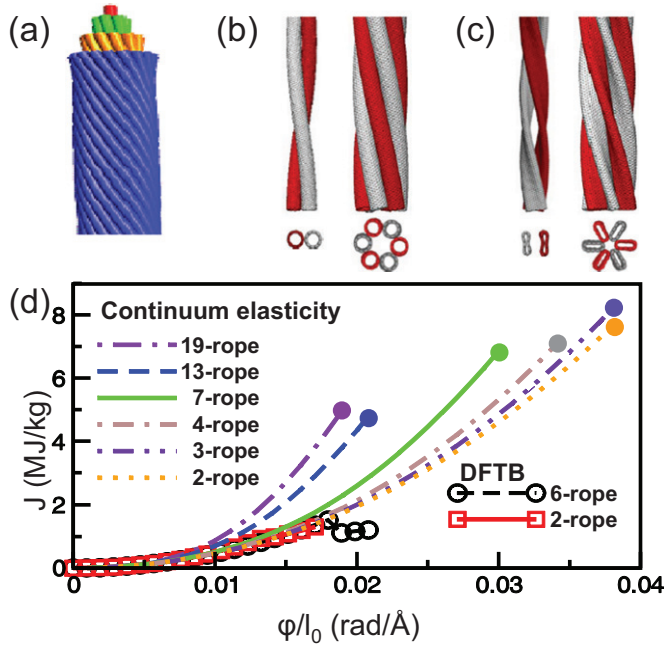


**Figure 50.** (a) Schematic diagram of a multi-layer macroscopic *rope* of carbon *nanotubes*. (b) Optimized structure of single-layer ropes containing 2 or 6 carbon nanotubes. (c) Deformations in these ropes caused by an applied torque. (d) Gravimetric *deformation energy* density $J$ in twisted nanotube ropes as a function of the rope twist rate $\varphi/l_0$. Circles at the end points indicate the elastic limit. (Adapted from Teich D *et al* 2012 *Phys. Rev. Lett.* **109** 255501, © 2012 American Physical Society.)

**Hexagonal graphite**, also called Bernal *graphite* and exhibiting AB layer stacking as shown in figure 44, this is the most stable form of graphite. Structural properties of hexagonal graphite are listed in table 11.

***Reference***

Bernal J D 1924 The structure of graphite *Proc. Roy. Soc.* A **106** 749

**Highly oriented pyrolytic graphite** (HOPG) is synthetic *graphite* with a high degree of preferred crystallographic orientation of the axes perpendicular to each *graphene* plane. Pyrolytic graphite is obtained by heating of pyrolytic carbon or by *chemical vapor deposition* (CVD) at temperatures above 2500 K. HOPG is obtained by hot working of pyrolytic graphite under compressive stress at approximately 3300 K. The physical properties of HOPG are close to those of the natural graphite mineral.

The **HiPCO process** refers to the high-pressure CO disproportionation which is an efficient technique for mass synthesis of *single-wall nanotubes*. The underlying *Boudouard reaction* occurs in the presence of $Fe(CO)_5$ or related transition metal *catalysts*.

**Reference**

Nikolaev P, Bronikowski M J, Bradley K R, Rohmund F, Colbert D T, Smith KA and Smalley R E 1999 Gas-phase catalytic growth of single-walled carbon nanotubes from carbon monoxide *Chem. Phys. Lett.* **313** 91

A **hook,** shown in figure 51, is a structure that may be formed by inserting

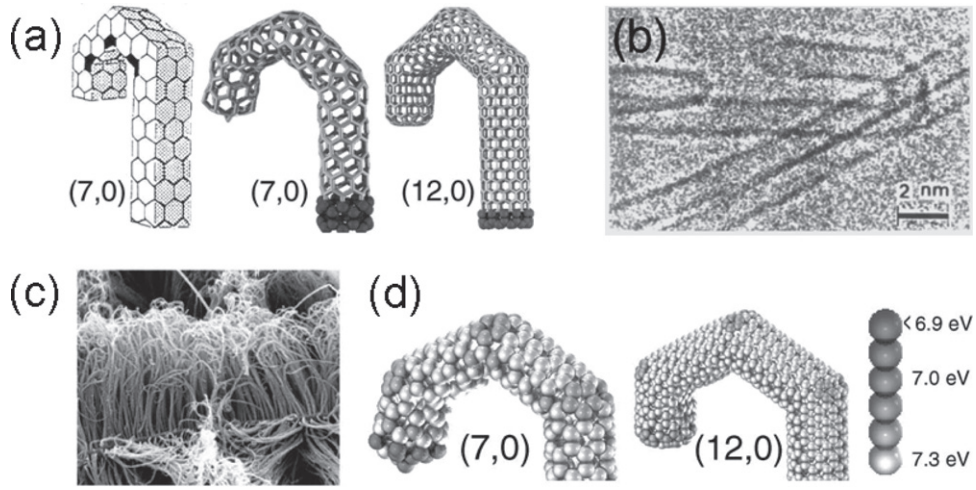


**Figure 51.** (a) Schematic view of a *nanotube*-based *hook*, formed by inserting pentagon–heptagon pairs in an all-hexagon tubular structure, and the equilibrium structure of hooks based on a (7, 0) and a (12, 0) nanotube. (b) *Transmission electron microscopy* image of an individual hook and (c) a *scanning electron microscopy* image of an array of nanohooks grown on a surface. (d) *Binding energy* of individual atoms in a hook structure. (Adapted from Berber S *et al* 2003 *Phys. Rev. Lett.* **91** 165503, © 2003 American Physical Society. Part of panel (a) and panel (b) reproduced from Iijima S 1994 MRS Bulletin **19**(11) 43, © 1994 Materials Research Society. Micrograph in panel (c) provided by Jean-Christophe Gabriel as a private communication (2003).)

*elbow bends* in a *nanotube*. Hook structures are very stable and resilient.

***Reference***

Berber S, Kwon Y-K and Tománek D 2003 Bonding and energy dissipation in a nanohook assembly *Phys. Rev. Lett.* **91** 165503

**HOPG** → *highly oriented pyrolytic graphite*

**HRTEM** → high-resolution *transmission electron microscopy*

The **Hückel molecular orbital method** (HMO), named after the German chemist Erich Hückel, is a commonly used simple approach to describe the *electronic band structure* of carbon nanostructures such as *chains*, *fullerenes*, *nanotubes* and *graphene*. The underlying single-band tight-binding Hamiltonian assumes that the electronic band structure near the Fermi level is dominated by the nearest-neighbor interaction between non-bonding C2$p_\pi$ orbitals, represented by the nearest-neighbor hopping integral $\gamma_0 \approx -2.9$ eV. The on-site energy $E(\mathrm{C}2p) = \alpha$ of a C2$p$ electron is typically set to zero and coincides with the Fermi level.

***Reference***

Hückel E 1931 Quantum contributions to the benzene problem' [in German; original title 'Quantentheoretische Beiträge zum Benzolproblem: I. Die Elektronenkonfiguration des Benzols und verwandter Verbindungen'] *Z. Phys.* **70** 204

**Hückel's rule** is a rule that estimates whether a planar carbon nanostructure, such as a flake of *graphene*, will display aromatic properties. Aromaticity is associated with the delocalization of C2$p_\pi$ electrons around a ring of carbon atoms, often illustrated by alternating single and double bonds that move around. The rule, based on the *Hückel molecular orbital method*, specifies that a planar nanostructure, which is formed of rings of carbon atoms, should be aromatic if it contains $4n + 2$ delocalized C2$p_\pi$ electrons (with integer $n = 0, 1, 2, \ldots$), and if each carbon atom in a ring may participate in the delocalization of these electrons. An equivalent rule for a *fullerene* with icosahedral symmetry to be aromatic requires $2(n+1)^2$ C2$p_\pi$ electrons. The C2$p_\pi$ electron count is particularly simple in $sp^2$ carbon nanostructures, where each carbon atom contributes one C2$p_\pi$ electron. As an example, the number of atoms in the $C_{60}$ fullerene does not have the form $2(n+1)^2$, indicating that this molecule is not aromatic.

***Reference***

Hirsch A, Chen Z and Jiao H 2000 Spherical aromaticity in symmetrical fullerenes: The 2(N+1)2 rule *Angew. Chem. Int. Ed. Engl.* **39** 3915

**Hydrogen storage** in pristine carbon nanostructures such as *nanotubes* may be achived reversibly with a capacity $\lesssim 3$ wt%. The storage capacity is enhanced significantly in the presence of alkali and alkaline earth intercalants.

**Hyperpolarizability** $\gamma$ describes deviations from the linear electronic *polarizability* $\alpha$ and is defined by the dependence of the electric dipole $p$ on the applied electric field $E$, given by $p = \alpha E + \gamma E^3$. Nanostructures with high dynamical hyperpolarizabilities are of interest for optical limitation.

# I

The **inter-layer distance** has a very similar value $d_i \approx 0.34$ nm in all *graphitic* structures with multiple layers.

The **inter-layer interaction** in *graphitic* systems, such as *graphite*, *multi-wall nanotubes* and *onions*, involves a weak covalent $p_\pi$–$p_\pi$ and a van der Waals interaction between neighboring walls with a typical separation $d_i \approx 0.335$ nm. The inter-layer interaction energy is $\varepsilon_i \approx 2.48$ eV nm$^{-2}$.

The **ionization potential** (IP) of a molecule or a finite system is the energy necessary to remove the least bound electron in the highest occupied molecular orbital (HOMO) and place it infinitely far away. The ionization potential of the $C_{60}$ molecule is IP=7.58 eV.

The **isolated pentagon rule** (IPR) states that the most stable *fullerene* structures contain no adjacent pentagons. The smallest fullerene satisfying this rule is the $C_{60}$ molecule.

An **isomer** is a well defined stable arrangement of atoms in a compound with a given chemical composition. Large nanostructures typically exhibit more than one stable structural isomer.

The **isotopic composition** of elements in a structure defines the fraction of particular isotopes, which are variants of the element with different numbers of neutrons in the nucleus. Naturally occurring carbon contains 98.9% $^{12}$C and 1.1% $^{13}$C. The large relative mass difference between $^{12}$C and $^{13}$C plays an important role in the *phonon spectra* that affect the *thermal conductivity* and the critical temperature $T_c$ of *superconductivity* in systems with different isotopic compositions.

**Isotopic defect** → *defect*

# K

The **Kataura plot** (see figure 52) displays the dependence of the optical transition energies $\Delta E = E_{ii}$ between pairs of van Hove singularities at $E(c_i)$ and $E(v_i)$ on the *diameter* $d_t$ of a *single-wall nanotube*. These transition energies are particularly useful for the identification of the *chiral index* $(n, m)$ of *single-wall nanotubes* using *photoluminescence*.

***Reference***

Kataura H, Kumazawa Y, Maniwa Y, Umezu I, Suzuki S, Ohtsuka Y and Achiba Y 1999 Optical properties of single-wall carbon nanotubes *Synth. Met.* **103** 2555

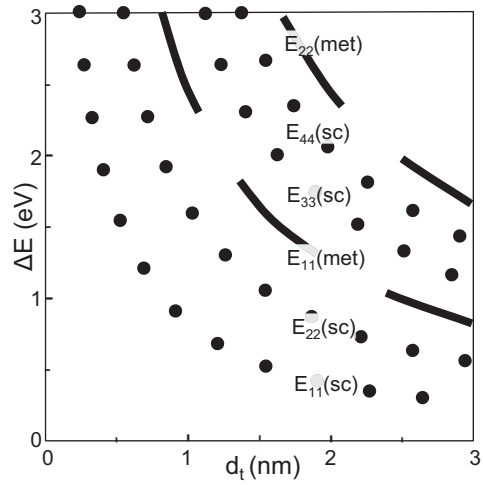


**Figure 52.** The *Kataura plot* depicting general trends in the dependence of optical transition energies between pairs of van Hove singularities on the *diameter* $d_t$ of semiconducting (sc) and metallic (met) *single-wall nanotubes*. The scatter of data for individual nanotubes is quite large and exceeds the separation between the trend lines for larger diameters.

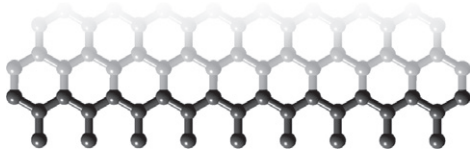

**Figure 53.** *Klein edge* of *graphene* (darker) in relation to the *zigzag edge*.

The **Klein edge** of *graphene*, shown in figure 53, is closely related to its *zigzag edge*. It is very reactive and much less stable than the *armchair edge* or the zigzag edge.

***References***

Klein D J 1994 Graphitic polymer strips with edge states *Chem. Phys. Lett.* **217** 261

Suenaga K and Koshino M 2010 Atom-by-atom spectroscopy at graphene edge *Nature* **468** 1088

**Klein tunneling** decribes the tunneling of carriers at the Fermi level of *graphene* and carbon *nanotubes*. The Klein paradox states that these electrons, which follow a linear band dispersion described by the *Dirac cone*, may tunnel efficiently through potential barriers of the order $V = mc^2$, where $m$ is the electron mass and $c$ the speed of light, corresponding to a barrier $V \approx 5 \times 10^5$ eV. Reduced scattering increases the *electron mobility*.

***References***

Klein O 1929 Die Reflexion von Elektronen an einem Potentialsprung nach der relativistischen Dynamik von Dirac *Z. Physik* **53** 157

Katsnelson M I, Novoselov K S and Geim A K 2006 Chiral tunnelling and the Klein paradox in graphene *Nature Phys.* **2** 620

# L

**Laser vaporization** is a common way to produce high-quality carbon nanostructures such as *fullerenes*, *nanotubes* and *nanohorns*. It often utilizes a pulsed beam in *pulsed laser vaporization* (PLV).

***References***

Kroto H W, Heath J R, O'Brien S C, Curl R F and Smalley R E 1985 $C_{60}$: buckminsterfullerene *Nature* **318** 162

Guo T, Nikolaev P, Thess A, Colbert D T and Smalley R E 1995 Catalytic growth of single-walled nanotubes by laser vaporization *Chem. Phys. Lett.* **243** 49

The **lattice constant** $a$ in *graphene* is the length of the Bravais lattice vectors spanning the lattice, $a = |\mathbf{a_1}| = |\mathbf{a_2}| = 0.246$ nm.

A **light-emitting diode** (LED) consisting of a *single-wall nanotube* is a source of *electroluminescence*. Light emission is caused by recombination of electrons and holes that are injected from opposite nanotube ends and move along the nanotube owing to its *ambipolar* transport character. The light-emitting diode is related to the *light-emitting transistor*, where the precise location of light emission is controlled by a gate voltage.

***Reference***

Wang S, Zeng Q, Yang L, Zhang Z, Wang Z, Pei T, Ding L, Liang X, Gao M, Li Y and Peng L-M 2011 High-performance carbon nanotube light-emitting diodes with asymmetric contacts *Nano Lett.* **11** 23

A **light-emitting transistor** (LET), consisting of a *single-wall nanotube* and shown in figure 54, is the smallest controllable localized light source. Light emission is caused by recombination of electrons and holes that are injected from opposite nanotube ends and move along the nanotube owing to its *ambipolar* transport character. The gate electrode controls the location of light emission.

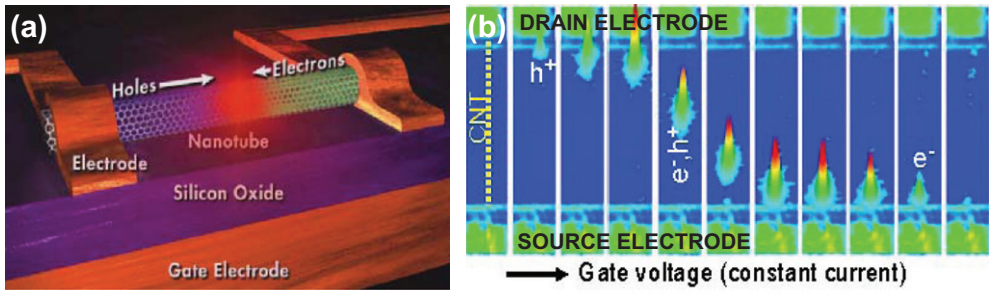


**Figure 54.** (a) Artistic rendition of a *light-emitting transistor* (LET) formed by a *single-wall nanotube*. (b) Infrared emission during a gate-voltage sweep. The color-coded light intensity is shown normal to the plane of the device in a 3D plot. (Private communication (2012), reproduced by permission of IBM and Phaedon Avouris.)

***References***

Misewich J A, Martel R, Avouris P, Tsang J C, Heinze S and Tersoff J 2003 Electrically induced optical emission from a carbon nanotube FET *Science* **300** 783

Freitag M, Chen J, Tersoff J, Tsang J C, Fu Q, Liu J and Avouris P 2004 Mobile Ambipolar Domain in Carbon-Nanotube Infrared Emitters *Phys. Rev. Lett.* **93** 076803

The **lip–lip interaction** stabilizes the growing end of a *multi-wall nanotube* and prevents premature *dome* closure by forming strong chemical bonds between edge atoms in neighboring walls, as illustrated in figure 55(a).

***References***

Guo T, Nikolaev P, Rinzler A G, Tománek D, Colbert D T and Smalley R E 1995 Self-assembly of tubular fullerenes *J. Phys. Chem.* **99** 10694

Kwon Y-H, Lee Y-H, Seong-Gon K, Jund P, Tománek D and Smalley R E 1997 Morphology and stability of growing multi-wall carbon nanotubes *Phys. Rev. Lett.* **79** 2065

Jin C, Suenaga K and Iijima S 2008 Direct evidence for lip-lip interactions in multi-walled carbon nanotubes *Nano Res.* **1** 434

**Logic circuits** may be constructed from semiconducting carbon *nanotubes*. Nonuniform *conductance* behavior may have an intrinsic origin, such as *chirality* change at an *elbow bend*, or can be achieved externally by nonuniform *p*- or *n*-*doping*. Multiple devices such as diodes or field-effect transistors (see figure 56) can be realized on one nanotube.

**Lonsdaleite** is hexagonal diamond. This less common form of *diamond* distinguishes itself from the common cubic diamond structure by its hexagonal crystal lattice. Like in cubic diamond, the tetrahedrally coordinated carbon atoms are connected by strong $sp^3$ bonds.

The **Luttinger liquid**, also called the Tomonaga Luttinger liquid (TLL), describes the electronic transport behavior in one-dimensional metallic systems, including carbon *nanotubes*. Whereas the behavior of electrons in conventional three-dimensional metals is described by the Fermi liquid, this ground state becomes unstable to Coulomb interactions and is replaced by the TLL state. The TLL state reveals itself through interaction-dependent anomalous exponents in the correlation functions, *electronic density of states* and momentum distribution of the electrons. The spin and charge degrees of freedom of electrons become decoupled in the TLL, which is known as spin-charge separation.

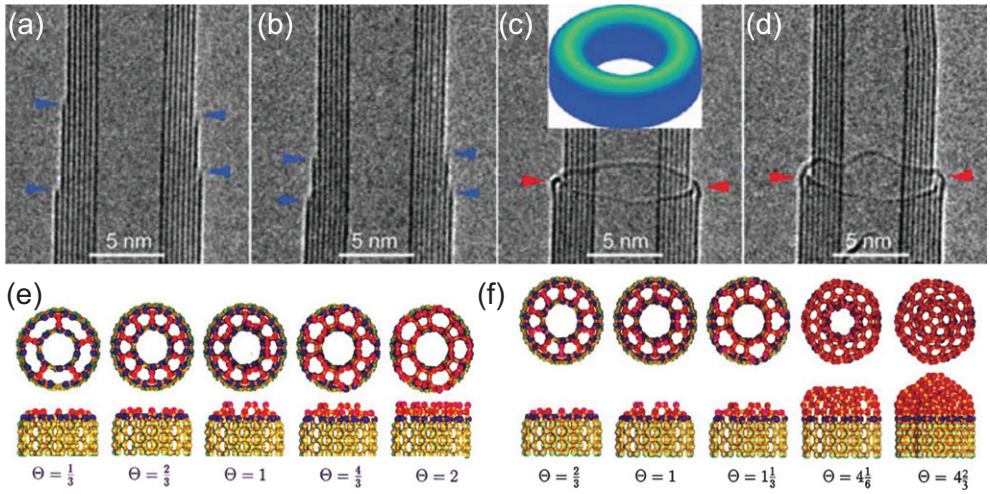


**Figure 55.** (a)–(d) Time sequence of high-resolution *transmission electron microscopy* (HRTEM) images of the fattening process of a *multi-wall nanotube*. Following a period of independent growth (a)–(b), the two outermost layers connect by *lip–lip interaction* (c) and continue growing at the end (d). (e)–(f) Optimum geometry near the end of a (5, 5) @ (10, 10) *double-wall nanotube* (DWNT), representing the two outermost layers in (c)–(d). The edge coverage $\Theta = N_{\mathrm{add}}/N_e$ is the ratio of the number of added atoms $N_{\mathrm{add}}$ and the number of edge atoms $N_{\mathrm{e}}$, which is the same as the number of atoms in any layer of the nanotube. (e) Covalent lip–lip interaction stabilizes the edges, yet does not stop continuous growth. (f) A possible scenario leading to a *dome* closure of the DWNT. The dome closure process requires an activation energy. Edge atoms are distinguished by color (dark blue) from added atoms (red) and atoms in the nanotube (light green). (Panels (a)–(d) are adapted from Jin C *et al* 2008 *Nano Res.* **1** 434, © 2008 Tsinghua Press and Springer-Verlag. Panel (f) is adapted from Kwon Y-K *et al* 1997 *Phys. Rev. Lett.* **79** 2065, © 1997 American Physical Society.)

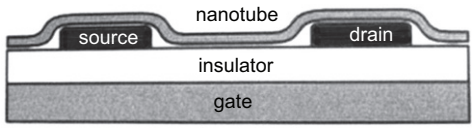


**Figure 56.** Schematic diagram of a carbon *nanotube* based field-effect transistor (CNT-FET). The current flowing from the source to the drain electrode is modulated by the voltage applied to the gate electrode.

***References***

Tomonaga S 1950 Remarks on Bloch's method of sound waves applied to many-fermion problems *Prog. Theor. Phys.* **5** 544

Luttinger J M 1963 An exactly soluble model of a many-fermion system *J. Math. Phys.* **4** 1154

Ishii H, Kataura H, Shiozawa H, Yoshioka H, Otsubo H, Takayama Y, Miyahara T, Suzuki S, Achiba Y, Nakatake M, Narimura T, Higashiguchi M, Shimada K, Namatame H and Taniguchi M 2003 Direct observation of Tomonaga-Luttinger-liquid state in carbon nanotubes at low temperatures *Nature* **426** 540

# M

The **M-carbon** phase is a dense phase of elemental carbon obtained by cold compression of *graphite* at pressures exceeding 19 GPa. This and related phases of cold-compressed graphite are believed to be harder than *diamond*.

***References***

Mao W L, Ho-kwang M, Eng P J, Trainor T P, Newville M, Chi-chang K, Heinz D L, Shu J, Meng Y and Hemley R J 2003 Bonding changes in compressed superhard graphite *Science* **302** 425

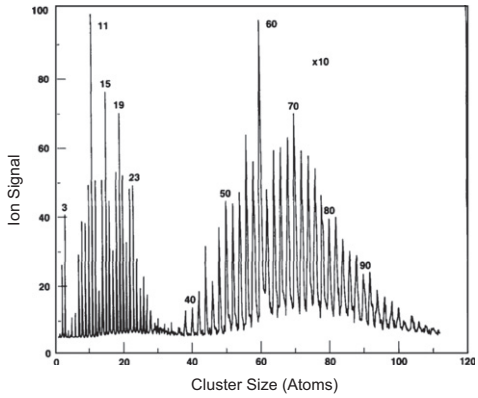


**Figure 57.** Time-of-flight mass spectra (TOF-MS) of $C_n^+$ clusters. The ion signal for $40 < n < 100$, which was obtained using different conditions than for $1n < 30$, has been increased by a factor of 10. An abundance of $C_{60}^+$ indicates that 60 is a *magic number* for carbon clusters. (Adapted from Rohlfing E A *et al* 1984 *J. Chem. Phys.* **81** 3322, © 2004 American Institute of Physics.)

Li Q, Ma Y, Oganov A R, Wang H, Wang H, Xu Y, Cui T, Ho-Kwang M and Zou G 2009 Superhard monoclinic polymorph of carbon *Phys. Rev. Lett.* **102** 175506

Wang Y, Panzik J E, Kiefer B and Lee K K M 2012 Crystal structure of graphite under room-temperature compression and decompression *Sci. Rep.* **2** 520

A **magic number** is a number of atoms in a nanostructure that indicates its high stability and its low likelihood to lose or acquire additional atoms. Magic numbers are characterized by abundances in time-of-flight mass spectra (TOF-MS). As seen in figure 57, 60 is a prominent magic number for carbon clusters.

***Reference***

Rohlfing E A, Cox D M and Kaldor A 1984 Production and characterization of supersonic carbon cluster beams *J. Chem. Phys.* **81** 3322

The **magnetic behavior** of nanocarbons depends sensitively on their structure and chemical modification. Pristine carbon nanostructures with no unsaturated bonds, including *fullerenes*, *nanotubes* and *graphene*, are diamagnetic ($\chi < 0$). The presence of pentagonal rings in fullerenes significantly lowers the absolute value of the diamagnetic susceptibility over other ring compounds. Magnetic instabilities may occur at the *zigzag edge* of *graphitic* nanostructures, including *zigzag nanotubes* or *graphene nanoribbons* with a zigzag edge. Antiferromagnetic coupling between spin-polarized zigzag edges of a graphene nanoribbon results in zero magnetic moment.

***References***

Makarova T L, Sundqvist B, Höhne R, Esquinazi P, Kopelevich Y, Scharff P, Davydov V A, Kashevarova L S and Rakhmanina A V 2001 Magnetic carbon *Nature* **413** 716 2005 *ibid.* **436** 1200 2006 *ibid.* **440** 707

Park N, Yoon M, Berber S, Ihm J, Osawa E and Tománek D 2003 Magnetism in all-carbon nanostructures with negative Gaussian curvature *Phys. Rev. Lett.* **91** 237204

The **mechanical properties** of carbon nanostructures, including toughness, reflect the excellent mechanical behavior of the bulk counterparts, but depend more sensitively on the presence of *defects*. Unlike *carbon fibers*, carbon *nanotubes* are highly resilient and capable of restoring their shape following deformation. The Young's modulus $Y = 1060$ GPa of a *graphene* monolayer has nearly the same value in carbon nanotubes. The large spread in reported values is mostly due to the choice of the assumed wall thickness; consistent values should be based on nanotube *ropes*. The wide spread of ≈50–150 GPa in the observed tensile strength values of single- and multi-wall carbon nanotubes

is likely caused by differences in defect types and concentrations. The observed shear modulus of *single-wall nanotube* ropes is 1 GPa.

***References***

Overney G, Zhong W and Tománek D 1993 Structural rigidity and low frequency vibrational modes of long carbon tubules *Z. Phys. D* **27** 93

Treacy M M J, Ebbesen T W and Gibson J M 1996 Exceptionally high Young's modulus observed for individual carbon nanotubes *Nature* **381** 678

Salvetat J-P, Briggs G A D, Bonard J-M, Bacsa R R, Kulik A J, Stöckli T, Burnham N A and Forró L 1999 Elastic and shear moduli of single-walled carbon nanotube ropes *Phys. Rev. Lett.* **82** 944

**Mechanochemical processes** induce changes in chemical bonding and structure by pressure, often introduced by hitting the material with a foreign object. A prominent example, the *ball milling* (BM) process, converts *boron nitride* and *graphite* to *nanotubes*.

The **melting temperature** of $sp^2$ carbon nanostructures, including *fullerenes* and *nanotubes*, should lie near 4000 K according to computer simulations, similar to high-*purity graphite*. The observed reduction of the melting point to above 3000 K has been linked to *defects* and residual oxygen under experimental conditions. The melting point of metal *catalyst* particles lies significantly lower than that of the bulk counterpart and may be further lowered in the presence of dissolved carbon, in particular close to the *eutectic* point.

A **metallofullerene** $M@C_n$ is the most common type of *endohedral fullerenes* containing one or several metal atoms M, usually from among the transition metal or rare earth elements. The formation of the enclosing $C_n$ *cage*, which contains typically $80 \lesssim n \lesssim 90$ carbon atoms, is catalyzed by the presence of the metal atoms during the arc synthesis.

**MLG (monolayer graphene)** → *graphene*

**Mobility** → *electron mobility* or hole mobility

The **mobility gap** in charge transport has a similar signature in the current–voltage ($I$–$V$) characteristic as the intrinsic *fundamental band gap*. It occurs in non-uniform systems including lithographically produced narrow *graphene nanoribbons*, where the edge roughness causes strong localization that suppresses transport at small applied voltages.

***References***

Stampfer C, Güttinger J, Hellmüller S, Molitor F, Ensslin K and Ihn T 2008 Energy gaps in etched graphene nanoribbons *Phys. Rev. Lett.* **102** 056403

Oostinga J B, Sacépé B, Craciun M F and Morpurgo A F 2010 Magnetotransport through graphene nanoribbons *Phys. Rev.* B **81** 193408

**Molecular dynamics** (MD) simulations are a powerful computational tool to track atomic motion during complex chemical reactions such as melting of *fullerenes* or the *catalytic growth* of *nanotubes*, shown in figure 58. Atomic trajectories are determined by solving Newton's equations of motion. The reliability of the results depends sensitively on the adequacy of the energy functional underlying the calculation of forces. Simulation runs for up to a few hundred atoms are typically limited to a few

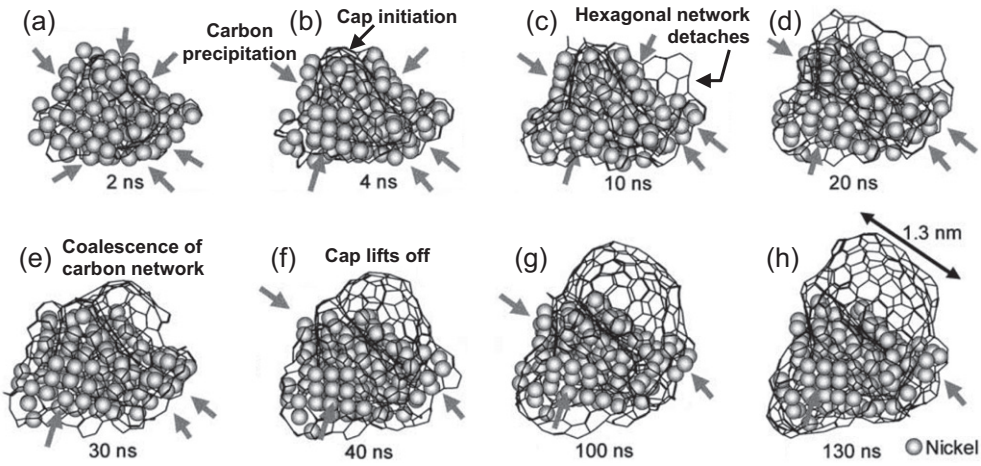


**Figure 58.** Snapshots of a *molecular dynamics* (MD) simulation depicting the first 130 ns of the *catalytic growth* process of a *nanotube* from a carbon-saturated $Ni_{108}$ particle. Kinetics has been accelerated by using a high temperature $T = 2500$ K. The growing *graphitic* network is represented by lines and nickel atoms are shown by gray spheres. Gray arrows indicate locations where carbon atoms precipitate to the surface. (Adapted from Shibuta Y and Maruyama S 2003 *Chem. Phys. Lett.* **382** 381, © 2003 Elsevier.)

picoseconds, since the calculation of forces at each time step of $\lesssim 0.5 \times 10^{-15}$ s using quantum mechanics is computationally very demanding even in the electronic ground state. While providing useful insight into the dynamics of possible processes, molecular dynamics simulations seldom represent most typical reactions, since the run times are limited and the outcome depends sensitively on the choice of system conditions and the selected starting geometry.

***References***

Kim S-G and Tománek D 1994 Melting the fullerenes: A molecular dynamics study *Phys. Rev. Lett.* **72** 2418

Shibuta Y and Maruyama S 2003 Molecular dynamics simulation of formation process of single-walled carbon nanotubes by CCVD method *Chem. Phys. Lett.* **382** 381

Ding F, Bolton K and Rosén A 2004 Nucleation and growth of single-walled carbon nanotubes: A molecular dynamics study *J. Phys. Chem.* B **108** 17369

**Momentum quantization** in carbon *nanotubes* is the consequence of the finite circumference given by the length of the *chiral vector* $\mathbf{C_h}$. Allowed momenta in the *Brillouin zone* of the generating *graphene* lattice occur along lines spaced by $2\pi/|\mathbf{C_h}|$ that run parallel to the tube axis (see figure 59). The orientation of the Brillouin zone is defined by the *chiral angle* $\theta$, and its center $\Gamma$ lies on one of the quantization lines. A carbon nanotube with the *chiral index* $(n, m)$ is conducting if any of the momentum quantization lines passes through a K or K′ point, which occurs when $n - m$ is divisible by 3.

***Reference***

Hamada N, Sawada S and Oshiyama A 1992 New one-dimensional conductors—graphitic microtubules *Phys. Rev. Lett.* **68** 1579

**Monolayer graphene** (MLG) → *graphene*

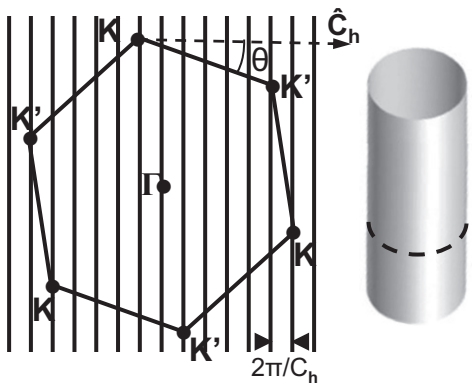


**Figure 59.** *Momentum quantization* in a carbon *nanotube*, illustrated in the *Brillouin zone* of *graphene*. Momentum quantization is the reason why carbon nanotubes may be metallic or semiconducting.

**Figure 60.** Schematic structure of a *multi-wall nanotube* (MWNT).

**Multi-layer graphene**, also known as 'multilayer epitaxial graphene' (MEG), is a structure that forms at the surface of heated SiC crystals. It differs from *graphite* by orientational disorder of constituent graphene layers, which suppresses electronic inter-layer coupling, resulting in a very similar electronic structure near the Fermi level to graphene.

***Reference***

Hass J, de Heer W A and Conrad EH 2008 The growth and morphology of epitaxial multilayer graphene *J. Phys.: Condens. Matter* **20** 323202

A **multi-wall nanotube** (MWNT) is a cylinder containing two or more nested *nanotubes*, shown in figure 60. The *inter-layer distance* $d_i$ is close to that in the corresponding layered material, such as *graphite* or layered *boron nitride*. The energy cost associated with forming a MWNT from *graphene* is shown in figure 61.

**MWNT** → *multi-wall nanotube*

# N

A **nanobud** is a carbon nanostructure resembling a tree branch with buds, consisting of *fullerenes* covalently attached to a *nanotube*, as shown in figure 62.

***Reference***

Nasibulin A G, Pikhitsa P V, Jiang H, Brown D P, Krasheninnikov A V, Anisimov A S, Queipo P, Moisala A, Gonzalez D, Lientschnig G, Hassanien A, Shandakov S D, Lolli G, Resasco D E, Choi M, Tománek D and Kauppinen E I 2007 A novel hybrid carbon material *Nature Nanotech.* **2** 156

**Nanocage** → *cage* or *capsule*

**Nanocapsule** → *cage* or *capsule*

**Nanocone** → *nanohorn*

A **nanohorn**, also called a *nanocone*, is a conical structure obtained by substituting $n_p$ hexagons in the honeycomb lattice of *graphene* by pentagons. It can be constructed by cutting a wedge from a

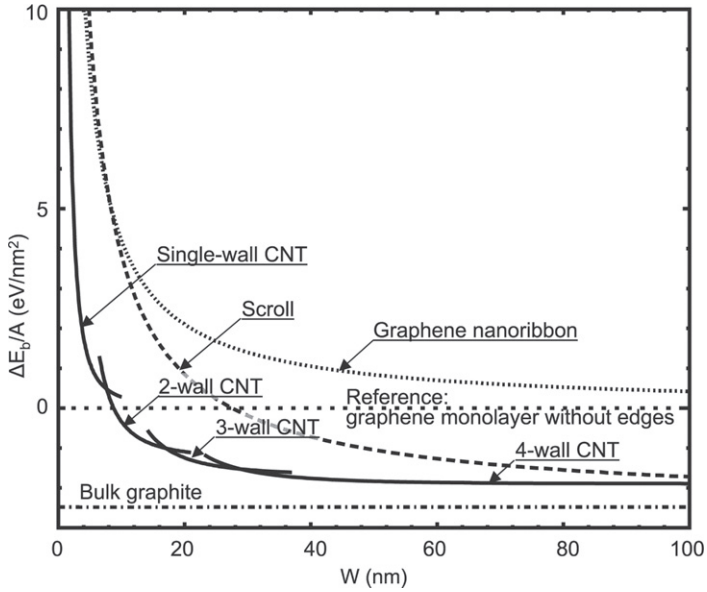


**Figure 61.** Difference *binding energy* $\Delta E_b$ per unit area $A$ associated with the conversion of a *graphene* monolayer strip of width $W$ with completely saturated edges into other cylindrical *graphitic* structures. (Adapted from Lavin J G *et al* 2002 *Carbon* **40** 1123, © 2002 Elsevier.)

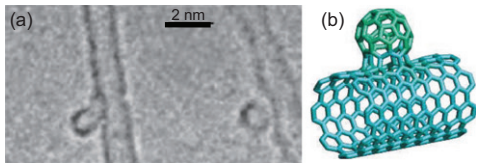


**Figure 62.** (a) High-resolution *transmission electron microscopy* image and (b) proposed structure of a *nanobud*. (Adapted from Nasibulin A G *et al* 2007 *Nature Nanotech.* **2** 156, © 2007 Nature Publishing Group.)

graphene monolayer and connecting the exposed edges in a seamless manner, as shown in figure 63(a). The opening angle of the wedge, called the disclination angle, is $\alpha = n_p \times 60^\circ$, with $0 < n_p < 6$. The number of pentagons $n_p$ at the apex, defining the disclination angle, is related to the opening angle $\theta$ of the cone by $\theta = 2\sin^{-1}(1 - n_p/6)$. Structural properties of nanohorns are summarized in table 8. The atomic structure of nanohorns with the smallest opening angle $\theta = 19.2^\circ$ is shown in figure 63(c). A planar graphene monolayer is associated with $n_p = 0$ and a *nanotube* is described by $n_p = 6$. All other possible *graphitic* cone structures with $0 < n_p < 6$ containing one or many walls, as shown in figure 63, may be formed by different *nanohorn synthesis* techniques.

***References***

Krishnan A, Dujardin E, Treacy M M J, Hugdahl J, Lynum S and Ebbesen T W 1997 Graphitic cones and the nucleation of curved carbon surfaces *Nature* **388** 451

Murata K, Kaneko K, Steele W A, Kokai F, Takahashi K, Kasuya D, Hirahara K, Yudasaka M and Iijima S 2001 Molecular potential structures of heat-treated single-wall carbon nanohorn assemblies *J. Phys. Chem.* B **105** 10210

**Nanohorn synthesis** generates samples by *pyrolysis* of hydrocarbons. Other

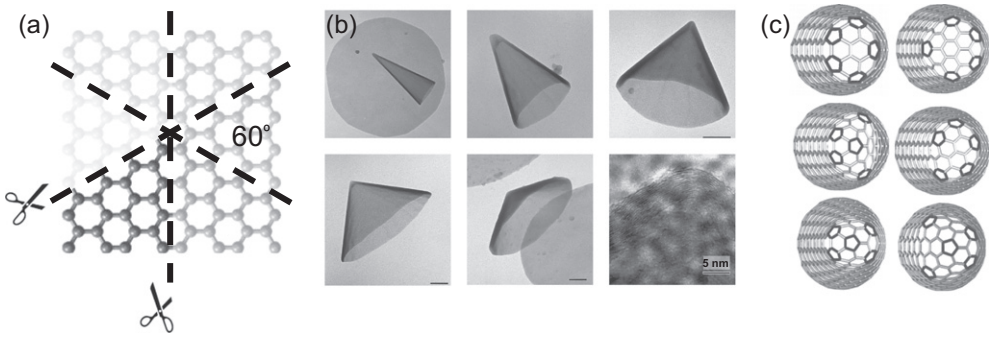


**Figure 63.** (a) Schematic diagram of *graphene* segments with disclination angles $\alpha = n_p \times 60^\circ$ $(0 < n_p < 6)$, which can be 'folded' to *nanohorn* structures by connecting the exposed edges. (b) *Transmission electron microscopy* images of nanohorns with $0 < n_p < 6$ pentagons at the apex. The scale bars in all but the bottom right panel are 200 nm. (Adapted from Krishnan A *et al* 1997 *Nature* **388** 451, © 1997 Nature Publishing Group.) (c) Possible arrangements of five pentagonal rings at the apex of a nanohorn with the opening angle $\theta = 19.2^\circ$. (Adapted following Berber S *et al* 2000 *Phys. Rev.* B **62** R2291, © 2000 American Physical Society.)

common synthesis techniques include $CO_2$ *laser vaporization* or *arc evaporation* of solid carbon in an inert gas atmosphere.

**Nanoribbon** → *graphene nanoribbon* (GNR)

A **nanotube** is a cylindrical structure consisting of one (*single-wall nanotube*, SWNT) or several (*multi-wall nanotube*, MWNT) walls formed by rolling a layered substance into a seamless cylinder. The structure of an individual nanotube is uniquely determined by the *chiral index* $(n, m)$. The time line of nanotube discoveries is listed in table 2.

***References***

Oberlin A, Endo M and Koyama T 1976 Filamentous growth of carbon through benzene decomposition *J. Cryst. Growth* **32** 335

Iijima S 1991 Helical microtubules of graphitic carbon *Nature* **354** 56

**Nanotube characterization** refers primarily to the identification of the *chiral index* $(n, m)$. The chiral index of an individual *nanotube* can be determined using electron diffraction in a high-resolution *transmission electron microscope* (HRTEM) and, to a limited degree, by *scanning tunneling microscopy* (STM). For semiconducting nanotubes that have been isolated from *ropes*, the most powerful characterization technique is *photoluminescence*. The chiral index of metallic nanotubes, which do not fluoresce, may be identified using *Rayleigh scattering*.

**Nanotube composites** are advanced materials, consisting of a small fraction of *nanotubes* in bulk polymers, ceramics and metals, that enhance the mechanical toughness and electrical and *thermal conductivity* of the host material. The relative benefit of inserting nanotubes depends on the degree of nanotube *dispersion* and on the bonding between nanotubes and the host material. The type and strength of these bonds determine the mechanical load transfer between the nanotube and the host, and the overall electrical and thermal conductivity of the composite. Typical loading rates are below 10 wt% nanotubes. 1% nanotube loading can cause

up to ≈50% increase in the *Young's modulus* of polymer materials. In nylon, the elastic modulus and yield strength has nearly doubled upon addition of 2 wt% carbon nanotubes. *Graphitic* carbon nanostructures may be used to improve electrical conductivity of low-cost bulk polymers. Combining elasticity with electrical *conductance* and optical transparency, nanotube–polymer composite materials are a viable alternative to indium tin oxide (ITO).

***References***

Schulte K and Windle A H 2007 Special issue on carbon nanotube—polymer composites *Composites Sci. Technol.* **67** 5

Moniruzzaman M, Chattopadhyay J, Edward B W and Winey K I 2007 Tuning the mechanical properties of SWNT/nylon 6,10 composites with flexible spacers at the interface *Nano Lett.* **7** 1178

**Nanotube electronic band structure** $E(k)$ is displayed in figure 64 for a metallic (10, 10) and a semiconducting (17, 0) carbon nanotube. Marked difference from the *graphene electronic band structure* is caused by quantum confinement of the states along the tube perimeter, as shown in figure 59. Similar to *graphite*, *supramolecular interactions* in *ropes* or *multi-wall nanotubes* may affect the electronic structure, as seen in figure 65.

***References***

Kwon Y-K, Saito S and Tománek D 1998 Effect of inter-tube coupling on the electronic structure of carbon nanotube ropes *Phys. Rev.* B **58** R13314

Delaney P, Choi H J, Ihm J, Louie S G and Cohen M L 1998 Broken symmetry and pseudogaps in ropes of carbon nanotubes *Nature* **391** 466

**Nanotube filling** → *capillary filling* of *nanotubes*

**Nanotube synthesis** involves high temperatures or energetic processes including *arc evaporation* (AE), *pulsed laser vaporization* (PLV), high-pressure carbon monoxide conversion in the *HiPCO process*, *chemical vapor deposition* (CVD), and *ball milling* (BM). Accelerated growth of *vertically aligned nanotube arrays* (VANTAs) on a substrate by CVD is sometimes referred to as *supergrowth*.

**Nanotube yarn** is a yarn that can be spun from carbon *nanotubes* for further processing to fabric or *ropes*. Two-ply nanotube yarns (see figure 66) can achieve a tensile strength of up to 0.5 TPa.

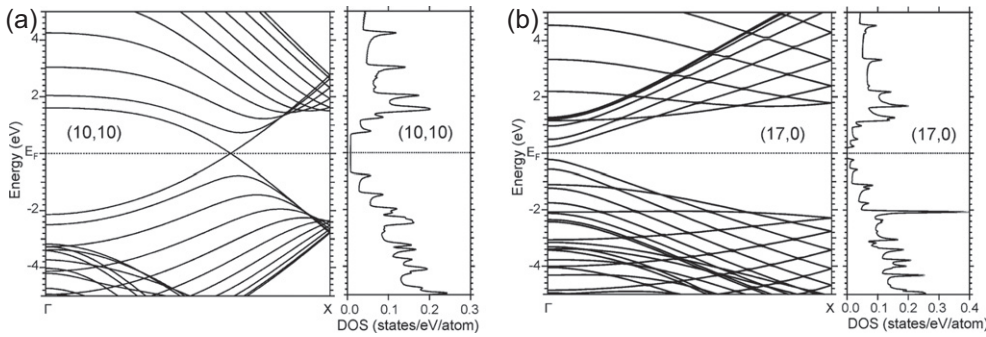


**Figure 64.** Electronic structure of (a) a metallic (10,10) and (b) a semiconducting (17, 0) carbon *nanotube*. The *electronic band structure* is shown in the left panels and the corresponding *electronic density of states* in the right panels.

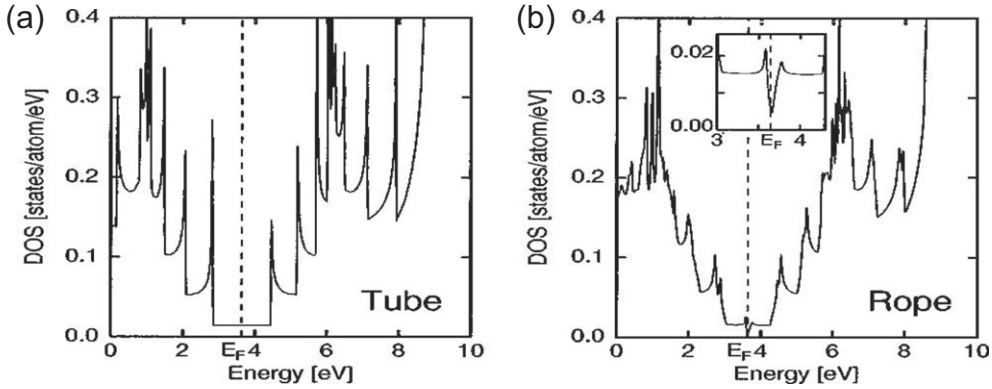


**Figure 65.** *Electronic density of states* of (a) an isolated (10,10) *nanotube* and (b) an infinite array or *rope* of such nanotubes. The structure of the pseudogap in the rope is displayed in the inset on an expanded energy scale. (Adapted from Kwon Y-K *et al* 1998 *Phys. Rev.* B **58** R13314, © 1998 American Physical Society.)

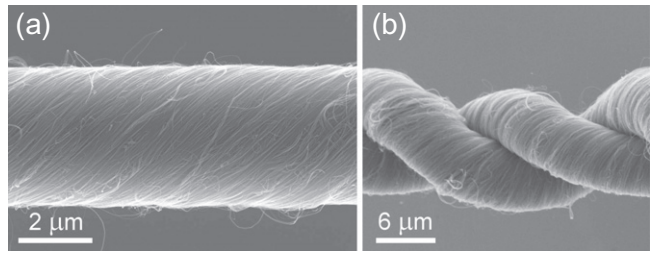


**Figure 66.** *Scanning electron microscopy* (SEM) images of (a) single and (b) two-ply multi-wall *nanotube yarns*. (Baughman R, Fang S, Lima M, Robles R, Chavez X L and Jung M 2012 private communication.)

***Reference***

Zhang M, Atkinson K R and Baughman R H 2004 Multifunctional carbon nanotube yarns by downsizing an ancient technology *Science* **306** 1358

**Nanowire** is a long cylinder with diameter not exceeding several nanometers. Nanowires consisting of substances ranging from metals to ice and *diamond* may assemble and solidify within the void of open-ended *nanotubes*.

***References***

Wang Z, Zhao Z and Qiu J 2006 In situ synthesis of super-long Cu nanowires inside carbon nanotubes with coal as carbon source *Carbon* **44** 1845

Koga K, Gao G T, Tanaka H and Zeng X C 2001 Formation of ordered ice nanotubes inside carbon nanotubes *Nature* **412** 802

Zhang J, Zhu Z, Feng Y, Ishiwata H, Miyata Y, Kitaura R, Dahl J E P, Carlson R M K, Fokina N A, Schreiner P R, Tománek D and Shinohara H 2013 Evidence of diamond nanowires formed inside carbon nanotubes from diamantane dicarboxylic acid *Angew. Chem. Int. Ed.* **52** 3717

# O

An **onion** is a spherical structure consisting of nested *fullerenes*, a counterpart to *multi-wall nanotubes* with cylindrical symmetry. The *inter-layer distance* $d_i$ is close to that in the corresponding layered material

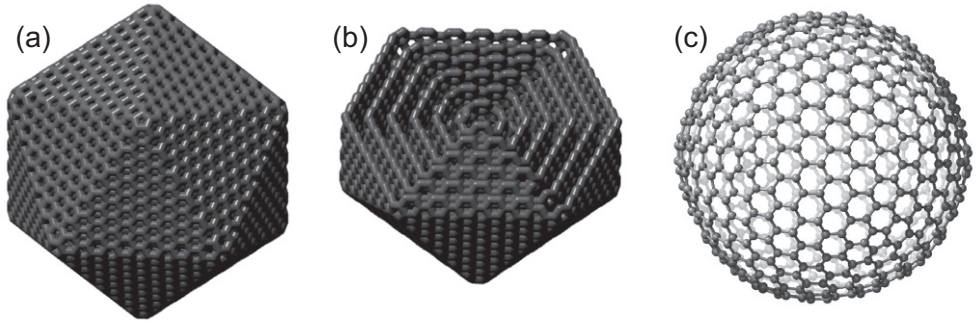


**Figure 67.** Schematic diagram of icosahedrally faceted nested *fullerenes* inside an *onion*. (a) Full and (b) bisected structure of an icosahedral $C_{5460}$ onion with six walls. Faceting is suppressed by orientational disorder and structural imperfections in the individual walls of naturally occurring onions. (c) The $C_{720}$ fullerene with its spherical shape may correspond to one wall in the observed onion structure, shown in figure 68.

($d_i \approx 0.34$ nm for carbon onions, shown in figures 67 and 68). Onions are formed under electron irradiation of carbon material and may be abundant in interstellar space. Their presence has been linked to the observed ultraviolet extinction band at $\lambda = 217.5$ nm. Carbon onions exposed to electron irradiation may change their size, as shown in figure 76.

***References***

Ugarte D 1992 Curling and closure of graphitic networks under electron-beam irradiation *Nature* **359** 707

Henrard H L, Lucas A A and Lambin P 1993 On the 2175 Å absorption band of hollow, onion-like carbon particles *Astrophys. J.* **406** 92

Wright E L 1988 The ultraviolet extinction from interstellar graphitic onions *Nature* **336** 227

Smith P P K and Buseck P R 1981 Graphitic carbon in the Allende meteorite—A microstructural study *Science* **212** 322

The **opening** of *dome*-closed *nanotube* ends can be achieved selectively in a mildly oxidizing environment, by heating the nanotubes at 950 °C in $CO_2$ atmosphere and making use of the 'reverse *Boudouard reaction*', $C(s) + CO_2(g) \rightarrow 2CO(g)$ or exposing them to boiling nitric acid. Alternatively, heating nanotubes to 850 °C in $O_2$ atmosphere also proved efficient in opening the tube ends, by corroding away a significant fraction of the material.

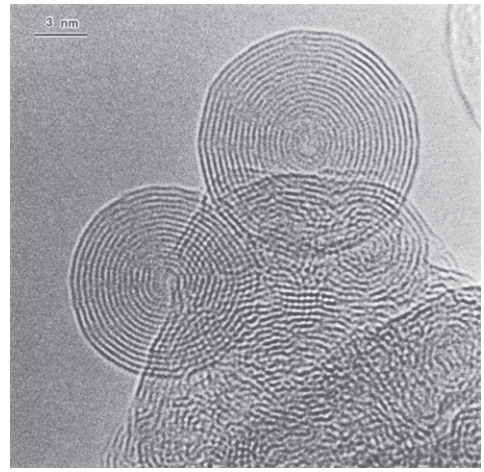


**Figure 68.** *Transmission electron microscopy* image of a carbon *onion*. (Adapted from Ugarte D 1992 *Nature* **359** 707, © 1992 Nature Publishing Group.)

***References***

Tsang S C, Harris P J F and Green M L H 1993 Thinning and opening of carbon nanotubes by oxidation using carbon dioxide *Nature* **362** 520

Ajayan P M, Ebbesen T W, Ichihashi T, Iijima S, Tanigaki K and Hiura H 1993 Opening carbon nanotubes with oxygen and implications for filling *Nature* **362** 522

Tsang S C, Chen Y K, Harris P J F and Green M L H 1994 A simple chemical method of opening and filling carbon nanotubes *Nature* **372** 159

The **optical properties** of nanocarbons vary strongly from structure to structure. A high density of free $\pi$ electrons causes absorption in the visible and the deep black color of *carbon black*. The semimetallic character gives *graphite* crystals a reflective grey metallic appearance. Films of pristine *fullerene* molecular solids and carbon *nanotubes* are rather transparent due to the high penetration depth of visible light caused by the low carrier density. *Diamondoids* share their sparkling transparency with *diamond* due to their large *fundamental band gaps*.

**Orientational melting** in *solid* $C_{60}$ describes changes in the orientation of individual $C_{60}$ molecules within the close-packed structure of the crystalline solid. Below 249 K, $C_{60}$ molecules do not rotate and form a simple cubic lattice with four molecules of different orientation per unit cell, as shown in figure 69. At temperatures above 249 K, $C_{60}$ molecules start rotating about their center in a correlated manner. Uncorrelated rotation of $C_{60}$ molecules sets on above 261 K. In this state, they convert to a face-centered cubic (fcc) lattice by lifting the orientational inequivalence of the different sites in the simple cubic supercell. In contrast to finite-size *fullerenes*, *nanotubes* do not rotate rigidly when aligned in a *rope*. In these ropes, orientational dislocations called *twistons* may move along the tube axis, corresponding to an effective *rotation* of individual nanotubes.

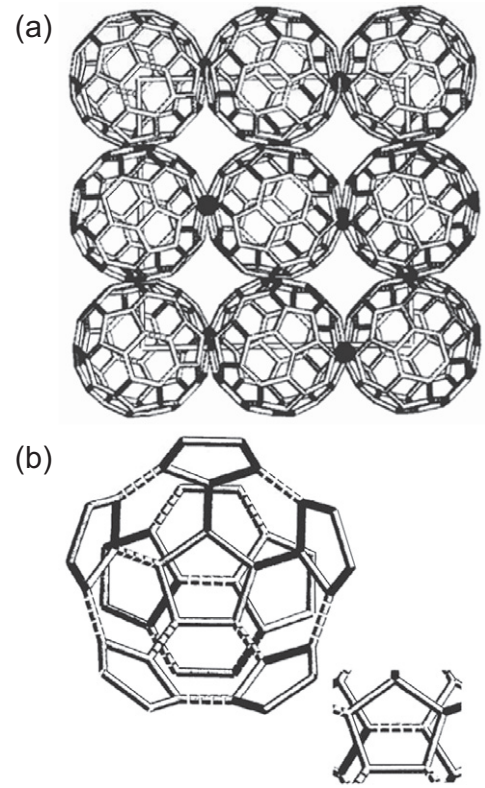


**Figure 69.** (a) Structure of the ordered simple cubic lattice of $C_{60}$ molecules near $T = 0$, viewed along the [001] direction. (b) Detailed structure at the interface of two neighboring molecules, viewed along the [110] direction, describing the center-to-center connection of adjacent $C_{60}$ molecules. (From David W I F *et al* 1991 *Nature* **353** 147, © 1991 Nature Publishing Group.)

***References***

Heiney P A, Fischer J E, McGhie A R, Romanow W J, Denenstein A M, McCauley Jr. J P, Smith A B and Cox D E 1991 Orientational ordering transition in solid $C_{60}$ *Phys. Rev. Lett.* **66** 2911

David W I F, Ibberson R M, Matthewman J C, Prassides K, Dennis T J S, Hare J P, Kroto H W, Taylor R and Walton D R M 1991 Crystal structure and bonding of ordered $C_{60}$ *Nature* **353** 147

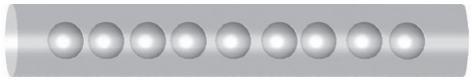

**Figure 70.** Schematic structure of a *peapod*.

Kwon Y-K and Tománek D 2000 Orientational melting in carbon nanotube ropes *Phys. Rev. Lett.* **84** 1483 2011 *ibid.* **106** 219901(E)

# P

**PAN-based carbon fiber** → polyacrylonitrile-based *carbon fiber*

A **peapod** is a tubular structure consisting of *fullerenes* enclosed in a *single-wall nanotube* (see figures 70 and 37(a)).

***Reference***

Smith B W, Monthioux M and Luzzi D E 1998 Encapsulated $C_{60}$ in carbon nanotubes *Nature* **396** 323

**PECVD** is the acronym for plasma-enhanced *chemical vapor deposition* (CVD).

**Peeling** or exfoliating the outermost walls of *onions* or *multi-wall nanotubes* may be achieved by a wet chemical reaction; this preferentially attaches hydrogen atoms to most stressed surface sites of these nanostructures. The presence of covalently bonded hydrogen locally weakens the *graphitic* structure, causing fracture and release of *strain energy*.

***References***

Miller G P, Kintigh J, Kim E, Weck P F, Berber S and Tománek D 2008 Hydrogenation of single-wall carbon nanotubes using polyamine reagents: combined experimental and theoretical study *J. Am. Chem. Soc.* **130** 2296

Berber S and Tománek D 2009 Hydrogen-induced disintegration of fullerenes and nanotubes: an ab initio study *Phys. Rev.* B **80** 075427

The **pentagon road** is a growth model that reflects the energetic benefit of introducing pentagonal rings in growing small flat hexagonal networks of carbon to reduce the *edge energy* associated with dangling bonds. If the temperature and timescale are such as to permit annealing, finite carbon aggregates will try to eliminate all dangling bonds by incorporating 12 pentagonal rings in accordance with *Euler's theorem*. Stable *fullerene isomers* follow the *isolated pentagon rule* (IPR).

***References***

Smalley R E 1992 Self-assembly of the fullerenes *Acc. Chem. Res.* **25** 98

Robertson D H, Brenner D W and White C T 1992 On the way to fullerenes: molecular dynamics study of the curling and closure of graphitic ribbons *J. Phys. Chem.* **96** 6133

**Periodic minimal surfaces** are space-filling layered structures related to *schwarzites*, which may be formed of $sp^2$ bonded carbon atoms. Periodic minimal surfaces can be classified as either primitive (P), diamond (D) or gyroid (G) surfaces.

A **phase diagram** describes the state of a system as a function of temperature $T$ and pressure $p$. Limits of solid *graphitic* and *diamond* phases, as well as liquid and vapor phases of elemental carbon, are shown in figure 71.

***Reference***

Bundy F P 1989 Pressure-temperature phase diagram of elemental carbon *Physica* A **156** 169

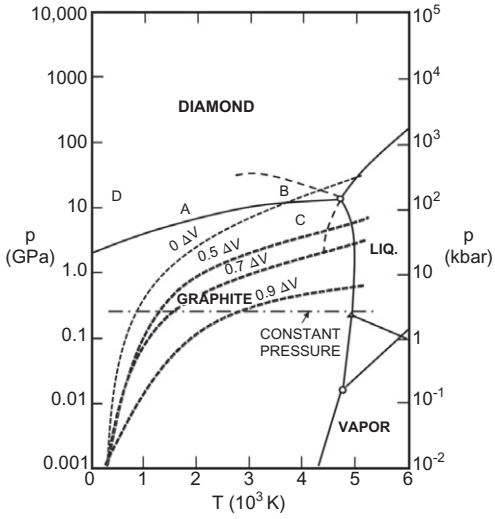


**Figure 71.** Pressure ($p$)–temperature ($T$) phase and reaction diagram of elemental carbon. (A) Region of *catalyst*/solvent *diamond* synthesis from *graphite*; (B) region of fast spontaneous graphite-to-diamond transformation; (C) region of fast spontaneous diamond-to-graphite transformation; (D) region of martensitic transformation of *hexagonal graphite* to hexagonal diamond. Dashed lines represent $p$, $T$ paths that a graphite specimen would take during fast energy insertion with various constraints on bulk expansion, with $0\Delta V$ describing transformation at constant volume. (Reproduced from Bundy F P 1989 *Physica* A **156** 169, © 1989 Elsevier.)

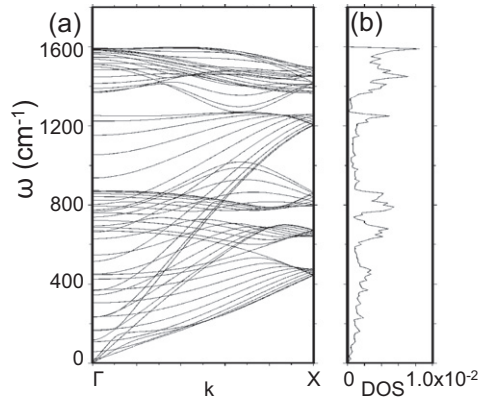


**Figure 72.** (a) *Phonon band structure* and (b) *phonon density of states* (DOS) of a (10,10) *armchair nanotube*. The units of the DOS are (states per carbon atom)/cm$^{-1}$. (Adapted from Saito R *et al* 1998 *Phys. Rev.* B **57** 4145, © 1998 American Physical Society.)

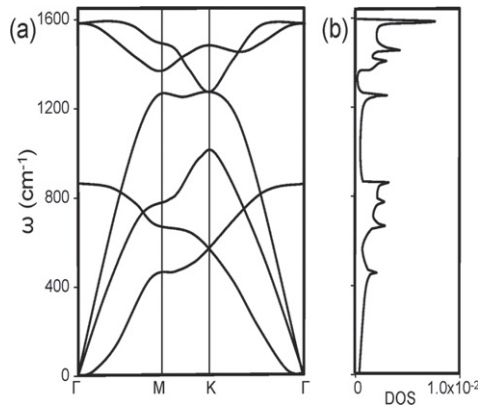


**Figure 73.** (a) *Phonon band structure*, plotted along high symmetry directions, and (b) *phonon density of states* (DOS) of a *graphene* monolayer. The units of the DOS are (states per carbon atom)/cm$^{-1}$. (Adapted from Jishi R *et al* 1993 *Chem. Phys. Lett.* **209** 77, © 1993 Elsevier.)

The **phonon band structure** $\omega(\mathbf{k})$ describes the dispersion of vibrational quantum states as a function of the crystal momentum **k** and is closely related to the *phonon density of states* (DOS). See also *phonon spectrum*.

The **phonon density of states** (DOS) $N(\omega)$, also called vibrational density of states, enumerates the number of vibration modes at angular frequency $\omega$ that are allowed to be occupied. $N(\omega)$ in clusters or *quantum dots*, such as *fullerenes* or *diamondoids*, consists of discrete levels. In one-dimensional wires, such as carbon *chains* and *nanotubes*, $N(\omega)$ is continuous and dominated by peaks called van Hove singularities (see figures 13(c) and 72(b)). $N(\omega)$ is also continuous in two-dimensional systems, such as *graphene* (see figure 73(b)), and three-dimensional systems, such as *diamond*.

The **phonon mean free path** $\lambda_p$ is the average distance a vibrational excitation travels without collisions. In isotopically pure *diamond*, *graphene* and *nanotubes*, the phonon mean free path at room temperature exceeds several hundred nanometers. $\lambda_p$ is strongly reduced by the presence of *defects*, including isotopic impurities.

**Phonon spectrum** → *phonon spectrum of a chain*, *phonon spectrum of graphene* or *phonon spectrum of a nanotube*

The **phonon spectrum of a chain** is shown in figure 13(b). The *phonon density of states* (DOS), depicted in figure 13(c), is dominated by sharp peaks representing van Hove singularities that are characteristic of 1D structures.

The **phonon spectrum of a nanotube** is shown in figure 72 and is closely related to the *phonon spectrum of graphene*. Similar to *graphite*, *supramolecular interactions* in *ropes* may affect the phonon spectrum.

***Reference***

Rao A M, Chen J, Richter E, Eklund P C, Haddon R C, Venkateswaran U D, Kwon Y-K and Tománek D 2001 Effect of van der Waals interactions on the Raman modes in single walled carbon nanotubes *Phys. Rev. Lett.* **86** 3895

The **phonon spectrum of graphene** is shown in figure 73.

**Photochemical processes** are a special case of *excited state dynamics* in nanocarbons that include photo-induced *polymerization* of *fullerenes* and other changes in their structure. The energy provided by the absorbed photon excites electrons from the ground state, thereby often reducing the activation barrier and thus facilitating a structural change during the lifetime of the photo-excitation, which can last in excess of a picosecond. Conversion of $CO_2$ to elemental carbon and $O_2$ in photosynthesis is a prominent example of a photochemical process.

***References***

Miyamoto Y, Zhang H and Tománek D 2010 Photo-exfoliation of graphene from graphite: An *ab initio* study *Phys. Rev. Lett.* **104** 208302

Raman R K, Murooka Y, Ruan C-Y, Yang T, Berber S and Tománek D 2008 Direct observation of optically induced transient structures in graphite using ultrafast electron crystallography *Phys. Rev. Lett.* **101** 077401

Nüuske R, Jurgilaitis A, Enquist H, Harb M, Fang Y, Håkanson U and Larsson J 2012 Transforming graphite to nanoscale diamonds by a femtosecond laser pulse *Appl. Phys. Lett.* **100** 043102

**Photocurrents** may be generated in *nanotubes* and *graphene* by coherent one-photon and *two-photon absorption* processes and set atoms into motion by electromigration.

***References***

Král P and Tománek D 1999 Laser driven atomic pump *Phys. Rev. Lett.* **82** 5373

Mele E J, Král P and Tománek D 2000 Coherent control of photocurrents in graphene and carbon nanotubes *Phys. Rev.* B **61** 7669

**Photoluminescence** spectroscopy allows the identification of the *chiral index* ($n$, $m$) of semiconducting *single-wall nanotubes*. Incident monochromatic light inducing a transition between the second

set of van Hove singularities from the Fermi level (see figure 29), $h\nu_i = E_{22} = E(c_2) - E(v_2)$, is re-emitted as a transition between the first set of van Hove singularities from the Fermi level, $h\nu_f = E_{11} = E(c_1) - E(v_1)$. The combination ($E_{11}$, $E_{22}$) uniquely identifies the chiral index of a *nanotube*.

***References***

O'Connell M J, Bachilo S M, Huffman C B, Moore V C, Strano M S, Haroz E H, Rialon K L, Boul P J, Noon W H, Kittrell C, Ma J, Hauge R H, Weisman R B and Smalley R E 2002 Band gap fluorescence from individual single-walled carbon nanotubes *Science* **297** 593

Bachilo S M, Strano M S, Kittrell C, Hauge R H, Smalley R E and Bruce W R 2002 Structure-assigned optical spectra of single--walled carbon nanotubes *Science* **298** 2361

A **photovoltaic device** consists of a semiconductor that absorbs energy provided by light and converts it to electrical energy by generating and spatially separating electron—hole pairs in a photodiode setup. Semiconducting *nanotubes* appear to be excellent candidates for future ultra-efficient photovoltaic devices.

***Reference***

Gabor N M, Zhong Z, Bosnick K, Park J and McEuen P L 2009 Extremely efficient multiple electron—hole pair generation in carbon nanotube photodiodes *Science* **325** 1367

The **plasmon mode** is a collective electronic excitation occurring in all polarizable (not necessarily metallic) carbon nanostructures including *graphite*, *fullerenes* and *nanotubes*. *Graphitic* nanostructures display the $\pi$-plasmon mode at $h\nu \approx 7$ eV and the $\sigma$-plasmon at $h\nu \approx 20$ eV. The $\pi$-plasmon involves mainly electrons in the non-bonding C2$p_\pi$ orbitals and is excited by an electric field polarized parallel to the plane of $sp^2$ bonded carbon atoms. The $\sigma$-plasmon involves mainly electrons in the bonding $sp\sigma$ states and is excited by an electric field polarized normal to the plane of $sp^2$ bonded carbon atoms.

***References***

Zeppenfeld K 1968 Anisotropy of plasma oscillations in graphite' [in German; original title 'Anisotropie der Plasmaschwingungen in Graphit'] *Z. Phys.* **211** 391

Bertsch G F, Bulgac A, Tománek D and Wang Y 1991 Collective plasmon excitations in $C_{60}$ clusters *Phys. Rev. Lett.* **67** 2690

Hertel I V, Steger H, de Vries J, Weisser B, Menzel C, Kamke B and Kamke W 1992 Giant plasmon excitation in free $C_{60}$ and $C_{60}$ molecules studied by photoionization *Phys. Rev. Lett.* **68** 784

Gensterblum G, Pireaux J J, Thiry P A, Caudano R, Vigneron J P, Lambin P, Lucas A A and Krätschmer W 1991 High-resolution electron-energy-loss spectroscopy of thin films of $C_{60}$ on Si(100) *Phys. Rev. Lett.* **67** 2171

**PLV** → *pulsed laser vaporization*

**Polarizability** $\alpha$, often taken synonymous with electronic polarizability, describes the displacement of the electric charge, which induces the dipole $p$ in response to an applied electric field $E$, and is defined by $p = \alpha E$. Static polarizability describes the response to a constant electric field, whereas dynamic polarizability $\alpha(\omega)$ describes the response to a time-dependent field $E(\omega)$. *Graphitic* carbon nanostructures, including *fullerenes*, *graphite*, *graphene* and metallic carbon *nanotubes*, have zero *fundamental band gaps* and are thus highly polarizable. Quantum size effects further enhance the polarizability of

nanocarbons. Higher-order terms, called *hyperpolarizability*, are needed to describe the dielectric response in systems and under conditions when $p$ is not proportional to $E$.

***Reference***

Kostov G K, Pacheco J M and Tománek D 2004 Quantum size effects in the polarizability of carbon fullerenes *Phys. Rev. Lett.* **92** 215501

**Polyhedral curvature C**, sometimes called the defect of a vertex, is used to characterize the local morphology at nanocarbon surfaces represented as polyhedra, and is related to the *Gaussian curvature*. Its value at each surface atom considered a vertex is given by $C = 360^\circ - \sum_i \phi_i$, where the summation extends over all face angles $\phi_i$ at the vertex. In a $C_n$ *fullerene* with completely planar faces, according to *Descartes' lost theorem*, the sum of polyhedral curvatures at all $n$ atoms is $\sum_i^n C_i = 720^\circ$. Deviations from planarity in $sp^2$-bonded structures come at an energy penalty that is associated with a non-zero value of $C$.

**Polymerization** is a chemical reaction that connects individual molecules, called monomers, into 1D, 2D or 3D networks called polymers. Polymerization of *fullerenes* may be induced by applying pressures exceeding 6 GPa, by exposure to an electron beam or to light, as a *photochemical process*. The initial step is often the 2+2 *cycloaddition* reaction depicted in figure 22.

***References***

Iwasa Y, Arima T, Fleming R M, Siegrist T, Zhou O, Haddon R C, Rothberg L J, Lyons K B, Carter Jr H L, Hebard A F, Tycko R, Dabbagh G, Krajewski J J, Thomas G A and Yagi T 1994 New phases of $C_{60}$ synthesized at high pressure *Science* **264** 1570

Zhao Y B, Poirier D M, Pechman R J and Weaver J H 1994 Electron stimulated polymerization of solid $C_{60}$ *Appl. Phys. Lett.* **64** 577

A **polyyne chain** is a specific *isomer* of a *chain* of carbon atoms (C−C≡C−C⋯) connected by alternating single and triple bonds.

**Pseudospin** $\sigma$ has nothing to do with the magnetic moment of a spinning electron. It is a quantum number associated with the motion of carriers in *graphitic* structures including *graphene* and *nanotubes*. The name implies a formal correspondence between the *electronic band structure* of graphene near the *Dirac points* K and K′ and that of relativistic electrons with zero rest mass. Such electrons are described by the Dirac–Weyl equation $H_{\mathrm{DW}}(\mathrm{K}) = v_{\mathrm{F}}\sigma \cdot \mathbf{p}$ and $H_{\mathrm{DW}}(\mathrm{K}') = v_{\mathrm{F}}\sigma' \cdot \mathbf{p}$. Here, $v_{\mathrm{F}}$ is the *Fermi velocity*, $\mathbf{p}$ the momentum of the electrons, $\sigma = (\sigma_x, \sigma_y)$ and $\sigma' = (-\sigma_x, \sigma_y)$. The right-handed Dirac–Weyl equation at K describes particles of opposite *chirality*, namely electrons and holes. The two spin directions in the true Dirac–Weyl equation correspond to the projection of the particle wavefunction onto *sublattice* $\alpha$ or $\beta$ in graphene. Electrons and holes with momentum near K and pseudospin $\sigma$ move on sublattice $\alpha$, those with momentum near K′ and pseudospin $\sigma'$ move on sublattice $\beta$. Absence of scattering from one sublattice to the other, described as conservation of pseudospin, lies behind the high *electron mobility*, and corresponding high hole mobility, in graphitic systems.

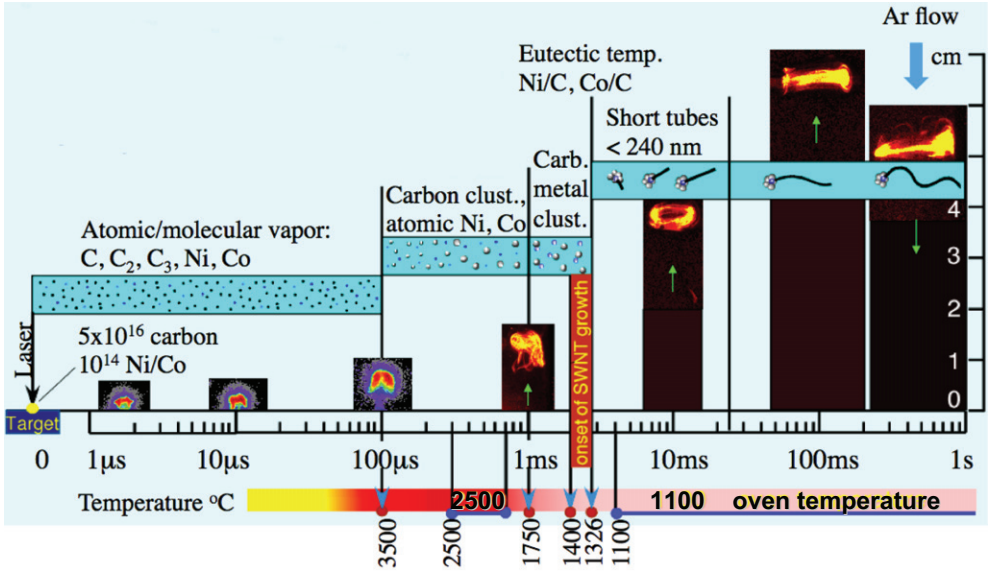


**Figure 74.** Summary of *in situ* imaging and spectroscopic characterization of *single-wall nanotube* growth using *pulsed laser vaporization*. The time evolution and the corresponding temperature are shown horizontally, the actual distance from the target vertically. *Rayleigh scattering* images of the plume, shown for $t > 200$ $\mu$s, depict the condensation of carbon atoms to nanotubes. (From Puretzky A A *et al* 2002 *Phys. Rev.* B **65** 245425, © 2002 American Physical Society.)

**Pulsed laser vaporization** (PLV) is a method to produce *fullerenes* or high quality *nanotubes* by irradiating pure solid carbon with a powerful laser beam. The *growth process* is depicted in figure 74 and, schematically, in figure 46.

***Reference***

Puretzky A A, Schittenhelm H, Fan X, Lance M J, Allard, Jr. L F and Geohegan D B 2002 Investigations of single-wall carbon nanotube growth by time-restricted laser vaporization *Phys. Rev.* B **65** 245425

The **purification** of carbon *nanotubes* often involves harsh acid treatment or exposure to oxidizing agents. Exposure to ultrasound helps in the process.

The **purity** of *graphitic* carbon nanostructures (*fullerenes*, *single-wall nanotubes*) is commonly assessed using *Raman spectroscopy*. A useful purity designator is the intensity ratio between the *D-band* and the *G-band*, which should be small. The presence of catalytic particles is commonly investigated using thermogravimetric analysis (TGA).

**Pyrolysis** is a thermochemical decomposition of a carbon-containing substance at high temperatures in the absence of oxygen. Pyrolysis is commonly used to produce charcoal or activated carbon, but may lead to the formation of *nanotubes* under specific conditions.

***Reference***

Terrones M, Grobert N, Olivares J, Zhang J P, Terrones H, Kordaros K, Hsu W K, Hare J P, Townsend P D, Prassides K,

Cheetham A K, Kroto H W and Walton D R M 1997 Controlled production of aligned-nanotube bundles *Nature* **388** 52

# Q

**Quantized conductance** → *conductance* or *conductance quantum*

A **quantum dot** is a nanostructure such as an atomic cluster, including a *fullerene*, or a nanometer-sized constrained region in a larger structure, where quantization of electronic levels plays a dominant role.

The **quantum Hall effect** (QHE) is a quantum mechanical enhancement of the Hall effect, which describes the response of electrons in a two-dimensional system such as *graphene* to a strong perpendicular magnetic field and is most pronounced at low temperatures. Discrete changes in the transverse Hall voltage occur at magnetic field values when electronic Landau orbits cross the Fermi surface. The Hall resistance $R_H = V_H/I$ is defined by the ratio of the Hall voltage $V_H$ and the current $I$. The Hall *conductance*, which is the inverse of the Hall resistance, is quantized as $1/R_H = \nu e^2/h$, where $e$ is the elementary charge, $h$ is Planck's constant and $R_K = h/e^2 = 25.8128$ kΩ is the von Klitzing resistance. The prefactor $\nu$, known as the 'filling factor', is either an integer in the 'integer quantum Hall effect' or a rational number (a fraction) in the 'fractional quantum Hall effect'. Graphene displays a half-integer quantum Hall effect.

***References***

Zheng Y and Ando T 2002 Hall conductivity of a two-dimensional graphite system *Phys. Rev.* B **65** 245420

Zhang Y, Tan Y-W, Stormer H L and Kim P 2005 Experimental observation of the quantum Hall effect and Berry's phase in graphene *Nature* **438** 201

# R

The **radial breathing mode** (RBM) is a *Raman-active* low-frequency mode of *fullerenes* and *single-wall nanotubes* (see figure 77). The RBM frequency in $C_{60}$ is $\omega_{RBM} = 497$ cm$^{-1}$. Its strong *diameter* dependence in carbon *nanotubes*, given by $\omega_{RBM} = 248\ \text{cm}^{-1} \times (1\ \text{nm}/d_t)$, is commonly used to determine the *nanotube diameter* $d_t$. This mode is not observed in multi-wall structures.

***Reference***

Rao A M, Richter E, Bandow S, Chase B, Eklund P C, Williams K A, Fang S, Subbaswamy K R, Menon M, Thess A, Smalley R E, Dresselhaus G and Dresselhaus M S 1997 Diameter-selective Raman scattering from vibrational modes in carbon nanotubes *Science* **275** 187

**Radiation hardness** is the resistance of a structure exposed to energetic particles or electromagnetic radiation. Carbon nanostructures are radiation hard (rad-hard) to a high degree. Structural changes, including the conversion of a *graphitic onion* into *diamond* shown in figure 75, have been observed in carbon nanostructures exposed to the energetic electron beam in an electron microscope.

***Reference***

Banhart F 1999 Irradiation effects in carbon nanostructures *Rep. Prog. Phys.* **62** 1181

**Radius** of a *fullerene* or a *single-wall nanotube* → *diameter of a fullerene* or *diameter of a nanotube*

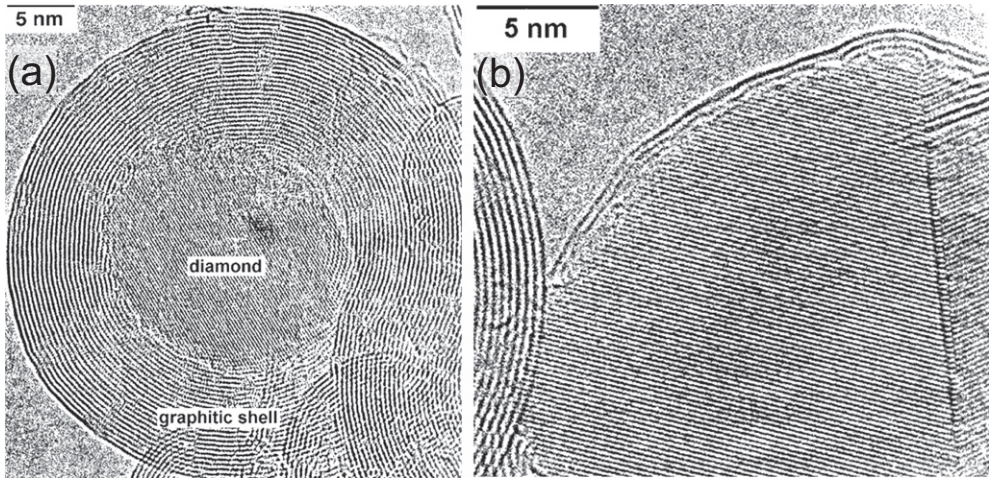


**Figure 75.** (a) Carbon *onion* structure with a *diamond* core. (b) Continuing conversion of the *graphitic* onion walls into diamond under extended electron irradiation. The monocrystalline nature of the core can be inferred from the dominating contribution of the (111) planes of diamond to the lattice image. (Adapted from Banhart F 1999 *Rep. Prog. Phys.* **62** 1181, © 1999 Institute of Physics.)

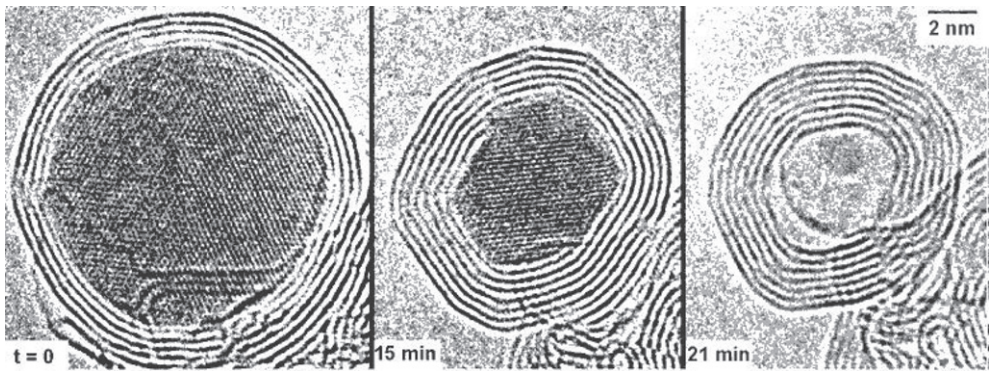


**Figure 76.** Gradual contraction of a carbon *onion* squeezing out an encapsulated cobalt nanoparticle during electron irradiation at 700 °C. (Adapted from Florian Banhart 1999 *Rep. Prog. Phys.* **62** 1181, © 1999 Institute of Physics.)

**Raman spectroscopy** is a powerful experimental technique based on inelastic scattering of visual light to measure vibrations in carbon nanostructures. The frequency of an incident laser beam is observed either to decrease (Stokes) by exciting or increase (anti-Stokes) by de-exciting a *Raman-active* vibrational mode. The observed signal is especially strong in the case of resonant Raman spectra, where the incident photon energy $h\nu$ matches electronic transitions with strong optical absorption between quantum levels with the same crystal momentum $k$. Micro-Raman spectroscopy achieves its high spatial resolution by focussing the laser beam onto a $1\,\mu$m spot. Nano-Raman

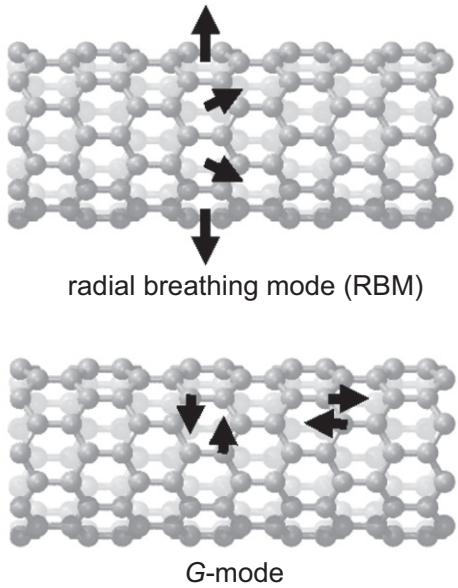


**Figure 77.** Atomic displacements during *radial breathing mode* (RBM) and *G-band* vibrations of a *nanotube*.

spectroscopy utilizes the fact that the Raman signal is enhanced by many orders of magnitude near a sharp noble metal tip. Scanning the tip across the sample yields Raman signals with ≈1 nm spatial resolution.

**Raman-active** modes are vibrational modes observable by *Raman spectroscopy*. Commonly discussed modes in *graphitic* nanostructures including *fullerenes* and *nanotubes* are the *radial breathing mode* (RBM) at low frequencies $\omega \lesssim 400\ \mathrm{cm}^{-1}$, the so-called *D-band* at $\omega \approx 1340\ \mathrm{cm}^{-1}$ that is associated with disordered graphitic material, and the *G-band* that is associated with C–C stretch modes occurring in *graphite* at $\omega = 1582\ \mathrm{cm}^{-1}$ (see figure 77).

***Reference***

Puretzky A A, Geohegan D B and Rouleau C M 2010 Narrow and intense resonances in the low-frequency region of surface-enhanced Raman spectra of single-wall carbon nanotubes *Phys. Rev.* B **82** 245402

**Rayleigh scattering** is a powerful spectroscopic technique based on elastic scattering of visible light, capable of determining the *chiral index* ($n$, $m$) of carbon *nanotubes* irrespective of their *conductance*.

***Reference***

Sfeir M Y, Wang F, Huang L, Chuang C-C, Hone J, O'Brien S P, Heinz T F and Brus L E 2004 Probing electronic transitions in individual carbon nanotubes by Rayleigh scattering *Science* **306** 1540

**Reconstruction** at the surface of *diamond*, the edge of *graphene* or a *nanotube* is a structural change causing chemical passivation by decreasing the *surface energy* or the *edge energy*. Possible reconstructions of bare graphene edges are illustrated in figure 78.

***Reference***

Koskinen P, Malola S and Häkkinen H 2008 Self-passivating edge reconstructions of graphene *Phys. Rev. Lett.* **101** 115502

**Rhombohedral graphite** is *graphite* exhibiting rhombohedral or ABC stacking of *graphene* layers. Rhombohedral graphite, with a primitive unit cell containing only two atoms, is nearly as stable as *hexagonal graphite*.

A **ribbon**, also called a *nanotube* ribbon, is a *graphitic* structure that forms spontaneously by the collapse of a wide nanotube with a *diameter* $d_t \gtrsim 5.4$ nm without breaking any bonds, as seen in figure 79. The edge of the ribbon resembles that of a *folded graphene*

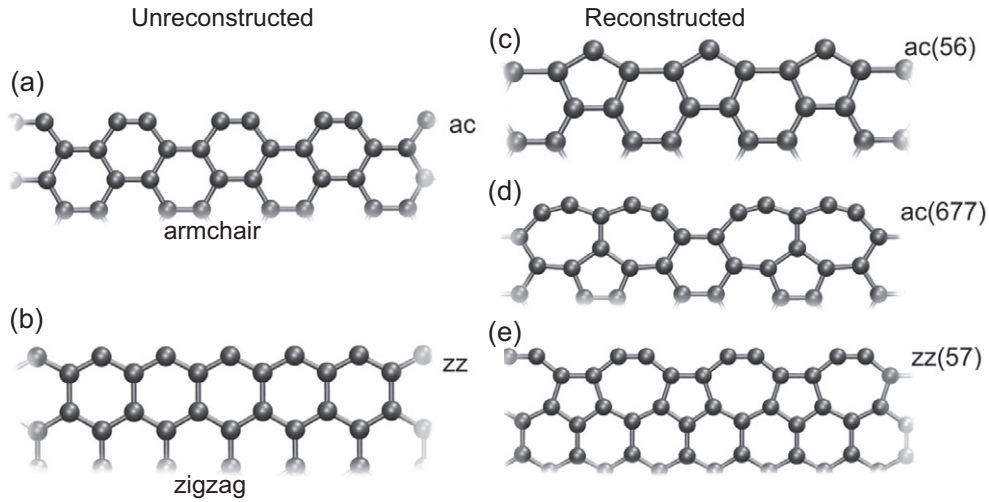


**Figure 78.** Atomic structure of unreconstructed and reconstructed bare *graphene* edges. (a) Unreconstructed *armchair edge* (ac) and (b) *zigzag edge* (zz) as reference systems. There are changes in the total energy due to *reconstruction* at the (c) ac(56) edge, (d) ac(677) edge and (e) zz(57) edge, which is the most stable of all. All geometries are strictly planar. (Adapted following Koskinen P *et al* 2008 *Phys. Rev. Lett.* **101** 115502, © 2008 American Physical Society.)

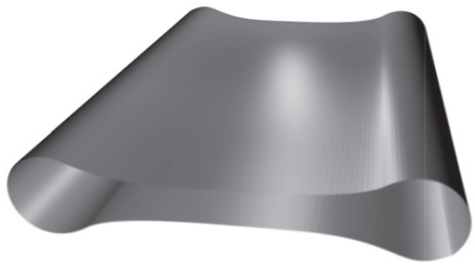

**Figure 79.** Schematic view of the collapse of a wide *nanotube* to a *ribbon*.

*nanoribbon*. It differs from the *graphene nanoribbon* (GNR) structure that contains under-coordinated edge atoms. The optimum shape maximizes the attractive *inter-layer interaction* while minimizing the *strain energy* associated with the *curvature* in the circular bulges near the edges. The inter-layer separation in the middle of wide ribbons is 0.34 nm, the same as in *graphite*. A helical ribbon structure may be produced by twisting a nanotube, as seen in figure 80.

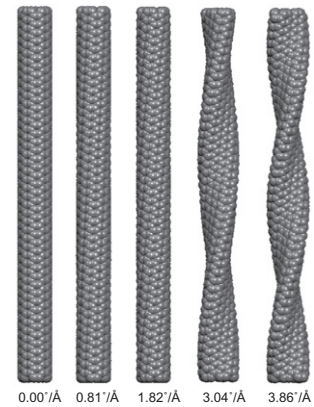


**Figure 80.** Transformation of a carbon *nanotube* to a helical *ribbon* by twisting about its axis. Equilibrium structure is shown at different twist rates.

***Reference***

Chopra N G, Benedict L X, Crespi V H, Cohen M L, Louie S G and Zettl A 1995 Fully collapsed carbon nanotubes *Nature* **377** 135

The **ring-stacking model** is a model of *fullerene* growth that assumes that the carbon network of the fullerene

containing pentagonal and hexagonal rings is assembled sequentially by stacking of monocyclic carbon rings. In contrast to the currently favored *pentagon road* growth mechanism, this early model ignores the energetics of the growing structure. Stable fullerene *isomers* follow the *isolated pentagon rule* (IPR).

***Reference***

Wakabayashi T and Achiba Y 1992 A model for the $C_{60}$ and $C_{70}$ growth mechanism *Chem. Phys. Lett.* **190** 465

**Rippling** is a phenomenon observed on free-standing *graphene* monolayers.

***Reference***

Lui C H, Liu L, Mak K F, Flynn G W and Heinz T F 2009 Ultraflat graphene *Nature* **462** 339

**Rope** is an aggregate of axially aligned-*single-wall nanotubes*, held together by weak *inter-layer interactions*, similar to those binding *graphene* layers in *graphite*.

***Reference***

Thess A, Lee R, Nikolaev P, Dai H, Petit P, Robert J, Xu C, Lee Y-H, Kim S G, Colbert D T, Scuseria G, Tománek D, Fischer J E and Smalley R E 1996 Crystalline ropes of metallic carbon nanotubes *Science* **273** 483

The **rotation** of individual nanostructures including *fullerenes* has been observed in *solid $C_{60}$* and in *nanotube peapods*.

# S

**Scanning electron microscopy** (SEM) is a technique that probes a sample by scanning a focused electron beam across its surface in a raster pattern. The image is constructed by mapping the intensity of secondary electrons, which are emitted from the surface in response to the excitation by the primary electron beam, with the beam position. SEM resolution, currently about 1 nm, is about one order of magnitude lower than that of *transmission electron microscopy* (TEM) images. Since the SEM image relies on electrons interacting with the surface rather than transmission in TEM, it is suitable to image bulk samples and provides a high depth of view, producing images that represent well the 3D structure of the sample.

**Scanning tunneling microscopy** (STM) is a local probe with atomic resolution that samples the spatial distribution of electronic states near the Fermi level. In *hexagonal graphite*, the STM signal shows a strong asymmetry between the inequivalent $\alpha$ and $\beta$ *sublattices*, shown in figure 44. As seen in figure 81, the signal is particularly strong at sites of the $\beta$ sublattice with no neighbors above and below in the adjacent layers, since the reduced band dispersion at these sites, shown in figure 45(b), increases the local *electronic density of states* at $E_F$. No such asymmetry occurs in *graphene*, *single-wall nanotubes* or other single-wall *graphitic* structures.

***References***

Tománek D, Louie S G, Mamin H J, Abraham D W, Thomson R E, Ganz E and Clarke J 1987 Theory and observation of highly asymmetric atomic structure in scanning tunneling microscopy images of graphite *Phys. Rev.* B **35** 7790(R)

Wildoer J W G, Venema L C, Rinzler A G, Smalley R E and Dekker C 1998 Electronic structure of atomically resolved carbon nanotubes *Nature* **391** 59

Odom T-W, Huang J-L, Kim P and Lieber C M 1998 Atomic structure and electronic properties of single-walled carbon nanotubes *Nature* **391** 62

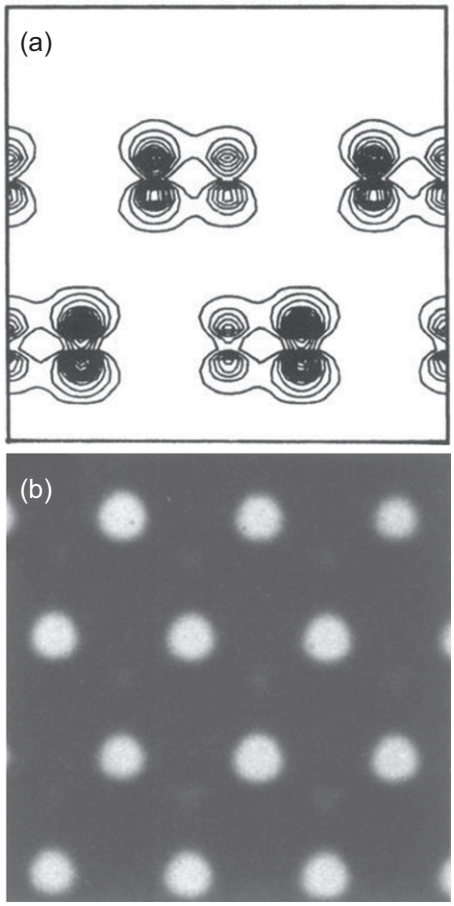


**Figure 81.** Spatial distribution of states contributing to *scanning tunneling microscopy* (STM) images of a *hexagonal graphite* surface at a bias voltage of 0.25 V. Calculated values are shown (a) in a plane normal to the surface and (b) in a plane parallel to the surface, at 1 Å separation from the topmost layer. (Adapted from Tománek D and Louie S G 1988 *Phys. Rev.* B **37** 8327, © 1988 American Physical Society.)

The **Schlegel diagram** is a schematic projection of a structure in three-dimensional space onto a plane. As seen in figure 82, the Schlegel diagram provides a convenient representation especially of *fullerene* structures, since it correctly reproduces the topological neighborhood of all atoms.

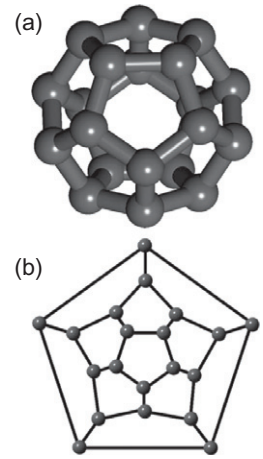


**Figure 82.** (a) A ball-and-stick model and (b) the corresponding *Schlegel diagram* of the $C_{20}$ *fullerene* structure.

**Schmutz**, from the German word for 'dirt', this is a common designation of a non-specific carbon overcoating commonly found on *nanotubes*. Often, such carbonaceous deposits are incorrectly referred to as *amorphous carbon*.

The **Schottky barrier** is a carrier-depleted region occurring at metal–semiconductor junctions. It is observed at metal *contacts* to semiconducting carbon *nanotubes* in nanotube-based *logic circuits*.

***Reference***

Heinze S, Tersoff J, Martel R, Derycke V, Appenzeller J and Avouris P 2002 Carbon nanotubes as Schottky barrier transistors *Phys. Rev. Lett.* **89** 106801

**Schwarzite** is a contiguous space-filling structure of $sp^2$ carbon with regions of negative *Gaussian curvature*. One possible schwarzite structure is shown in figure 83. The name derives from the German mathematician H A Schwarz (1843–1921), who studied minimal surfaces. Schwarzites, *periodic minimal surfaces* formed of *graphene* with

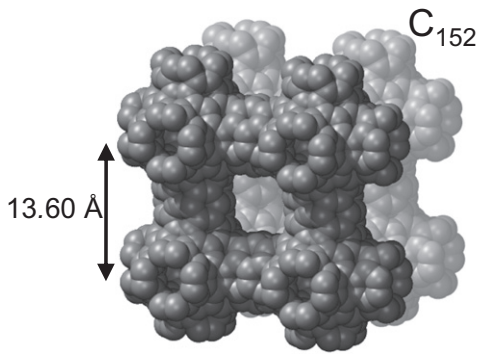


**Figure 83.** Equilibrium structure of a *schwarzite* lattice with 152 atoms per unit cell. (Adapted from Park S *et al* 2010 *J. Phys.: Condens. Matter* **22** 334220, © 2010 Institute of Physics.)

heptagonal *defects*, are unique in their ability to subdivide space into two disjoint, contiguous subspaces with labyrinthine morphology and infinite spatial extent. Negative Gaussian curvature in *graphitic* structures is favored near boron substitutional impurities. Schwarzites are related to *foams*, may be structurally rigid and exhibit unusual electronic and magnetic properties.

***References***

Mackay A L and Terrones H 1991 Diamond from graphite *Nature* **352** 762

Park S, Kittimanapun K, Ahn J-S, Kwon Y-K and Tománek D 2010 Designing rigid carbon foams *J. Phys.: Condens. Matter* **22** 334220

Jana P and Ganesan V 2009 Synthesis, characterization and radionuclide ($^{137}$Cs) trapping properties of a carbon foam *Carbon* **47** 3001

Hashim D P, Narayanan N T, Romo-Herrera J M, Cullen D A, Hahm M G, Lezzi P, Suttle J R, Kelkhoff D, Muñoz-Sandoval E, Ganguli S, Roy A K, Smith D J, Vajtai R, Sumpter B G, Meunier V, Terrones H, Terrones M and Ajayan P M 2012 Covalently bonded three-dimensional carbon nanotube solids via boron induced nanojunctions *Sci. Rep.* **2** 363

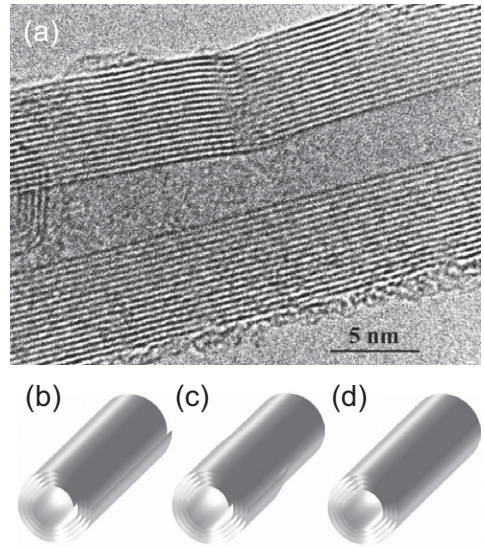


**Figure 84.** Coexistence of a *scroll* and a *multi-wall nanotube* (MWNT) in a single structure. (a) *Transmission electron microscopy* image and schematic representations of (b) a scroll, (c) a scroll–nanotube junction containing a slip-plane *defect*, and (d) a multi-wall nanotube. (Panel (a) reproduced from Lavin J G *et al* 2002 *Carbon* **40** 1123, © 2002 Elsevier.)

The **scooter model** is a growth model for *single-wall nanotubes* in the presence of a *catalyst*. A covalently bonded catalyst metal atom may diffuse fast along the growing edge and selectively suppress the formation of pentagons from accumulating carbon feedstock, thus preventing premature closure by a *dome*. Current understanding is that this represents an oversimplification of the *growth process*.

***Reference***

Lee Y H, Kim S G and Tománek D 1997 Catalytic growth of single-wall nanotubes: An *ab initio* study *Phys. Rev. Lett.* **78** 2393

A **scroll** is a cylindrical structure consisting of a contiguous layer that has been rolled up (see figure 84(b)). It is

very similar in morphology and energy to a *multi-wall nanotube* (MWNT), shown in figure 84(d), with the exception of exposed edges at the innermost and outermost radii. Unlike a MWNT, a scroll consists of a single contiguous *graphene* layer and can change its diameter. The energy cost associated with forming a scroll is shown in figure 61. As seen in figure 84, scrolls and multi-wall nanotubes may coexist in one tubular structure.

***Reference***

Lavin J G, Subramoney S, Ruoff R S, Berber S and Tománek D 2002 Scrolls and nested tubes in multiwall carbon nanotubes *Carbon* **40** 1123

A **sea urchin**, also known as a *dahlia* structure, is a colloquial designation for a compact agglomerate of carbon *nanohorns* formed during the laser ablation process.

**SEM** → *Scanning electron microscopy*

**Separation** → *dispersion*

**Sharpening** of *multi-wall nanotubes* may be achieved by tapering at the point of contact between the nanotube and a metal electrode by electrically driven local vaporization of outer-wall atoms, as seen in figure 85.

***Reference***

Cumings J, Collins P G and Zettl A 2000 Materials: Peeling and sharpening multi-wall nanotubes *Nature* **406** 586

**Shungite** is a natural glassy-like carbon structure containing *fullerenes* and *onions*. The name derives from Shunga in the Karelia region of Russia, where the mineral is mined.

***Reference***

Kovalevski V V, Buseck P R and Cowley J M 2001 Comparison of carbon in shungite rocks to other natural carbons: An X-ray and TEM study *Carbon* **39** 243

A **single-electron transistor** (SET) is a device consisting of a low-capacitance *quantum dot* such as a *fullerene* that is weakly coupled to source and drain electrodes by tunneling *contacts*. At low applied voltages and low temperatures, *Coulomb blockade* dominates charge transport between source and drain. The alignment of the quantized energy levels of the quantum dot with the Fermi level of the electrodes may be changed by a gate voltage causing a potential change at the quantum dot. This in turn controls the current passing through the device.

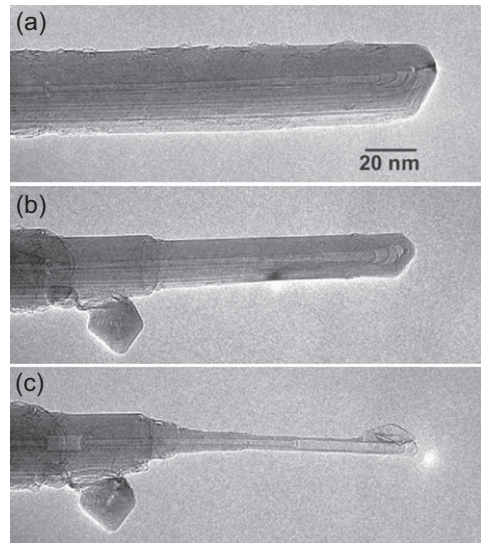


**Figure 85.** *Sharpening* of a *multi-wall nanotube* (MWNT) tip that has been approached successively by an electrode using a nano-manipulator inside a *transmission electron microscope*. (Adapted from Cumings J *et al* 2000 *Nature* **406** 586, © 2000 Nature Publishing Group.)

***Reference***

Park H, Park J, Lim A K. L, Anderson E H, Alivisatos P A and McEuen P L 2000 Nanomechanical oscillations in a single-$C_{60}$ transistor *Nature* **407** 57

A **single-wall nanotube** (SWNT) is a *nanotube* with one wall only. Unlike *multi-wall nanotubes* of carbon, synthesis of single-wall carbon nanotubes (SWCNTs) typically requires the presence of a *catalyst*.

***References***

Iijima S and Ichihashi T 1993 Single-shell carbon nanotubes of 1-nm diameter *Nature* **363** 603

Bethune D S, Kiang C H, DeVries M S, Gorman G, Savoy R and Beyers R 1993 Cobalt-catalysed growth of carbon nanotubes with single-atomic-layer walls *Nature* **363** 605

**Solid $C_{60}$**, also called fullerite, is a molecular crystal consisting of closely packed *$C_{60}$* molecules. The crystal undergoes a first-order *orientational melting* phase transition at $T = 261$ K. The $C_{60}$ molecules rotate independently about their center for $T > 261$ K in the face-centered cubic (fcc) lattice with the *lattice constant* $a = 1.417$ nm. For $T < 261$ K, the orientations of neighboring $C_{60}$ molecules are correlated, causing hindered *rotation*, and the lattice constant drops to $a = 1.404$ nm at $T = 11$ K. At these low temperatures, fullerite is a solid with the simple cubic (sc) structure and four $C_{60}$ molecules with different orientations per unit cell.

***References***

Krätschmer W, Lamb L D, Fostiropoulos K and Huffman D R 1990 Solid $C_{60}$ : a new form of carbon *Nature* **347** 354

Heiney P A, Fischer J E, McGhie A R, Romanow W J, Denenstein A M, McCauley Jr. J P, Smith A B and Cox D E 1991 Orientational ordering transition in solid $C_{60}$ *Phys. Rev. Lett.* **66** 2911

**Sorting of nanotubes** according to *chiral index* $(n, m)$ is an extremely challenging endeavor, since their behavior depends sensitively on their length, their propensity to form nanotube *ropes*, chemical *functionalization* and intrinsic *defects*. Sorting of pristine *nanotubes*, isolated from nanotube ropes, into metallic and semiconducting nanotubes is best achieved using *dielectrophoresis*. Progress towards sorting nanotubes by *chirality* has been made by exposing a nanotube mixture to synthetic single-stranded DNA with a designer base sequence that wraps preferentially around nanotubes of a given chiral index $(n, m)$.

***Reference***

Tu X, Manohar S, Jagota A and Zheng M 2009 DNA sequence motifs for structure-specific recognition and separation of carbon nanotubes *Nature* **460** 250

***sp*$^1$** hybrid orbitals are formed by mixing the $s$ orbital and one of the $p$ orbitals ($p_x$) of carbon. The set of two equivalent $sp^1$ hybrid orbitals, shown in figure 86(a), forms a linear arrangement; the angle between the orbitals is 180°. Strong $sp^1$ $\sigma$ bonds connect carbon atoms in a one-dimensional *chain*. $p$ orbitals not involved in the $sp^1$ bond ($p_y$, $p_z$) form weak $pp$ $\pi$ bonds that dominate the states near the Fermi level, which are important for conduction.

***sp*$^2$** hybrid orbitals are formed by mixing the $s$ orbital and two of the $p$ orbitals ($p_x$, $p_y$) of carbon. The set of three equivalent $sp^2$ hybrid orbitals, shown in

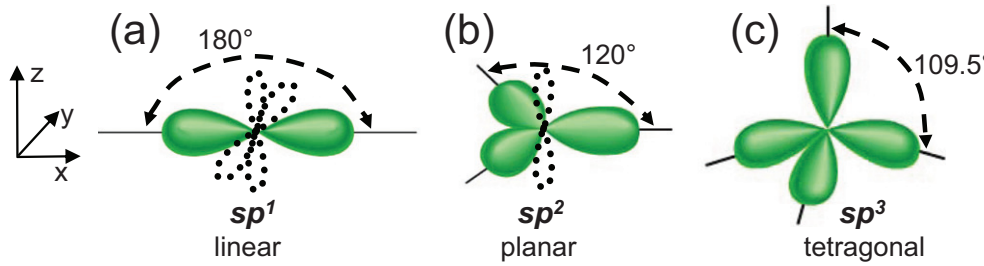


**Figure 86.** Schematic representation of the (a) $sp^1$, (b) $sp^2$ and (c) $sp^3$ hybridization in carbon. Hybrid $sp^n$ ($n$=1–3) orbitals shown in solid color form strong $sp\sigma$ bonds. Dotted $p$ orbitals form weak $pp\pi$ bonds.

figure 86(b), forms a trigonal planar arrangement; the angle between the orbitals is 120°. Strong $sp^2$ $\sigma$ bonds connect carbon atoms in the two-dimensional *graphene* lattice with a locally planar arrangement of carbon atoms, which have three nearest neighbors. Other related $sp^2$ bonded structures include *fullerenes* and *nanotubes*. The $p$ orbital not involved in the $sp^2$ bond ($p_z$) forms weak $pp\pi$ bonds that dominate the states near the Fermi level, which are important for conduction. Carbon atoms in $sp^2$ bonded systems have three neighbors.

***sp*³** hybrid orbitals are formed by mixing the s orbital and all three $p$ orbitals ($p_x$, $p_y$, $p_z$) of carbon. The set of four equivalent $sp^3$ hybrid orbitals, shown in figure 86(c), forms a tetragonal arrangement; the angle between the orbitals is 109.5°. The absence of $pp$ $\pi$ states in $sp^3$ bonded solids is the reason for their insulating behavior. Strong $sp^3$ $\sigma$ bonds, formed of $s$ and all three $p$ orbitals ($p_x$, $p_y$, $p_z$), connect carbon atoms in the three-dimensional *diamond* lattice, where carbon atoms have four nearest neighbors.

The **specific heat** $C_V$ or the heat capacity of a substance at constant volume $V$ describes the amount of heat necessary to raise the temperature of 1 mole of the substance by 1 degree Kelvin. $C_V$ contains contributions from lattice vibrations (phonons) and, in metals, from electrons. $C_V = 0$ at $T = 0$ and $C_V = 3N_A k_B$ for $T \rightarrow \infty$, where $N_A$ is Avogadro's number and $k_B$ is Boltzmann's constant. At low temperatures $T \rightarrow 0$, the electronic contribution is $C_{V,\mathrm{el}} = \frac{1}{3}\pi^2 N(E_\mathrm{F}) k_\mathrm{B}^2 T = \gamma T$, where $N(E_\mathrm{F})$ is the *electronic density of states* at the Fermi energy. The phonon contribution for $T \rightarrow 0$ is $C_{V,ph} = \frac{12}{5}\pi^4 N_A k_B \left(T/T_\mathrm{D}\right)^3 = \delta T^3$, where $T_\mathrm{D}$ is the *Debye temperature*. Phonon contributions dominate in pristine carbon nanostructures, since $N(E_\mathrm{F})$ either vanishes (e.g. in *diamond* or *graphene*) or is very small.

The **speed of sound** $v_\mathrm{s}$ in a substance is given by $v_\mathrm{s} = \sqrt{E/\rho}$, where $E$ is the elastic modulus quantifying the rigidity and $\rho$ is the *gravimetric density*. The low gravimetric density and high elastic modulus of *diamond* are responsible for its high speed of sound of $v_\mathrm{s} = 12\,000$ m s$^{-1}$. Also *graphene* displays high in-plane rigidity, giving rise to a similar in-plane speed of sound of $v_\mathrm{s} = 12\,000$ m s$^{-1}$. The speed of sound along the close-packed (111) direction of *solid* $C_{60}$ has a significantly lower value, $v_\mathrm{s} = 3390$ m s$^{-1}$.

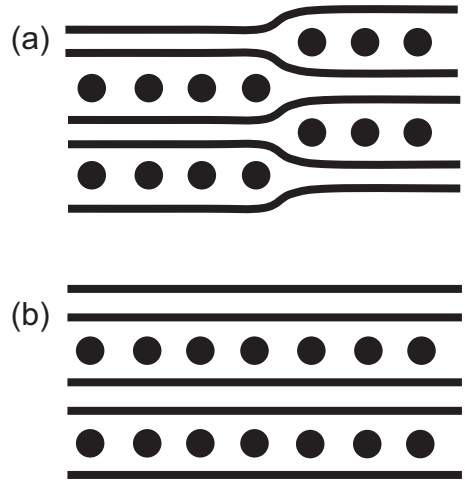


**Figure 87.** Schematic side view of a stage-2 *graphite intercalation compound* (GIC), with solid lines representing the *graphene* layers. Favorable rearrangement of intercalants within the *graphite* galleries (a) gives the appearance of *staging* (b).

***Reference***

Soifer Y, Kobelev N and Levin V 2000 Internal friction and elastic properties of the high pressure-induced phases of solid $C_{60}$ *J. Alloys Compounds* **310** 292

A **staggered edge configuration** in a *graphene nanoribbon* (GNR), different from an *eclipsed edge configuration*, is a geometrical configuration, where the edges are not mirror images with respect to the GNR axis. The difference between the eclipsed and the *staggered edge configuration* is shown in figure 27.

**Staging** is the common term describing the spatial ordering of intercalants in *graphite intercalation compounds* (GICs). Stage-1 compounds contain the same local concentration of intercalants in every inter-layer gallery. In stage-*n* compounds, intercalants appear to be present only in every *n*th gallery. In reality, intercalants are present in all galleries even at low concentrations. They aggregate in regions with high concentration, separated from intercalant-free regions, as seen in figure 87. Staging is a consequence of most efficiently arranging full and empty gallery regions throughout the GIC.

***Reference***

Daumas N and Hérold A 1969 Relations between phase concept and reaction mechanics in graphite insertion compounds *C.R. Hebd. Séances Acad. Sci. Ser.* C **268** 373

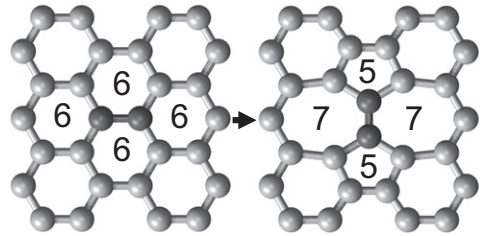


**Figure 88.** Schematic of a *Stone–Wales transformation* that involves a bond rotation within a *Stone–Thrower–Wales defect*.

The **Stone–Thrower–Wales defect** (often called the 'Stone–Wales' defect) consists of a pair of pentagons and a pair of heptagons in a structure of $sp^2$ bonded carbon (see the right panel in figure 88), formed by a *Stone–Wales transformation* of four adjacent hexagons in the honeycomb lattice of a *graphene* layer. The energy cost of a *Stone–Thrower–Wales defect* in *graphene* is $\approx 6$ eV.

***References***

Thrower P A 1969 'Study of defects in graphite by transmission electron microscopy' Walker P L Jr Chemistry and physics of carbon **5** (New York: Marcel Dekker) pp 217–319

Stone A J and Wales D J 1986 Theoretical studies of icosahedral $C_{60}$ and some related species *Chem. Phys. Lett.* **128** 501

The **Stone–Wales transformation** is a chemical process with an activation energy of $\lesssim 6$ eV that causes a $90^\circ$ rotation of an individual C–C bond in an *$sp^2$* lattice (see figure 88). This transformation creates pentagon–heptagon pairs, called *Stone–Thrower–Wales defects* in honeycomb lattices containing hexagons only, or may change the arrangement of pentagons in *fullerenes* or other structures containing pentagons.

The **strain energy** $\Delta E_s$ is the energy penalty associated with the deformation of a reference structure, defined for planar structures in figure 89. The strain energy associated with the deformation of *graphene* to spherical objects is presented in figure 18(a) and to cylindrical objects in figure 61. *Continuum elasticity theory* determines the internal strain energy in a spherical $C_n$ *fullerene* of any size to be $\Delta E_s = 4\ \pi\ D(\alpha + 1) \approx 20.6$ eV, where $D$ is the flexural rigidity and $\alpha$ is the Poisson ratio. This approach furthermore approximates the internal strain energy in a *single-wall nanotube* segment of *radius* $R_t$ and length $L_t$ by $\Delta E_s = \pi D(L_t/R_t) \approx (L_t/R_t) \times 4.43$ eV. Bending a *graphene nanoribbon* (GNR) of area $A$ to become part of a cylinder wall with radius $R_t$ is associated with the strain energy $\Delta E_s \approx (A/R_t^2) \times 0.71$ eV. Bending a graphene flake of area $A$ to form a hemispherical cap of radius $R_s$ is associated with the strain energy $\Delta E_s \approx (A/R_s^2) \times 1.64$ eV. Since the covalent bonds connecting carbon atoms are very strong, elastic deformations caused by external forces require a very large energy investment, making carbon nanostructures very tough.

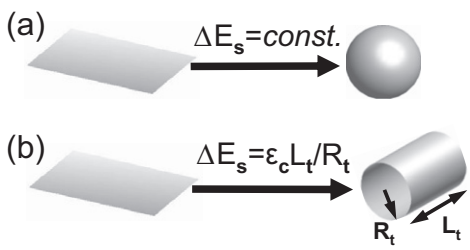


**Figure 89.** Definition and behavior of the *strain energy* in (a) *fullerenes* and (b)*single-wall nanotubes*.

***Reference***

Tománek D, Zhong W and Krastev E 1993 Stability of multi-shell fullerenes *Phys. Rev.* B **48** 15461

A **sublattice** is a periodic structure within a lattice. The honeycomb lattice of *graphene* with two atoms per unit cell consists of two interpenetrating triangular sublattices $\alpha$ and $\beta$, illustrated in figure 44. The *diamond* lattice consists of two interpenetrating face-centered cubic sublattices.

**Superconductivity** with critical temperatures $T_c \lesssim 45$ K has been observed in alkali metal intercalated *solid $C_{60}$* with the composition $M_3C_{60}$ (see figure 90). Superconductivity with critical temperatures $T_c \lesssim 15$ K has been observed in very narrow *single-wall nanotubes* and in *multi-wall nanotubes*. In all these cases superconducting behavior is a consequence of electron–phonon coupling.

***References***

Hebard A F, Rosseinsky M J, Haddon R C, Murphy D W, Glarum S H, Palstra T T M,

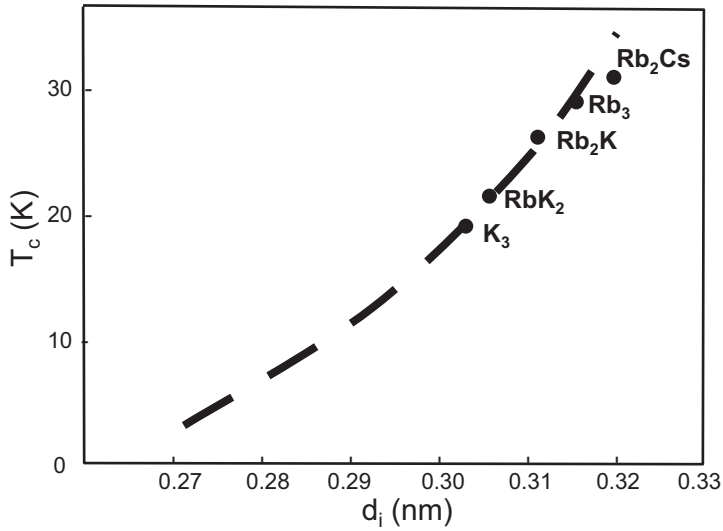


**Figure 90.** Critical temperature $T_c$ for *superconductivity* in solid $M_3C_{60}$, with M denoting an alkali metal, as a function of the wall-to-wall distance $d_i$ of adjacent $C_{60}$ molecules. (Adapted following Schlüter M *et al* 1992 *J. Phys. Chem. Solids* **53** 1473, © 1992 Elsevier.)

Ramirez A P and Kortan A R 1991 Superconductivity at 18 K in potassium-doped $C_{60}$ *Nature* **350** 600

Rosseinsky M J, Ramirez A P, Glarum S H, Murphy D W, Haddon R C, Hebard A F, Palstra T T M, Kortan A R, Zahurak S M and Makhija A V 1991 Superconductivity at 28 K in Rb $C_{60}$ *Phys. Rev. Lett.* **66** 2830

Schluter M, Lannoo M, Needels M, Baraff G A and Tománek D 1992 Electron—phonon coupling and superconductivity in alkali intercalated $C_{60}$ solid *Phys. Rev. Lett.* **68** 526

Kociak M, Kasumov A Y, Guéron S, Reulet B, Khodos I I, Gorbatov Y B, Volkov V T, Vaccarini L and Bouchiat H 2001 Superconductivity in ropes of single-walled carbon nanotubes *Phys. Rev. Lett.* **86** 2416

**Supergrowth** is a common designation for accelerated *nanotube synthesis* by *chemical vapor deposition* (CVD) that leads to the formation of *vertically aligned nanotube arrays* (VANTAs) on a substrate, typically silicon, in the presence of water.

***References***

Hata K, Futaba D N, Mizuno K, Namai T, Yumura M and Iijima S 2004 Water-assisted highly efficient synthesis of impurity-free single-walled carbon nanotubes *Science* **306** 1362

Noda S, Hasegawa K, Sugime H, Kakehi K, Zhang Z, Maruyama S and Yamaguchi Y 2007 Millimeter-thick single-walled carbon nanotube forests: hidden role of catalyst support *Japan. J. Appl. Phys.* **46** L399

**Supramolecular interactions** are interactions between carbon nanostructures and their environment, including a solid substrate. These interactions cause the aggregation of $C_{60}$ molecules to *solid* $C_{60}$, carbon *nanotubes* to *bundles* or *ropes*. Supramolecular interactions may modify the *phonon spectrum of a*

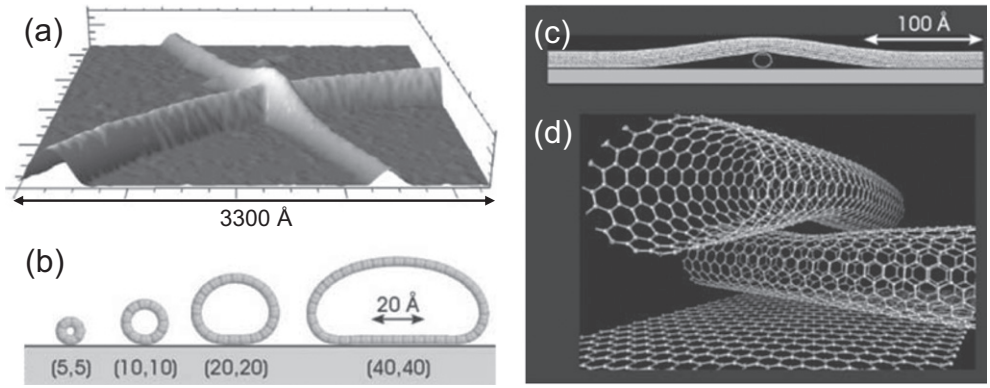


**Figure 91.** Structure of two *nanotubes* crossing on a substrate. (a) Non-contact AFM image of two overlapping nanotubes on a substrate. (b)–(d) Results of molecular mechanics calculations for axial and radial deformations of single-wall carbon nanotubes adsorbed on *graphite*. (Adapted from Avouris P *et al* 1999 *Appl. Surf. Sci.* **141** 201, © 1999 Elsevier.)

*nanotube* or cause deformations, as seen in figure 91 for nanotubes on a substrate.

**Surface energy**, also known as surface tension $\gamma = \Delta E/A$, is given by the ratio of the energy $\Delta E$ needed to cleave an infinite bulk structure and the total area $A$ of the two surfaces. The surface energy is the 3D counterpart of the *edge energy* in 2D systems, and its precise value depends on the surface morphology. Surface *reconstruction* reflects the general tendency to reduce surface energy. Systems with a low surface energy, such as *graphite*, are often unreactive.

A **surfactant** such as sodium dodecyl sulphate (SDS) is a substance used to separate *single-wall nanotubes* from within *ropes*.

**SWNT** → *single-wall nanotube*

The **synthesis temperature** of *graphitic* carbon nanostructures in all common *growth processes* (*arc evaporation* (AE), *pulsed laser vaporization* (PLV), the *HiPCO process*, *chemical vapor deposition* (CVD)), with the exception of *ball milling* (BM), is close to 1000 °C.

# T

**Telescopic motion** is associated with the pulling out of interior walls axially from within the outer walls of a *multi-wall nanotube* structure.

***Reference***

Kis A, Jensen K, Aloni S, Mickelson W and Zettl A 2006 Interlayer forces and ultralow sliding friction in multiwalled carbon nanotubes *Phys. Rev. Lett.* **97** 025501

**TEM** → *Transmission electron microscopy*

**Therapeutic applications** of carbon *nanotubes* exploit their combination of high rigidity at small *diameters*, their *thermal stability* and electronic as well as *optical properties*. Drug delivery has been achieved by attaching biomolecules to nanotubes that can

pass through cell membranes without damage, by endocytosis, whereby the nanostructure is engulfed with protrusions of the cell membrane. Selective attachment of carbon nanotubes to cancerous cells and subsequent irradiation by infrared light has been used for photodynamic therapy of cancer.

**Thermal conductivity** $\kappa$ of carbon nanostructures varies strongly from system to system and, except at extremely low temperatures, is dominated by the contribution of vibrations. $\kappa$ is proportional to the *speed of sound* $v_s$, the *Debye frequency* $\nu_D$, and the *phonon mean free path* $\lambda_p$. Phonon transport is *ballistic* in *single-wall nanotubes* for distances $d < \lambda_p$. Very high values of the product $v_s \cdot \nu_D \cdot \lambda_p$ are responsible for the record value $\kappa \approx 40\,000$ W m$^{-1}$ K$^{-1}$ in isotopically pure *diamond* and single-wall carbon nanotubes (SWNTs) at $T = 100$ K. At room temperature this value drops to $\kappa \approx 3300$ W m$^{-1}$ K$^{-1}$ in $^{12}$C diamond and $\kappa \lesssim 6600$ W m$^{-1}$ K$^{-1}$ in SWNTs and *graphene*. The in-plane thermal conductivity of *graphite* is one order of magnitude smaller than that of graphene due to the reduced value of $\lambda_p$.

***Reference***

Berber S, Kwon Y-K and Tománek D 2000 Unusually high thermal conductivity of carbon nanotubes *Phys. Rev. Lett.* **84** 4613

**Thermal contraction** is negative *thermal expansion*.

**Thermal expansion** is the commonly observed increase in length and volume in response to an increase in temperature. Thermal contraction (described as negative thermal expansion) occurs in filamentous systems such as *nanotubes* and layered systems such as *graphene* or *graphite* up to $\approx 1000$ °C. It is caused mainly by the thermal activation of long-wavelength transverse vibrational modes that increase entropy and reduce the lateral system size.

***Reference***

Kwon Y-K, Berber S and Tománek D 2004 Thermal contraction of carbon fullerenes and nanotubes *Phys. Rev. Lett.* **92** 015901

**Thermal stability** of all-carbon structures such as *fullerenes*, *diamond*, *graphene*, *graphite* and *nanotubes* under vacuum conditions extends to $T \approx 3000$ °C. The presence of oxygen lowers the onset temperature of disintegration.

A **torus** is a hypothetical *nanotube*-based structure in the shape of a donut, shown schematically in figure 92. Observed structures resembling a torus, shown in figure 93, are in reality nanotubes coiled

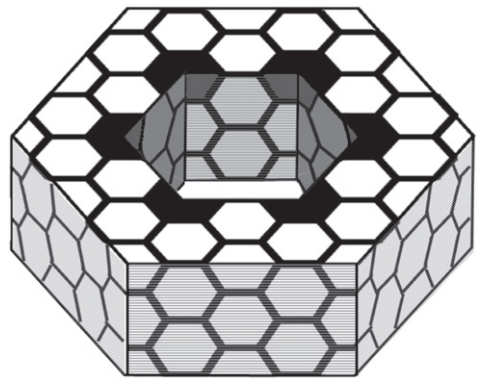

**Figure 92.** Schematic model of a *nanotube torus*. Heptagons in the inner corners, enhanced by the dark color, are paired with pentagonal rings at the outer corners. (Adapted following Iijima S 1994 *MRS Bulletin* **19**(11) 43 , © 1994 Materials Research Society.)

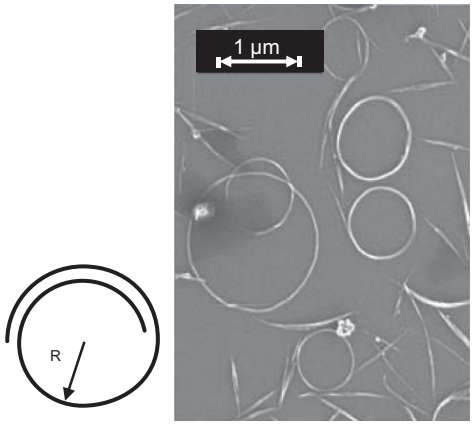


**Figure 93.** Schematic model and *scanning electron microscopy* (SEM) image of rings of *single-wall nanotubes* dispersed on a hydrogen-passivated silicon substrate. (Adapted from Martel R *et al* 1999 *J. Phys. Chem.* B **103** 7551, © 1999 American Chemical Society.)

into a large ring. The optimum radius $R$ is a compromise between the bending energy, which favors large $R$, and the inter-tube interaction, which favors small $R$ to maximize the number of turns.

The **toxicity** of carbon nanoparticles is an intensely researched topic, on which the final consensus has yet to emerge. For carbon *nanotubes*, the occurrence of pathogenic response depends sensitively on the presence of *catalyst* particles, side-wall *functionalization*, length-to-*diameter* aspect ratio, degree of aggregation, the tissue exposed and the type of exposure. Since most nanostructures will be constituents of complex systems, the occurrence of bio-hazards is limited to the fabrication process.

The **translational vector T** is the unit vector spanning the unit cell of a (1D) *nanotube*, *graphene nanoribbon* or a *chain*.

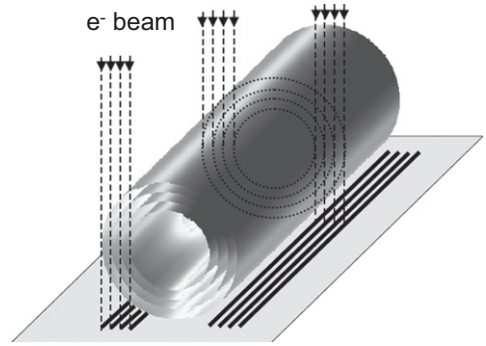


**Figure 94.** Principle of imaging in *transmission electron microscopy* (TEM), illustrated for a *multi-wall nanotube*. Schematic TEM images of other carbon nanostructures are reproduced in figure 95.

**Transmission electron microscopy** (TEM) is a powerful imaging technique using an energetic electron beam. TEM images are generated by electrons with a narrow energy distribution around typically $10^2$ keV. In contrast to *scanning electron microscopy* (SEM), where a focused electron beam probes the surface, electrons in a TEM are transmitted through a thin film containing carbon nanostructures, are subsequently magnified and focused on a screen. Resolution down to 0.1 nm is possible in the latest generation of high-resolution transmission electron microscopes (HRTEMs) with aberration correction even at reduced acceleration voltages of 60 keV. As seen in figure 94, *graphitic* segments parallel to the beam block transmission and often appear as dark lines. Typical images of graphitic carbon nanostructures are shown in figure 95. Since the electron beam interacting with the nanostructures undergoes electron diffraction, quantitative interpretation of TEM images is non-trivial.

A **triple-wall nanotube** (TWNT) is a *multi-wall nanotube* with three walls.

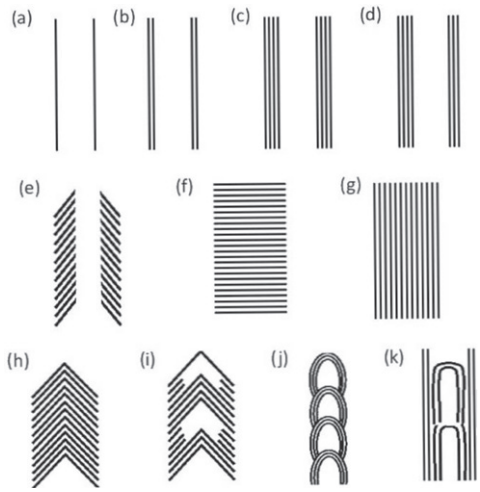


**Figure 95.** Typical schematic *transmission electron microscopy* images of (a) a *single-wall nanotube* (SWNT), (b) a *double-wall nanotube* (DWNT), (c) a *multi-wall nanotube* (MWNT), (d) a graphitic *scroll*, (e) hollow-core stacked *nanocones*, (f) a stacked curved platelet *carbon fiber*, (g) a full-core *nanotube*, (h) stacked nanocones in a *cup-stacked fiber*, (i) partitioned stacked nanocones, (j) stacked open multi-wall *fullerenes* resembling open *onions* and (k) a partitioned nanotube, commonly called *bucky bamboo*. (From Suarez-Martinez I *et al* 2012 *Carbon* **50** 741, © 2012 Elsevier.)

Triple-wall nanotubes can be prepared by the *fusion of fullerenes* inside *peapods*, where the tubular enclosure consists of *double-wall nanotubes* (DWNTs) with a sufficiently large inner *diameter*. This synthesis route is closely related to the growth of high- *purity* pristine DWNTs by *fullerene* coalescence inside *single-wall nanotubes* (SWNTs), shown in figure 37.

***Reference***

Hirschmann T C, Araujo P T, Muramatsu H, Zhang X, Nielsch K, Kim Y A and Dresselhaus M S 2013 Characterization of bundled and individual triple-walled carbon nanotubes by resonant Raman spectroscopy *ACS Nano* **7** 2381

**Turbostratic graphite** is a *graphitic* structure with a random orientation of *graphene* layers about their normal.

A **twiston** is an orientational dislocation in a *nanotube* that is stabilized by *interlayer interactions* in *multi-wall nanotubes* or nanotube *ropes*. The presence of twistons reduces the *conductance* of nanotubes.

***References***

Kwon Y-K and Tománek D 2000 Orientational melting in carbon nanotube ropes *Phys. Rev. Lett.* **84** 1483 2011 *ibid.* **106** 219901(E)

Bailey S W D, Tománek D, Kwon Y-K and Lambert C J 2002 Giant magneto-conductance in twisted carbon nanotubes *Europhys. Lett.* **59** 75

**TWNT** → *triple-wall nanotube*

**Two-photon absorption** is an ultra-fast optical technique using high-intensity light pulses, which allows two photons to be absorbed before emission occurs. Two-photon absorption studies in semiconducting *single-wall nanotubes* provided experimental evidence that *photoluminescence* stemming from low-lying $E_{11}$ transitions is *excitonic* in nature.

***Reference***

Wang F, Dukovic G, Brus L E and Heinz T F 2005 The optical resonances in carbon nanotubes arise from excitons *Science* **308** 838

# V

**VANTA** → *vertically aligned nanotube array*

**Vapor grown carbon fibers** (VGCFs) are continuous *graphitic* filaments with a

typical *diameter* exceeding one micrometer. VGCFs form typically when iron *catalyst* particles are introduced into carbon feedstock vapor in the reactor. Yield increases significantly at temperatures above the iron/carbon *eutectic* point. Initially poor degree of *graphitization* improves upon annealing, yielding good *mechanical properties*.

***Reference***

Oberlin A, Endo M and Koyama T 1976 Filamentous growth of carbon through benzene decomposition *J. Cryst. Growth* **32** 335

The **vapor–liquid–solid** (VLS) *catalytic growth* model of *nanotubes* is depicted schematically in figure 96. The basic assumption is that carbon feedstock in the vapor phase first condenses on small metal *catalyst* nanoparticles. Next, carbon atoms diffuse inside the metal nanoparticle until reaching saturation, transforming the nanoparticle to carbide. The nanoparticles are liquid under synthesis conditions, since the *melting temperature* $T_M$ of metal nanoparticles is substantially lower than that of bulk metals. Further lowering of $T_M$ occurs near the *eutectic* composition. Finally, carbon precipitates to the surface of a supersaturated catalyst particle and condenses to a solid nanotube, as seen in figure 58. In many cases, the *diameter* of the nanotube is similar to that of the catalyst nanoparticle.

***Reference***

Gavillet J, Loiseau A, Journet C, Willaime F, Ducastelle F and Charlier J-C 2001 Root-growth mechanism for single-wall carbon nanotubes *Phys. Rev. Lett.* **87** 275504

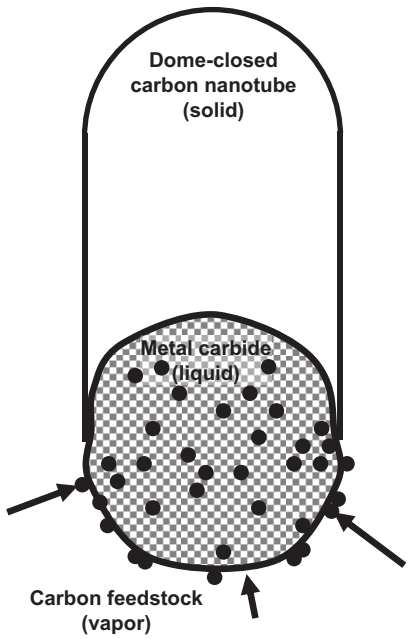


**Figure 96.** Schematic diagram of the *vapor–liquid–solid* (VLS) *catalytic growth* model of *nanotubes*. (After Bolton K *et al* 2006 *J. Nanosci. Nanotech.* **6** 1211, © 2006 American Scientific Publishers.)

A **vertically aligned nanotube array** (VANTA) is a dense array of carbon *nanotubes* growing vertically on a substrate, typically silicon with adsorbed transition metal *catalyst* particles (see figure 97). Accelerated growth of VANTAs is often called *supergrowth*.

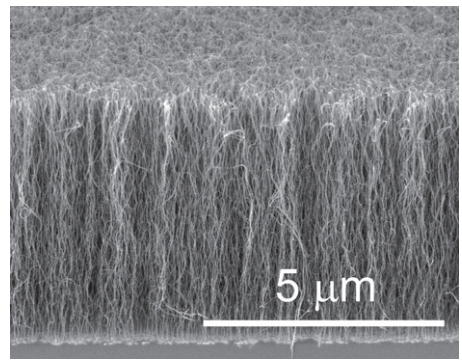


**Figure 97.** *Scanning electron microscopy* (SEM) image of a *vertically aligned nanotube array* (VANTA) grown on a quartz substrate (Shigeo Maruyama 2012 private communication).

***Reference***

Murakami Y, Chiashi S, Miyauchi Y, Hu M, Ogura M, Okubo T and Maruyama S 2004 Growth of vertically aligned single-walled carbon nanotube films on quartz substrates and their optical anisotropy *Chem. Phys. Lett.* **385** 298

The **Veselago lens** is a proposed planar lens made of a composite material with simultaneously negative values of the electric permittivity $\varepsilon$ and the magnetic permeability $\mu$ that could provide greatly improved resolution. A sharp n–p–n junction in *graphene* is expected to act as a Veselago lens for electrons.

***References***

Veselago V G 1968 The electrodynamics of substances with simultaneously negative values of ε and $\mu$ *Sov. Phys. Usp.* **10** 509 (Russian original appeared in 1967)

Cheianov V V, Fal'ko V and Altshuler B L 2007 The focusing of electron flow and a Veselago lens in graphene p-n junctions *Science* **315** 1252

The **vibration spectrum** is the set of atomic vibration frequencies. It is referred to as the *phonon spectrum* in infinite periodic structures.

**Viscoelasticity** is a behavior that combines elasticity and viscosity, and is typically attributed to rubbers. Carbon *nanotube* mats exhibit viscoelastic behavior in the temperature range from −196°C to 1000°C, significantly exceeding the corresponding temperature range in rubber compounds.

***Reference***

Xu M, Futaba D N, Yamada T, Yumura M and Hata K 2010 Carbon nanotubes with temperature-invariant viscoelasticity from to -196° *to* 1000° C *Science* **330** 1364

**VLS** → *Vapor–Liquid–Solid* growth model.

# W

**Wet chemical synthesis** of the $C_{60}$ *fullerene* may be accomplished by a multistep process from aromatic precursor molecules.

***References***

Scott L T, Boorum M M, McMahon B J, Hagen S, Mack J, Blank J, Wegner H and Armin de M 2002 A rational chemical synthesis of $C_{60}$ *Science* **295** 1500

Otero G, Biddau G, Sánchez-Sánchez C, Caillard R, López M F, Rogero C, Javier Palomares F, Cabello N, Basanta M A, Ortega J, Méndez J, Echavarren A M, Pérez R, Gómez-Lor B and Martin-Gago J A 2008 Fullerenes from aromatic precursors by surface-catalysed cyclodehydrogenation *Nature* **454** 865

The **Wigner–Seitz cell** is a primitive unit cell of a periodic structure that preserves its symmetry properties. The Wigner–Seitz cell in the reciprocal lattice of the momentum space is called the *Brillouin zone*. In *graphene*, the Wigner–Seitz cell of the direct lattice of the atoms and the Brillouin zone are hexagons that are rotated by 30° with respect to each other, as shown in figure 99.

The **work function** $\Phi$ of an extended system is the macroscopic counterpart of the first *ionization potential* (*IP*) or the *electron affinity* (*EA*). It is the energy necessary to remove the least bound electron and place it infinitely far from the structure. The work function of a molecular solid lies in between the ionization potential and the electron affinity of the molecules; the observed

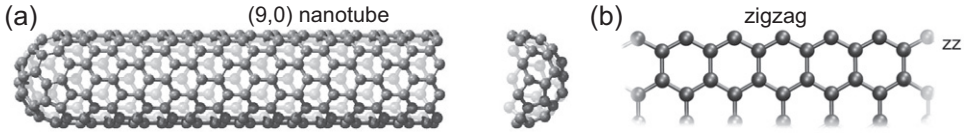


**Figure 98.** Structure of a (9,0) *zigzag nanotube* (a), terminated by a *zigzag edge* (b) at one end and capped by a *dome* at the other end.

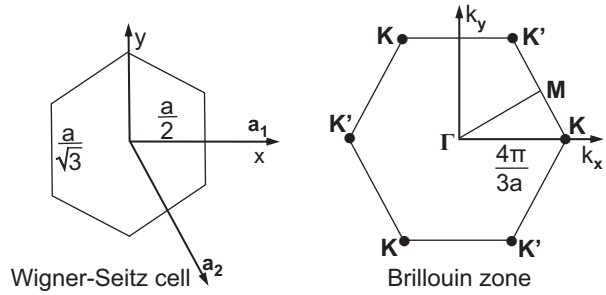


**Figure 99.** The *Wigner–Seitz cell* and the *Brillouin zone* of *graphene*, with cell sizes depending on the *lattice constant a*. Note the different orientation of the delimiting hexagons.

values for $C_{60}$ are $\Phi(C_{60}$ solid) = 4.7 eV, $IP(C_{60}$ molecule) = 7.58 eV and $EA(C_{60}$ molecule) = 2.65 eV.

# Y

**Young's modulus** → *mechanical properties*

# Z

The **zigzag edge** morphology of a *graphene* layer is shown in figure 98(b).

A **zigzag nanoribbon** is a *graphene nanoribbon* (GNR) with a *zigzag edge*. See also *graphene nanoribbon morphology*.

A **zigzag nanotube** is a common name for a *nanotube* with *chiral index* ($n$, 0), referring to the *zigzag edge* morphology at the open nanotube end (see figure 98).

# Further information

## History of Nanotubes in Pictures

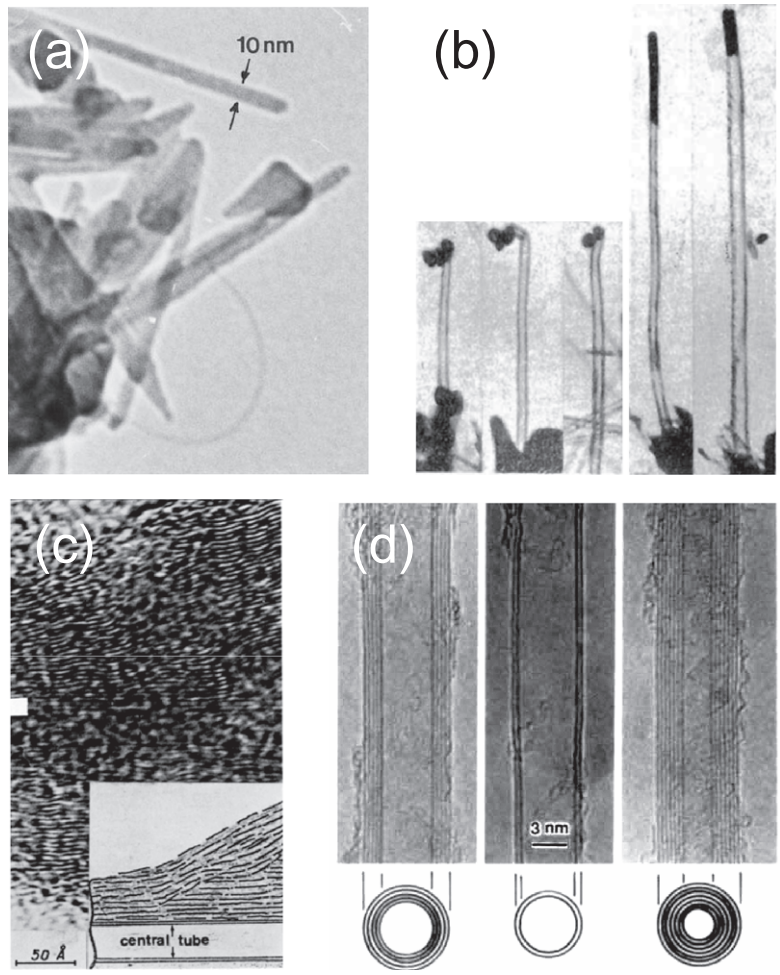


**Figure 100.** First electron microscopy observations of filamentous carbon related to carbon *nanotubes*. (a) Nanotubes observed in 10 000 year-old ice[a]. (b) A 1952 image of filamentous carbon formed by an ancestor of the *HiPCO process*[b]. (c) A 1976 image of a nanotube in the core of a *carbon fiber* formed by the *chemical vapor deposition (CVD)* process[c]. (d) A 1991 image of a multi-wall nanotube formed by the *arc evaporation (AE)* process[d].

[a]Murr L E, Esquivel E V, Bang J J, de la Rosa G and Gardea-Torresdey J L 2004 Chemistry and nano-particulate compositions of a 10,000 year-old ice core melt water *Water Res.* **38** 4282

[b]Radushkevich L V and Lukyanovich V M 1952 On the structure of carbon formed by thermal decomposition of carbon monoxide on iron substrate' [in Russian; original title 'O strukture ugleroda, obrazujucegosja pri termiceskom razlozenii okisi ugleroda na zeleznom kontakte'] *Zurn. Fisic. Chim.* **26** 88

[c]Oberlin A, Endo M and Koyama T 1976 Filamentous growth of carbon through benzene decomposition *J. Cryst. Growth* **32** 335

[d]Iijima S 1991 Helical microtubules of graphitic carbon *Nature* **354** 56

**Table 1. Time Line of Fullerenes**

| | |
|---|---|
| **1970** | **Theoretical postulate of the fullerene structure** |
| | Osawa E 1970 Superaromaticity' [in Japanese] *Kagaku (Kyoto)* **25** 854 |
| **1984** | **Synthesis of small carbon clusters** |
| | Rohlfing E A, Cox D M and Kaldor A 1984 Production and characterization of supersonic carbon cluster beams' *J. Chem. Phys.* **81** 3322 |
| **1985** | **$C_{60}$ synthesis and structure identification** |
| | Kroto H W, Heath J R, O'Brien S C, Curl R F and Smalley R E 1985 $C_{60}$: buckminsterfullerene *Nature* **318** 162 |
| **1990** | **Mass synthesis of $C_{60}$ in a carbon arc** |
| | Krätschmer W, Lamb L D, Fostiropoulos K and Huffman D R 1990 Solid $C_{60}$: a new form of carbon *Nature* **347** 354 |
| **1996** | **Nobel prize in Chemistry** |
| | The Nobel Prize in Chemistry 1996 was awarded jointly to Curl Jr R F, Kroto S H W and Smalley R E "for their discovery of fullerenes". |
| **1998** | **Synthesis of nanotube peapods** |
| | Smith B W, Monthioux M and Luzzi D E 1998 Encapsulated $C_{60}$ in carbon nanotubes *Nature* **396** 323 |
| **2002** | **Wet chemical synthesis** |
| | Scott L T, Boorum M M, McMahon B J, Hagen S, Mack J, Blank J, Wegner H and Armin de M 2002 A rational chemical synthesis of $C_{60}$ *Science* **295** 1500 |

**Table 2. Time Line of Nanotubes**

| | |
|---|---|
| **1952** | **Electron microscopy observation of carbon filaments** |
| | Radushkevich L V and Lukyanovich V M 1952 On the structure of carbon formed by thermal decomposition of carbon monoxide on iron substrate' [in Russian; original title 'O strukture ugleroda, obrazujucegosja pri termiceskom razlozenii okisi ugleroda na zeleznom kontakte'] *Zurn. Fisic. Chim.* **26** 88 |
| **1973** | **Structure of filamentous carbon** |
| | Baker R T K, Harris P S, Thomas R B and Waite R J 1973 Formation of filamentous carbon from iron, cobalt and chromium catalyzed decomposition of acetylene *J. Catal.* **30** 86 |
| **1976** | **Nanotube core observed in a carbon fiber** |
| | Oberlin A, Endo M and Koyama T 1976 Filamentous growth of carbon through benzene decomposition *J. Cryst. Growth* **32** 335 |
| **1991** | **Synthesis of multi-wall carbon nanotubes** |
| | Iijima S 1991 Helical microtubules of graphitic carbon *Nature* **354** 56 |
| **1992** | **Conductivity of carbon nanotubes** |
| | Mintmire J W, Dunlap BI and White C T 1992 Are fullerene tubules metallic? *Phys. Rev. Lett.* **68** 631 |
| | Hamada N, Sawada S and Oshiyama A 1992 New one-dimensional conductors - graphitic microtubules *Phys. Rev. Lett.* **68** 1579 |
| | Saito R, Fujita M, Dresselhaus G and Dresselhaus M S 1992 Electronic structure of graphene tubules based on $C_{60}$ *Phys. Rev.* B **46** 1804 |

**Table 2.** (*Continued*)

| | |
|---|---|
| **1993** | **High elastic modulus of carbon nanotubes** |
| | Overney G, Zhong W and Tománek D 1993 Structural rigidity and low frequency vibrational modes of long carbon tubules *Z. Phys. D* **27** 93 |
| **1993** | **Synthesis of single-wall nanotubes** |
| | Iijima S and Ichihashi T 1993 Single-shell carbon nanotubes of 1-nm diameter *Nature* **363** 603 |
| | Bethune D S, Kiang C H, DeVries M S, Gorman G, Savoy R and Beyers R 1993 Cobalt-catalysed growth of carbon nanotubes with single-atomic-layer walls *Nature* **363** 605 |
| **1995** | **Nanotubes as field emitters** |
| | Rinzler A G, Hafner J H, Nikolaev P, Lou L, Kim S G, Tománek D, Nordlander P, Colbert D T and Smalley R E 1995 Unraveling nanotubes: field emission from an atomic wire *Science* **269** 1550 |
| | de Heer W A, Châtelain A and Ugarte D 1995 A Carbon Nanotube Field-Emission Electron Source *Science* **270** 1179 |
| **1996** | **Ropes of single-wall nanotubes** |
| | Thess A, Lee R, Nikolaev P, Dai H, Petit P, Robert J, Xu C, Lee Y H, Kim S G, Colbert D T, Scuseria G, Tománek D, Fischer J E and Smalley R E 1996 Crystalline ropes of metallic carbon nanotubes *Science* **273** 483 |
| **1996** | **CVD synthesis of SWNTs (HiPCO)** |
| | Dai H J, Rinzler A G, Nikolaev P, Thess A, Colbert D T and Smalley R E 1996 Single-wall nanotubes produced by metal-catalyzed disproportionation of carbon monoxide *Chem. Phys. Lett.* **260** 471 |
| **1997** | **Quantum conductance of carbon nanotubes** |
| | Tans S J, Devoret M H, Dai H, Thess A, Smalley R E, Geerligs L J and Dekker C 1997 Individual single-wall carbon nanotubes as quantum wires *Nature* **386** 474 |
| **1997** | **Hydrogen storage in nanotubes** |
| | Dillon A C, Jones K M, Bekkendahl T A, Kiang C H, Bethune D S and Heben M J 1997 Storage of hydrogen in single-walled carbon nanotubes *Nature* **386** 377 |
| **1998** | **Chemical vapor deposition synthesis of aligned nanotube films** |
| | Ren Z F, Huang Z P, Xu J W, Wang J H, Bush P, Siegal M P and Provencio P N 1998 Synthesis of large arrays of well-aligned carbon nanotubes on glass *Science* **282** 1105 |
| **1998** | **Synthesis of nanotube peapods** |
| | Smith B W, Monthioux M and Luzzi D E 1998 Encapsulated $C_{60}$ in carbon nanotubes *Nature* **396** 323 |
| **2000** | **Thermal conductivity of nanotubes** |
| | Berber S, Young-Kyun K and Tománek D 2000 Unusually high thermal conductivity of carbon nanotubes *Phys. Rev. Lett.* **84** 4613 |
| **2000** | **Macroscopically aligned nanotubes in yarns** |
| | Vigolo B, Pénicaud A, Coulon C, Sauder C, Pailler R, Journet C, Bernier P and Poulin P 2000 Macroscopic fibers and ribbons of oriented carbon nanotubes *Science* **290** 1331 |

(*Continued*)

**Table 2.** (*Continued*)

| | |
|---|---|
| **2001** | **Integration of carbon nanotubes for logic circuits** |
| | Collins P C, Arnold M S and Avouris P 2001 Engineering Carbon Nanotubes and Nanotube Circuits Using Electrical Breakdown *Science* **292** 706 |
| **2001** | **Intrinsic superconductivity of carbon nanotubes** |
| | Kociak M, Kasumov A Y, Guéron S, Reulet B, Khodos I I, Gorbatov Y B, Volkov V T, Vaccarini L and Bouchiat H 2001 Superconductivity in ropes of single-walled carbon nanotubes *Phys. Rev. Lett.* **86** 2416 |
| **2004** | **Supergrowth of carbon nanotube arrays** |
| | Hata K, Futaba D N, Mizuno K, Namai T, Yumura M and Iijima S 2004 Water-assisted highly efficient synthesis of impurity-free single-walled carbon nanotubes *Science* **306** 1362 |
| **2009** | **Chirality-specific separation of carbon nanotubes** |
| | Tu X, Manohar S, Jagota A and Zheng M 2009 DNA sequence motifs for structure-specific recognition and separation of carbon nanotubes *Nature* **460** 250 |

**Table 3. Time Line of Graphene**

| | |
|---|---|
| **1907** | **Discovery of graphene** |
| | Acheson E G 1907 Deflocculated graphite *J. Frankl. Inst.* **164** 375 |
| **1947** | **Electronic band structure of graphene and the Dirac cone** |
| | Wallace P R 1947 The band theory of graphite *Phys. Rev.* **71** 622 |
| **1962** | **Term 'graphene' coined for chemically exfoliated graphite** |
| | Boehm H P, Clauss A, Fisher G, Hofman U and Fischer G O 1962 Thinnest carbon foils' [in German; original title 'Dünnste Kohlenstoff-Folien'] *Z. Naturforsch.* B **17** 150 |
| **1975** | **Graphene growth on SiC at 800°C** |
| | van Bommel A J, Crombeen J E and van Tooren A 1975 LEED and Auger electron observations of the SiC(0001) surface *Surf. Sci.* **48** 463 |
| **1998** | **Non-trivial Berry's phase and pseudo-spin** |
| | Ando T, Nakanishi T and Saito R 1998 Berry's phase and absence of back scattering in carbon nanotubes *J. Phys. Soc. Japan* **67** 2857 |
| **2004** | **Growth and electronic properties of multilayered graphene** |
| | Berger C, Song Z, Li T, Li X, Ogbazghi A Y, Feng R, Dai Z, Marchenkov A N, Conrad E H, First P N and de Heer W A 2004 Ultrathin epitaxial graphite: 2D electron gas properties and a route toward graphene-based nanoelectronics *J. Phys. Chem.* B **108** 19912 |
| **2004** | **Electronic properties of supported graphene** |
| | Novoselov K S, Geim A K, Morozov S V, Jiang D, Zhang Y, Dubonos S V, Grigorieva I V and Firsov A A 2004 Electric field effect in atomically thin carbon films *Science* **306** 666 |
| **2005** | **Quantum Hall effect and Berry's phase in graphene** |
| | Zhang Y, Tan Y-W, Stormer H L and Kim P 2005 Experimental observation of the quantum Hall effect and Berry's phase in graphene *Nature* **438** 201 |

**Table 3.** (*Continued*)

| | |
|---|---|
| **2005** | **Scotch tape method of isolating graphene from graphite** |
| | Novoselov K S, Jiang D, Schedin F, Booth T J, Khotkevich V V, Morozov S V and Geim A K 2005 Two-dimensional atomic crystals *Proc. Natl. Acad. Sci.* **102** 10451 |
| **2008** | **Graphene formed by surface segregation on carbon-saturated metals** |
| | Yu Q, Lian J, Siriponglert S, Li H, Chen Y P and Pei S-S 2008 Graphene segregated on Ni surfaces and transferred to insulators *Appl. Phys. Lett.* **93** 113103 |
| **2009** | **Chemical vapor deposition synthesis of graphene** |
| | Reina A, Jia X, Ho J, Nezich D, Son H, Bulovic V, Dresselhaus M S and Kong J 2009 Large area, few-layer graphene films on arbitrary substrates by chemical vapor deposition *Nano Lett.* **9** 30 |
| **2009** | **CVD growth of macroscopic graphene films** |
| | Kim K S, Zhao Y, Jang H, Lee S Y, Kim J M, Kim K S, Ahn J-H, Kim P, Choi J-Y and Hong B H 2009 Large-scale pattern growth of graphene films for stretchable transparent electrodes *Nature* **457** 706 |
| **2010** | **Nobel prize in Physics** |
| | The Nobel Prize in Physics 2010 was awarded jointly to Geim A and Novoselov K for 'groundbreaking experiments regarding the two-dimensional material graphene'. |

**Table 4. List of Common Acronyms**

| | |
|---|---|
| A@$C_n$ | Complex A enclosed inside a $C_n$ fullerene |
| A@(n, m) | Complex A enclosed inside an ($n$, $m$) nanotube |
| AFM | Atomic force microscopy, a common variant of SPM |
| CNT | Carbon nanotube |
| CVD | Chemical vapor deposition |
| DFS | Damping force spectroscopy, a variant of SPM |
| DOS | Density of states |
| DWNT | Double-wall nanotube |
| EG | Exfoliated graphite |
| ESR | Electron spin resonance |
| FEM | Field emission microscopy |
| GIC | Graphite intercalation compounds |
| GNR | Graphene nanoribbon |
| HOPG | Highly oriented pyrolytic graphite |
| HPLC | High-pressure liquid chromatographye |
| HREM | High-resolution electron microscopy |
| HRTEM | High-resolution transmission electron microscopy |
| ICP | Inductively coupled plasma |
| IR | Infrared spectroscopy |
| LDOS | Local density of states |
| MD | Molecular dynamics |

(*Continued*)

**Table 4. (*Continued*)**

| | |
|---|---|
| MR | Magnetoresistance |
| MWNT | Multi-wall nanotube |
| NH | Nanohorn |
| NT | Nanotube |
| (n, m) | Nanotube with the chiral index ($n$, $m$) |
| PVD | Physical vapor deposition |
| QHE | Quantum Hall effect |
| RBM | Radial breathing mode |
| SEM | Scanning electron microscopy |
| SERS | Surface enhanced Raman spectroscopy |
| SPM | Scanning probe microscopy |
| STM | Scanning tunneling microscopy, a common variant of SPM |
| STS | Scanning tunneling spectroscopy |
| SWCNT | Single-wall carbon nanotube |
| SWNT | Single-wall nanotube |
| TEM | Transmission electron microscopy |
| TGA | Thermogravimetric analysis |
| VANTA | Vertically aligned nanotube array |
| VLS | Vapor–liquid–solid model of nanotube growth |
| XRD | X-ray diffraction |

**Table 5. Common Quantities and Units**

| Quantity | Name | Equivalent quantity | Use |
|---|---|---|---|
| 1 Å | Angstrom | $10^{-10}$ m | length unit |
| 1 $a_0$ | Bohr radius | 0.52918 Å | length unit |
| 1 eV | electron-volt | $1.6022 \times 10^{-19}$ J | energy unit |
| 1 Ry | Rydberg | 13.606 eV | energy unit |
| 1 Ha | Hartree | 27.212 eV | energy unit |
| 1 amu | atomic mass unit | $1.661 \times 10^{-27}$ kg | mass unit |
| $h$ | Planck's constant | $4.1357 \times 10^{-15}$ eV s | quantum unit |
| $k_B$ | Boltzmann's constant | $8.617 \times 10^{-5}$ eV $K^{-1}$ | thermodynamic unit |
| $N_A$ | Avogadro's number | $6.0221 \times 10^{23}$ $mol^{-1}$ | number of particles per mole |
| $c$ | speed of light | $2.998 \times 10^{8}$ m $s^{-1}$ | speed of light in vacuum |
| $e$ | electron charge | $1.6022 \times 10^{-19}$ C | electrical charge |

**Table 6. Useful Conversion Factors**

| Quantity | Equivalent Quantity | Use |
|---|---|---|
| 1 eV/particle | 23.06 kcal/mol | binding energy |
| 1 eV/particle | 96.49 kJ/mol | binding energy |
| $k_BT$ (300 K) | $2.585 \times 10^{-2}$ eV | energy $k_BT$ at room temperature |
| 1 eV | $2.418 \times 10^{14}$ Hz | energy represented by frequency $\nu$ (conversion using $E = h\nu$) |
| 1 eV | $8.066 \times 10^{3}$ cm$^{-1}$ | energy represented by spectroscopic wavenumber $\lambda^{-1}$ (conversion using $E = hc\lambda^{-1}$) |
| 1 eV | $1.160 \times 10^{4}$ K | energy represented by temperature $T$ (conversion using $E = k_BT$) |

**Table 7. Structural Aspects of Nanocarbons**

| Quantity | Value |
|---|---|
| C–C distance (C–C *'single bond'* in $C_2H_6$) | $d_{CC} = 0.154$ nm |
| C–C distance (C = C *'double bond'* in $C_2H_4$) | $d_{CC} = 0.134$ nm |
| C–C distance (C ≡ C *'triple bond'* in $C_2H_2$) | $d_{CC} = 0.120$ nm |
| C–C distance ($sp^1$ carbons) | $d_{CC} = 0.129$ nm |
| C–C distance ($sp^2$ carbons) | $d_{CC} = 0.142$ nm |
| C–C distance ($sp^3$ carbons) | $d_{CC} = 0.154$ nm |
| Area per C atom ($sp^2$ carbons) | $A_C = 2.62 \times 10^{-2}$ nm$^2$ |
| Volume per C atom ($sp^3$ carbons) | $V_C = 5.69 \times 10^{-3}$ nm$^3$ |

**Table 8. Structural Properties of Nanohorns**

| Disclination angle | Opening angle $\theta$ |
|---|---|
| 300° | 19.2° |
| 240° | 38.9° |
| 180° | 60.0° |
| 120° | 84.6° |
| 60° | 112.9° |

**Table 9. Structural Parameters of the (Cubic) Diamond Lattices**

| | | |
|---|---|---|
| Structure characterization | face-centered cubic (fcc) lattice with a 2-atom basis | |
| Space group | $Fd3m\ (O_h^7)$ | |
| Lattice constant | $a = 0.357$ nm | |
| Interatomic distance | $d_{CC} = 0.154$ nm | |
| Bravais lattice vectors | *Cartesian coordinates* | |
| | $\vec{a}_1 = (0.0000, 0.1785, 0.1785)$ nm | |
| | $\vec{a}_2 = (0.1785, 0.0000, 0.1785)$ nm | |
| | $\vec{a}_3 = (0.1785, 0.1785, 0.0000)$ nm | |
| Basis vectors | *Cartesian coordinates* | |
| | $\vec{\tau}_1 = (0.0000, 0.0000, 0.0000)$ nm | |
| | $\vec{\tau}_2 = (0.0893, 0.0893, 0.0893)$ nm | |
| Reciprocal lattice vectors | *Cartesian coordinates* | *Fractional coordinates* |
| | $\vec{b}_1 = (-17.600, 17.600, 17.600)$ nm$^{-1}$ | $=(1, 0, 0)$ |
| | $\vec{b}_2 = (17.600, -17.600, 17.600)$ nm$^{-1}$ | $=(0, 1, 0)$ |
| | $\vec{b}_3 = (17.600, 17.600, -17.600)$ nm$^{-1}$ | $=(0, 0, 1)$ |
| High-symmetry points | *Cartesian coordinates* | *Fractional coordinates* |
| in the reciprocal lattice | $\Gamma = (0, 0, 0)$ nm$^{-1}$ | $= (0, 0, 0)$ |
| | $\mathrm{X} = (17.600, 0.000, 0.000)$ nm$^{-1}$ | $=(0.000,0.500,0.500)$ |
| | $\mathrm{W} = (17.600, 8.800, 0.000)$ nm$^{-1}$ | $=(0.250,0.500,0.750)$ |
| | $\mathrm{U} = (17.600, 4.400, 4.400)$ nm$^{-1}$ | $=(0.250,0.625,0.625)$ |
| | $\mathrm{L} = (8.800, 8.800, 8.800)$ nm$^{-1}$ | $=(0.500,0.500,0.500)$ |
| | $\mathrm{K} = (13.200, 13.200, 0.000)$ nm$^{-1}$ | $=(0.375,0.375,0.750)$ |

The figure display (a) the conventional unit cell and (b) the Brillouin zone.

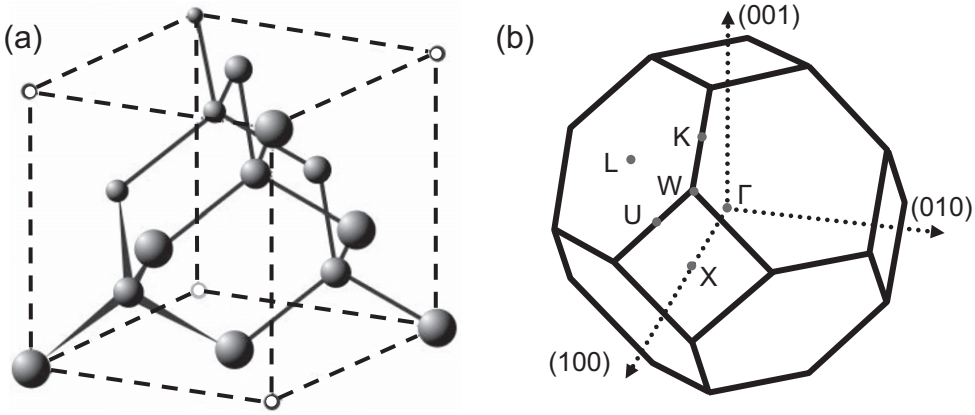

**Table 10. Structural Parameters of the Graphene Lattice**

| | | |
|---|---|---|
| Structure characterization | honeycomb lattice<br>(triangular lattice with a 2-atom basis) | |
| Lattice constant | $a = 0.246$ nm | |
| Interatomic distance | $d_{CC} = 0.142$ nm | |
| Bravais lattice vectors | *Cartesian coordinates* | |
| | $\vec{a}_1 = (0.2130, -0.1230)$ nm | |
| | $\vec{a}_2 = (0.2130, 0.1230)$ nm | |
| Basis vectors | *Cartesian coordinates* | |
| | $\vec{\tau}_1 = (0.0000, 0.0000)$ nm | |
| | $\vec{\tau}_2 = (1.4200, 0.0000)$ nm | |
| Reciprocal lattice vectors | *Cartesian coordinates* | *Fractional coordinates* |
| | $\vec{b}_1 = (25.546, -44.248)$ nm$^{-1}$ | $= (1, 0)$ |
| | $\vec{b}_2 = (25.546, 44.248)$ nm$^{-1}$ | $= (0, 1)$ |
| High-symmetry points | *Cartesian coordinates* | *Fractional coordinates* |
| in the reciprocal lattice | $\Gamma = (0, 0)$ nm$^{-1}$ | $= (0, 0)$ |
| | M $= (25.546, 0.000)$ nm$^{-1}$ | $= (0.5, 0.5, 0)$ |
| | K $= (25.546, 14.749)$ nm$^{-1}$ | $= (0.333, 0.667)$ |
| | K$' = (25.546, -14.749)$ nm$^{-1}$ | $= (0.667, 0.333)$ |

The figure displays (a) the atomic structure including the primitive unit cell and (b) the Brillouin zone.

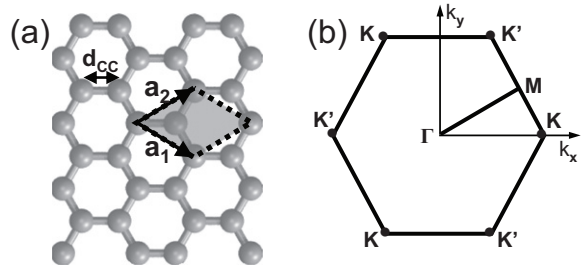

**Table 11. Structural Parameters of Hexagonal Graphite**

| | | |
|---|---|---|
| Structure characterization | hexagonal lattice with a 4-atom basis | |
| Space group | $P6_3/mmc \quad (D_{6h}^4)$ | |
| Lattice constant | $a = 0.246$ nm, $c = 0.690$ nm | |
| Interatomic distance | $d_{CC} = 0.142$ nm (in-plane) | |
| Interlayer distance | $c/2 = 0.345$ nm | |
| Bravais lattice vectors | *Cartesian coordinates* | |
| | $\vec{a}_1 = (0.2130, -0.1230, 0.0000)$ nm | |
| | $\vec{a}_2 = (0.2130, 0.1230, 0.0000)$ nm | |
| | $\vec{a}_3 = (0.0000, 0.0000, 0.6900)$ nm | |
| Basis vectors | *Cartesian coordinates* | |
| | $\vec{\tau}_1 = (0.0000, 0.0000, 0.0000)$ nm | |
| | $\vec{\tau}_2 = (0.1420, 0.0000, 0.0000)$ nm | |
| | $\vec{\tau}_3 = (0.0000, 0.0000, 0.3450)$ nm | |
| | $\vec{\tau}_4 = (-0.1420, 0.0000, 0.3450)$ nm | |
| Reciprocal lattice vectors | *Cartesian coordinates* | *Fractional coordinates* |
| | $\vec{b}_1 = (25.546, -44.248, 0.000)$ nm$^{-1}$ | $=(1, 0, 0)$ |
| | $\vec{b}_2 = (25.546, 44.248, 0.000)$ nm$^{-1}$ | $=(0, 1, 0)$ |
| | $\vec{b}_3 = (0.000, 0.000, 9.106)$ nm$^{-1}$ | $=(0, 0, 1)$ |
| High-symmetry points in the reciprocal lattice | *Cartesian coordinates* | *Fractional coordinates* |
| | $\Gamma = (0, 0, 0)$ nm$^{-1}$ | $= (0, 0, 0)$ |
| | $\mathrm{M} = (25.546, 0.000, 0.000)$ nm$^{-1}$ | $= (0.5, 0.5, 0)$ |
| | $\mathrm{K} = (25.546, 14.749, 0.000)$ nm$^{-1}$ | $= (0.333, 0.667, 0)$ |
| | $\mathrm{K}' = (25.546, -14.749, 0.000)$ nm$^{-1}$ | $= (0.667, 0.333, 0)$ |
| | $\mathrm{H} = (25.546, 14.749, 4.553)$ nm$^{-1}$ | $= (0.333, 0.667, 0.5)$ |
| | $\mathrm{A} = (0.000, 0.000, 4.553)$ nm$^{-1}$ | $= (0, 0, 0.5)$ |
| | $\mathrm{L} = (25.546, 0.000, 4.5530)$ nm$^{-1}$ | $= (0.5, 0.5, 0.5)$ |

The figure displays (a) the atomic structure and (b) the Brillouin zone.

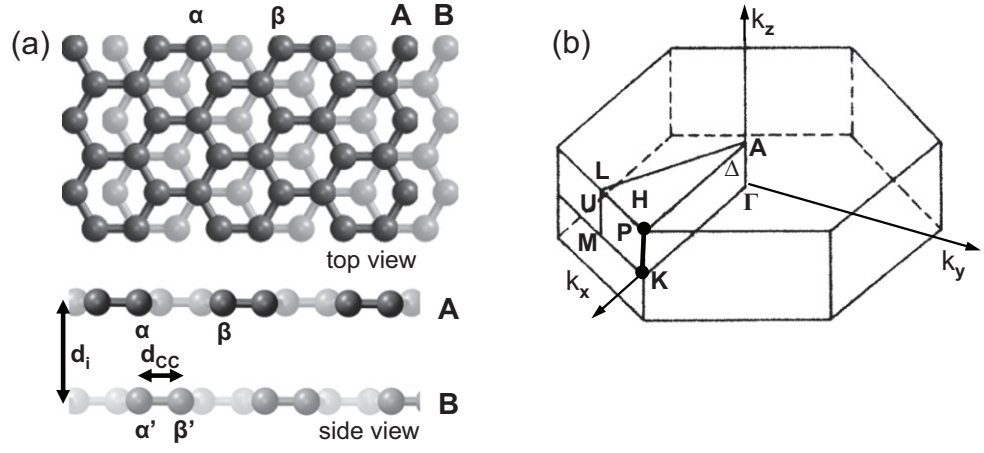

**Table 12. Structure of Fullerenes and Nanotubes**

| Quantity | Expression |
|---|---|
| Diameter of a $C_n$ fullerene | $d_f \approx \sqrt{n} \times 0.0913$ nm |
| Diameter of an ($n$, $m$) nanotube | $d_t \approx \sqrt{m^2 + mn + n^2} \times 0.0783$ nm |
| Chiral angle of an ($n$, $m$) nanotube | $\theta = \sin^{-1}\left(\frac{\sqrt{3}m}{2\sqrt{n^2 + nm + m^2}}\right)$ |
| Length of the chiral vector of an ($n$, $m$) nanotube | $C_h \approx 0.246 \times \sqrt{m^2 + mn + n^2}$ nm |

**Table 13. Useful textbooks on carbon nanostructures**

Dresselhaus M S, Dresselhaus G and Eklund P 1996 *Science of Fullerenes and Carbon Nanotubes* (San Diego: Academic Press)

Harris P J F 2009 *Carbon Nanotube Science* (Cambridge: Cambridge University Press).

Jorio A, Dresselhaus M and Dresselhaus G 2008 *Carbon Nanotubes: Advanced Topics in the Synthesis, Structure, Properties and Applications* Topics in Applied Physics No. 111 (Berlin: Springer).

Fowler P W and Manolopoulos D E 2006 *An Atlas of Fullerenes* Dover.